

# Round-Trip Time-Division Distributed Beamforming

by

Tyson Coey

A Thesis

Submitted to the Faculty

of the

WORCESTER POLYTECHNIC INSTITUTE

In partial fulfillment of the requirements for the

Degree of Master of Science

in

Electrical and Computer Engineering

by

---

June 2007

APPROVED:

---

Dr. D. Richard Brown, Advisor

---

Dr. John McNeill, Committee Member

---

Dr. Fred Looft, Department Head

---

Dr. Richard Vaz, Committee Member

## **Abstract**

This thesis develops a system for synchronizing two wireless transmitters so that they are able to implement a distributed beamformer in several different channel models. This thesis considers a specific implementation of the system and proposes a metric to quantify its performance. The system's performance is investigated in single-path and multi-path time-invariant channel scenarios, as well as in single-path time-varying channel scenarios. Where prior systems have difficulty in implementing a distributed beamformer in multi-path channels and/or mobile scenarios, the results of this thesis show that the Round-Trip Time-Division distributed beamforming system is able to perform as a beamformer in all three of the channel models considered.

## **Acknowledgements**

I would like to express my gratitude to my advisor, Rick Brown, who has been very patient with me throughout this endeavor. Not only did he help me expand my technical knowledge, but his understanding and appreciation for the research process enabled an education beyond the field of electrical engineering.

While most of my family and friends will never understand exactly what I have done for the past two years, many of them offered a significant amount of support. I would like to thank those who encouraged me throughout my education and those who helped make it possible.

I would also like to thank Professor John McNeill and Professor Richard Vaz for reviewing my thesis and participating in my defense.

# Contents

<b>1</b>	<b>Introduction</b>	<b>1</b>
1.1	Thesis Organization . . . . .	3
<b>2</b>	<b>Background</b>	<b>5</b>
2.1	Principles of Conventional Transmit Beamforming . . . . .	5
2.2	Distributed Beamforming . . . . .	9
2.3	Synchronization Architectures and Techniques . . . . .	10
2.3.1	The Mutual Synchronization Architecture . . . . .	11
2.3.2	The Master-Slave Synchronization Architecture . . . . .	13
2.3.3	The Round-Trip Synchronization Architecture . . . . .	15
2.4	Phase Locked Loop Basics . . . . .	21
2.4.1	PLL Operation . . . . .	24
<b>3</b>	<b>Round-Trip Time-Division Distributed Beamforming</b>	<b>28</b>
3.1	RTTD Protocol Description . . . . .	28
3.2	RTTD Source Node Design Considerations . . . . .	33
3.2.1	Source Requirements and PLL Design Methodology . . . . .	34
3.2.2	RTTD Source PLL Implementation . . . . .	38
3.2.3	RTTD Source PLL Design Guideline . . . . .	40
<b>4</b>	<b>RTTD Distributed Beamforming in Time Invariant Channels</b>	<b>47</b>
4.1	RTTD System Performance Measure . . . . .	48
4.2	RTTD System Operation in SPTI Channels . . . . .	49
4.2.1	SPTI Channel Effects and Synchronization Overhead . . . . .	49
4.2.2	Effects of PLL Design on RTTD System Efficiency . . . . .	52
4.2.3	Worst-Case Performance Analysis for SPTI Channels . . . . .	54
4.2.4	RTTD System Performance in SPTI Channels . . . . .	60
4.3	RTTD System Operation in MPTI Channels . . . . .	63
4.3.1	MPTI Channel Effects and Synchronization Overhead . . . . .	65
4.3.2	Worst-Case Performance Analysis for MPTI Channels . . . . .	68
4.3.3	RTTD System Performance in MPTI Channels . . . . .	70

<b>5</b>	<b>RTTD Distributed Beamforming in Time-Varying Channels</b>	<b>73</b>
5.1	Time-Varying Channel Model . . . . .	74
5.1.1	Statistical Properties of Channel Delays . . . . .	75
5.2	Initial Phase Error Distribution . . . . .	79
5.3	Simulation Results: Initial Phase Error . . . . .	83
5.3.1	Effects of Movement Speed . . . . .	84
5.3.2	Effects of Velocity Variation . . . . .	86
5.3.3	Initial Phase Error in Mobile Scenarios . . . . .	89
5.4	Phase Error During Beamforming . . . . .	92
5.5	Simulation Results: Beamformer Phase Error . . . . .	94
5.5.1	Beamformer Duration and Phase Error . . . . .	94
5.5.2	Efficiency in Mobile Scenarios . . . . .	96
<b>6</b>	<b>Conclusions</b>	<b>98</b>
<b>A</b>	<b>Appendices</b>	<b>101</b>
A.1	Time-to-Lock . . . . .	101
A.2	High-Frequency Feedthrough Magnitude . . . . .	103

# Chapter 1

## Introduction

Antenna arrays have been commonly used in communication systems for many years to achieve a directional radiation pattern. Beamforming is used to isolate communication to a specific receiver, increase power efficiency in cases when isotropic radiation is not needed, and increase signal reliability. The direction of focused transmission energy is controlled by the orientation of the antennas used in the array, or by changing the phases of the excitation signals for each antenna, i.e. phased arrays.

With the increased interest in wireless products and wireless sensor networks, *distributed beamforming* is gaining the interest of many researchers. The size of most wireless devices, i.e., cellular handsets and low-powered sensors, restrict the use of multiple antennas, so beamforming with a conventional phased array is not possible. Distributed beamforming is the concept of many wireless devices forming a virtual antenna array in order to implement a beamformer. Each single-antenna device, however, is controlled independently by a separate local oscillator, so carrier synchronization is necessary among the distributed sources.

Previous work in the field of distributed beamforming and carrier synchroniza-

tion can be categorized into three major areas by the architecture in which the transmitters are organized. The *mutual*, *master-slave*, and *round-trip* synchronization architectures have unique attributes in the way that the transmitters are organized, and therefore the way in which the transmitters are able to achieve carrier synchronization is significantly affected.

Mutual synchronization methods are considered in [3] and [10] in the context of clock synchronization, but as shown in [11], this architecture is not suitable for RF distributed beamforming. In mutual synchronization there is no consideration of phase steering to realize a beamformer in a predictable direction, and the commonly imposed half-duplex constraint is violated.

Master-slave synchronization systems for distributed beamforming are proposed in [12], [13], and [14], but common pitfalls of these systems are channel estimation and limited mobility. The system proposed in [12] requires substantial time to measure the channel phase delays to each distributed source, which limits mobility and requires precise channel estimation. The system in [13] requires the sources to be static, and the system in [14] relies on random convergence behavior so mobility may inhibit this system from implementing a beamformer.

The round-trip synchronization system proposed in [15] is shown to be effective in mobile scenarios and does not require explicit channel estimation, but its performance degrades in general multipath channels. Hence, a distributed beamforming system that performs well in mobile scenarios, as well as in general multi-path channels, does not exist.

This thesis considers an implementation of a round-trip synchronization system that performs well in general multipath channels, and although limited, also in mobile scenarios. The system described in this thesis may perform better in mobile scenarios when compared to the master-slave synchronization systems in [12], [13], and [14]

because no explicit channel estimation is required, and the time in which synchronization is achieved is relatively small. This thesis introduces the Round-Trip Time-Division (RTTD) distributed beamforming system and outlines a specific implementation. This thesis also investigates the system's performance in single-path and multipath time-invariant channels, as well as single-path time-varying channels.

## 1.1 Thesis Organization

This thesis is comprised of four major chapters:

- Background Material
- Presentation of the Round-Trip Distributed Beamforming System
- Analysis of the RTTD System in Time-Invariant Channels
- Analysis of the RTTD System in Time-Varying Channels

Background material is provided in Chapter 2 and consists of three major sections. The first discusses conventional beamforming with phased arrays. The second reviews the research field of distributed beamforming and investigates previous attempts of carrier synchronization and phase control. The third reviews the basic operation of phase locked loops and introduces a key tradeoff in designing PLLs.

The Round-Trip Time-Division (RTTD) distributed beamforming system is presented and described in detail in Chapter 3. The synchronization protocol is outlined, the construction of the distributed sources is considered, and assumptions regarding inherent source knowledge and ability are presented. A specific implementation of the source components is chosen, and then a design example is provided.

Chapter 4 investigates the performance of the RTTD system when the channels are modeled as single-path, and multi-path, time-invariant channels. The effects

of each channel model are considered, and a worst-case analysis of the system performance is conducted. Simulation results are presented to support the analytical work, and to investigate the achievable performance in each channel model.

Chapter 5 analyzes the performance of the RTTD system in single-path time-varying channels. The statistical channel model is described, and then the phase error distribution at the start of beamforming and during beamforming is found analytically. Simulation results are used to verify the analytical work and are used to investigate the achievable performance for a range of mobile scenarios.

# Chapter 2

## Background

This chapter provides background material for better understanding of the distributed beamforming system proposed in this thesis. This chapter begins with a discussion of the basic principles of conventional beamforming. The concept of distributed beamforming is introduced and motivated by potential applications, and descriptions of published synchronization architectures are given. Finally, a review of phase locked loops is given to aid in the understanding of the distributed beamforming system proposed in this thesis.

### 2.1 Principles of Conventional Transmit Beamforming

Antenna arrays that produce a directional radiation pattern have been commonly used in communication systems since the introduction of shortwave radio equipment in the 1920s [1]. Directional radiation patterns are used to increase power efficiency where isotropic radiation is not necessary, and in cases where it is important to focus transmission energy to a single receiver, i.e., isolating communication from enemy

receivers in military applications. The direction of the focused transmission energy is specific to the orientation of the isotropic antennas used in an array, but also to the phase of the excitations for each antenna.

When isotropic antennas are spaced by some non-zero distance from each another, there are phase differences in their radiated fields. These phase differences result in the radiated fields constructively and destructively interfering in different directions. Hence, the resultant radiation pattern is directional and a beamformer is realized. To better understand this basic principle of transmit beamforming, consider Figure 2.1 where two isotropic antennas are separated by half a wavelength. It is assumed that the interference is evaluated at a distance from the antenna array that is in the far-field region [2], and that the source signals are narrowband such that the time delay of one signal relative to another can be expressed as a simple phase shift of the signals' frequency.

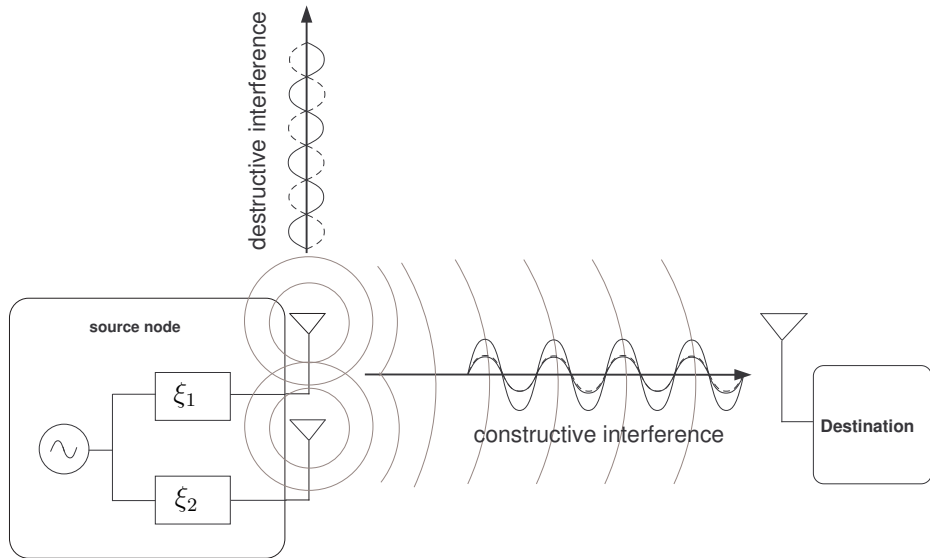


Figure 2.1: System model for conventional transmit beamforming where the source has a single oscillator and two phase adjusters,  $\xi_1$ ,  $\xi_2$ , for the two antennas spaced by a half-wavelength.

In Figure 2.1, the signals emitted are of the same frequency and phase, i.e., the phase adjusters are set equal,  $\xi_1 = \xi_2$ . Along the vertical axis on which the antennas lie, the signals are  $180^\circ$  out of phase in the far-field because of the half-wavelength spacing, and therefore the signals cancel each other. In the horizontal direction, however, the signals coherently combine in the far-field because they are in phase, giving the maximum possible amplitude and the direction of the beamformer. The radiation pattern, or normalized array factor [1], for two isotropic antennas with identical amplitude and phase feeds spaced a half-wavelength apart in the orientation shown in Figure 2.1 can be expressed by

$$f(\psi) = \sin\left(\frac{d\pi}{\lambda} \cos \psi\right) = \sin\left(\frac{\pi}{2} \cos \psi\right), \quad (2.1)$$

where  $d$  is the spacing distance and  $\lambda$  is the wavelength. The array factor  $f(\psi)$  for this configuration is plotted in Figure 2.2.

Notice that the transmission energy in this case is actually focused in two directions,  $\psi = 0^\circ$  and  $\psi = 180^\circ$ . The radiation pattern can be changed by physically altering the orientation of the antennas or by adjusting the phase of the excitation signals for each antenna, i.e.,  $\xi_1 \neq \xi_2$ . The later approach, commonly known as a phased array, offers quicker adaptability and there is no need for mechanical moving parts [1].

The transmitter depicted in Figure 2.1 drives its antennas with the same oscillator, and has explicit control of the phase for each antenna. As a result, the direction of the beamformer is easily controlled by the single transmitter. In many applications, however, a transmitter may only have a single antenna, e.g. cellular handsets and low-powered sensor networks. Hence, many researchers have been motivated to work in the research field of *distributed beamforming*. Distributed beamforming is

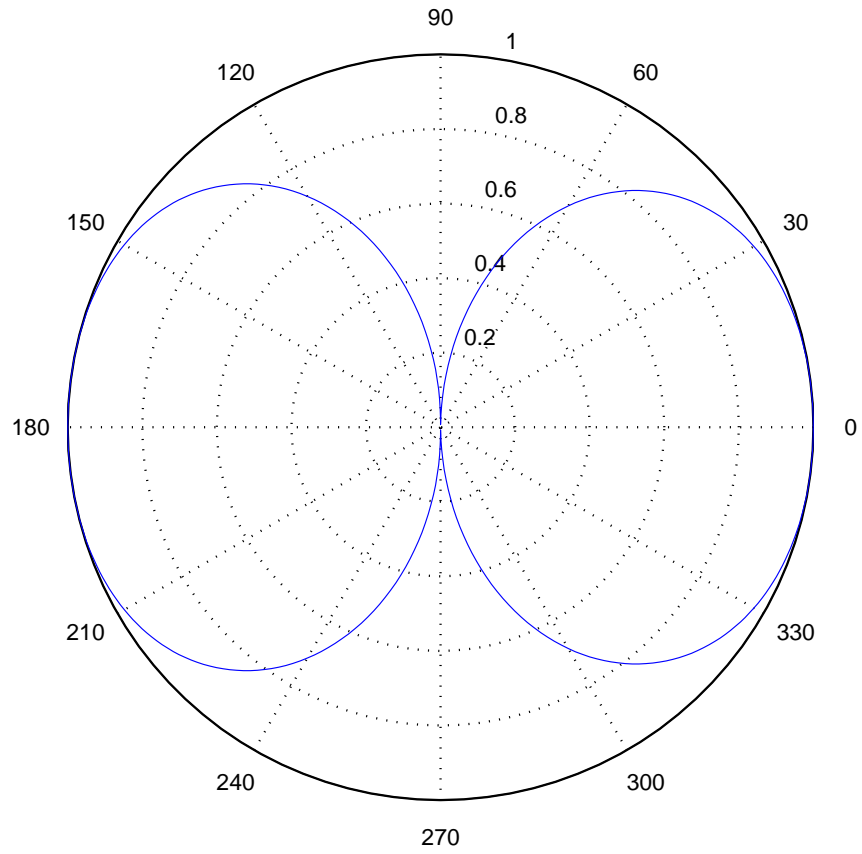


Figure 2.2: Polar plot of the array factor  $f(\psi)$  for two isotropic antennas with identical amplitude and phase excitations spaced a half-wavelength apart in a vertical orientation.

the concept of multiple single-antenna transmitters realizing the behavior of a conventional phased array. The next section discusses the concept of distributed beamforming and identifies the added challenges.

## 2.2 Distributed Beamforming

Distributed beamforming is the concept of multiple single-antenna transmitters behaving as a conventional phased array despite being disconnected and driven by separate independent local oscillators as shown in Figure 2.3. One reason the concept of distributed beamforming gained the interest of many researchers recently is because there are many wireless devices, such as cellular handsets and sensors, that would see power consumption and quality of service improvements through distributed beamforming. Researchers have considered the sensor reachback problem where multiple sensors are deployed in a field and it is desired that they act as a distributed transmission array to send information back to a base station or overhead aircraft [3]. Others have considered cooperation protocols that require beamforming amongst distributed autonomous cell users [4–6]. The wireless devices considered in these examples, however, are small in size and the use of multiple antennas is prohibited. Therefore conventional beamforming is not feasible, but distributed beamforming may allow these devices to realize a beamformer.

Distributed beamforming has many challenges considering the autonomous and mobile nature of wireless devices. Figure 2.3 shows that the transmitters have independent frequency references  $\omega_i$ , and each transmitter has control over its individual phase  $\xi_i$ . Distributed beamforming requires the synchronization of the independent oscillators, and the coordination amongst the disconnected transmitters to phase their transmissions in such a way that the energy is steered in the desired direction.

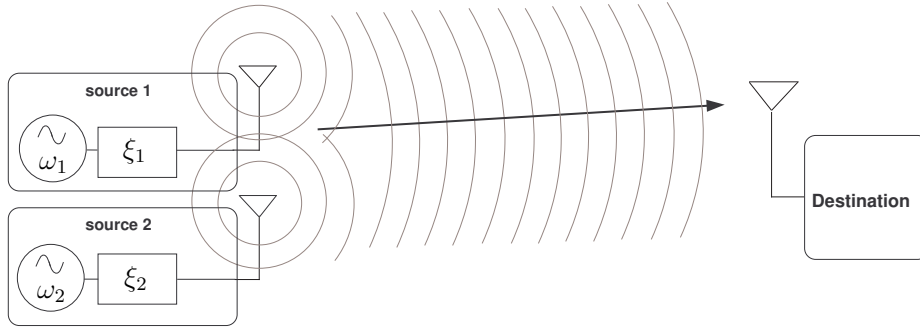


Figure 2.3: Two-source, one-destination system model for distributed beamforming. Note that unlike conventional beamforming, each antenna in distributed beamforming is driven by an independent local oscillator.

Although it was shown in [7] that even with a phase error of  $30^\circ$ , the distributed beamformer amplitude is still 96% percent of the maximum possible value, these challenges are difficult to overcome considering the mobile nature and typical high RF frequencies characteristic of modern communication systems. For example, GPS which has an accuracy of about 10 ns, is not accurate enough for carrier synchronization at RF frequencies such as 2.4 GHz. A phase error of  $30^\circ$  translates to a timing error of about 35 ps (and a position error of 10 mm).

Recent work in the field of distributed beamforming and carrier synchronization has considered several multi-user synchronization architectures to achieve carrier synchronization at RF frequencies and precise phase control. This work is reviewed in the next section.

## 2.3 Synchronization Architectures and Techniques

There have been two multi-user/network architectures considered in the field of carrier synchronization that are easily distinguishable from one another, but a third that is more of a hybrid architecture and has been consider only once previous

to this thesis. In this section, conceptual descriptions are given for the *mutual*, *master – slave*, and *round – trip* synchronization architectures, and specific techniques utilizing these architectures are discussed. Each conceptual description will be facilitated using the two-source one-destination system model shown in Figure 2.3, although many of the techniques proposed in the previous work are not limited to two sources.

### 2.3.1 The Mutual Synchronization Architecture

The mutual synchronization architecture is inspired by Southern Asian fireflies that synchronize their flashes of light with each other with no master coordinator or outside influence. As discussed in [8] and [9], these fireflies, modeled as pulse-coupled oscillators, synchronize their flashes of light on a common time scale. Each firefly would advance or delay (in time) its event of a light flash based on the observations of light flashes by surrounding fireflies. Thus, each firefly synchronizes the frequency of their flashes to the frequency of other close proximity fireflies while they are, in return, doing the same.

A mutual synchronization architecture was considered in [3] and [10] in the context of clock synchronization. As shown in [11], however, this architecture is not suitable for RF distributed beamforming because there is no consideration of phase steering to realize the beamformer in a predictable direction. In addition, the mutual synchronization architecture requires that the transmitters transmit and receive on the same frequency simultaneously, which violates the commonly imposed constraint that the transmitters operate in half-duplex mode. To further illustrate why mutual synchronization does not work well for distributed beamforming consider Figure 2.4.

In this figure, the sources are receiving a transmission from the other source, estimating the frequency and phase, and then controlling their oscillators  $\omega_i$  and

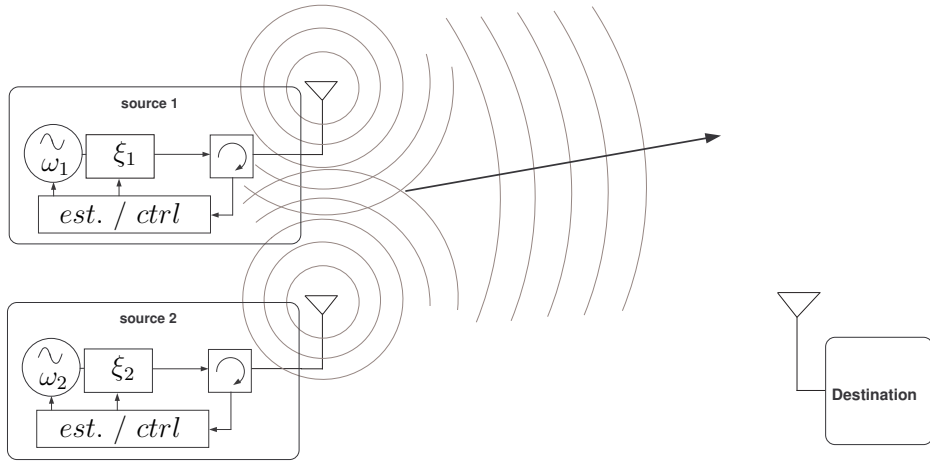


Figure 2.4: Mutual synchronization system model where the transmissions are not guaranteed to coherently combine in the direction of the destination.

phases  $\xi_i$  accordingly. The transmissions that are to realize the beamformer are also acting as synchronization signals to which the oscillators are locked, but the phases are not synchronized in such a way that the direction of the beamformer is predictable. Therefore phase coherency cannot be guaranteed in the direction of the destination.

Although the mutual synchronization architecture does not lend itself well to distributed beamforming, the architecture offers an elegant solution to frequency synchronization in multi-user wireless communication systems. In a mutual synchronization architecture there is low synchronization overhead, meaning that the sources are able to transmit to one another with relatively low power and the signals used for synchronization are also the actual communication signals. The next section discusses a synchronization architecture that has additional synchronization overhead, but is more suitable for distributed beamforming.

### 2.3.2 The Master-Slave Synchronization Architecture

In a master-slave network architecture there is a master transmitter amongst the distributed source transmitters, or, as is more common, the destination acts as a master to the sources. The master is responsible for coordinating the synchronization effort, commonly employing feedback to the sources to achieve frequency and phase synchronization. The master can be compared to an orchestrator of a symphony, giving instruction to the sources (i.e., musicians) in order to synchronize (i.e., play a musical piece in unison). The master-slave architecture, as it applies to a two-source one-destination system model, is illustrated in Figure 2.5.

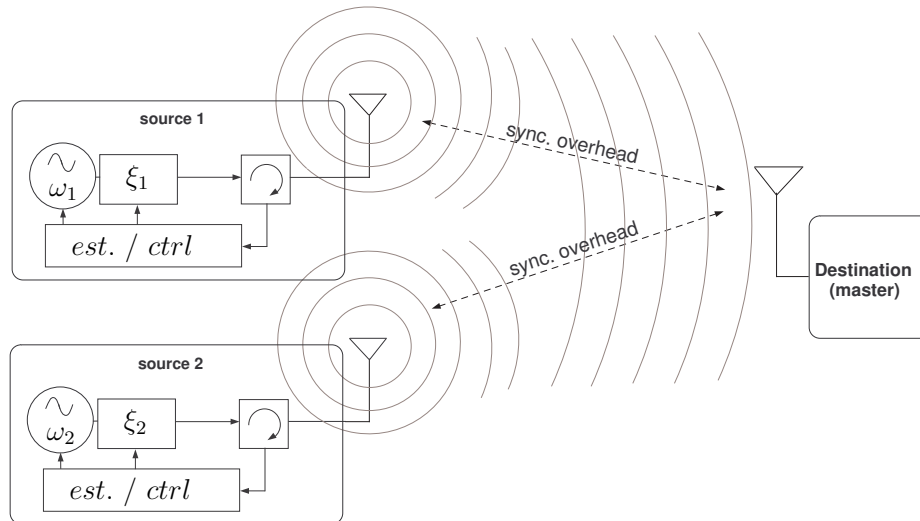


Figure 2.5: Master-slave system model where feedback from the destination is used to direct the beamformer in the direction of the destination.

With instructional feedback from the master to the sources, the sources in a master-slave architecture are able to adjust their phases  $\xi_i$  to focus the beamformer in a predictable direction, which is not possible in a mutual synchronization architecture. While the instructional feedback is the key to realizing a distributed beamformer in a master-slave architecture, it generally causes the master-slave syn-

chronization techniques to be less power efficient compared to mutual synchronization techniques. The destination is commonly assumed to be at a distance from the sources that is much greater than the distance between the two sources. This corresponds to the common assumption that sources can transmit to one another with relatively low power through high SNR channels compared to transmissions to the destination, e.g. sensor networks transmitting to a base station or close proximity cellular handsets transmitting to a cell tower. Therefore, the synchronization signals fed back and forth between the master and the sources often use valuable transmit power. Although master-slave synchronization techniques tend to be less power efficient, the synchronization signals, often containing channel estimates or instructions for phase adjustment, are necessary in a master-slave architecture in order to realize the distributed beamformer.

A master-slave synchronization method for distributed beamforming was proposed in [12] where a master beacon from the destination and a response from the sources is used to measure the phase delays to each source. The destination estimates the delays, sends the estimates back to the sources, and the sources pre-compensate for their respective channel phase delay. The estimation, feedback, and pre-compensation cycle of this protocol limits the amount of mobility. Moreover, accurate channel estimates must be obtained for maximum phase coherency.

Another master-slave carrier synchronization method was proposed in [13] where phase coherency is achieved by static sources that are precisely placed such that the phase delays to the destination are identical for all sources. Although this technique has no explicit channel estimation and has minimal feedback, distributed beamforming is achieved at the cost of mobility. In addition, the high frequency carriers commonly used in wireless networks require that the placement of the static sources be very accurate in order to realize the beamformer in the desired direction.

The placement of such sources would need to be accurate within centimeters for typical RF frequencies.

In [14] a protocol was introduced that requires continuous feedback from the destination to the sources based on the power of received signal at the destination. The synchronization process begins when the sources apply an arbitrary phase perturbation to their unsynchronized phase. The sources then wait for feedback from the destination notifying whether the phase perturbation increased or decreased the received signal power at the destination. If the applied phase perturbation is beneficial then the sources keep their new phases, otherwise a different phase perturbation is used for the next time step. According to [14], the phases of the sources converge to values that maximize the power of the distributed beamformer. Although this protocol is attractive because of the potential for synchronizing a large number of sources and no explicit channel estimation is performed, it is susceptible to ill performance if the sources are mobile. Mobility hinders the convergence of the sources' phases because the channel phase delays continually change and the phase perturbations are arbitrarily chosen.

Unlike mutual synchronization, master-slave synchronization techniques are able to realize a distributed beamformer, but this approach may have limitations caused by channel estimation, limited mobility, and continuous feedback that may not converge if the sources are mobile.

### **2.3.3 The Round-Trip Synchronization Architecture**

The round-trip synchronization architecture first proposed in [15] is a hybrid strategy in that it shares properties with the master-slave architecture and the mutual synchronization architecture. Round-trip synchronization is similar to master-slave synchronization in that the destination acts as a master initializing the synchro-

nization process, but it differs because it does not use explicit channel estimation nor instructional phase adjustment feedback. It is similar to mutual synchronization in that the sources and destination equally contribute to the synchronization process, but differs because the destination acts as a master. The system model for round-trip synchronization is shown in Figure 2.6.

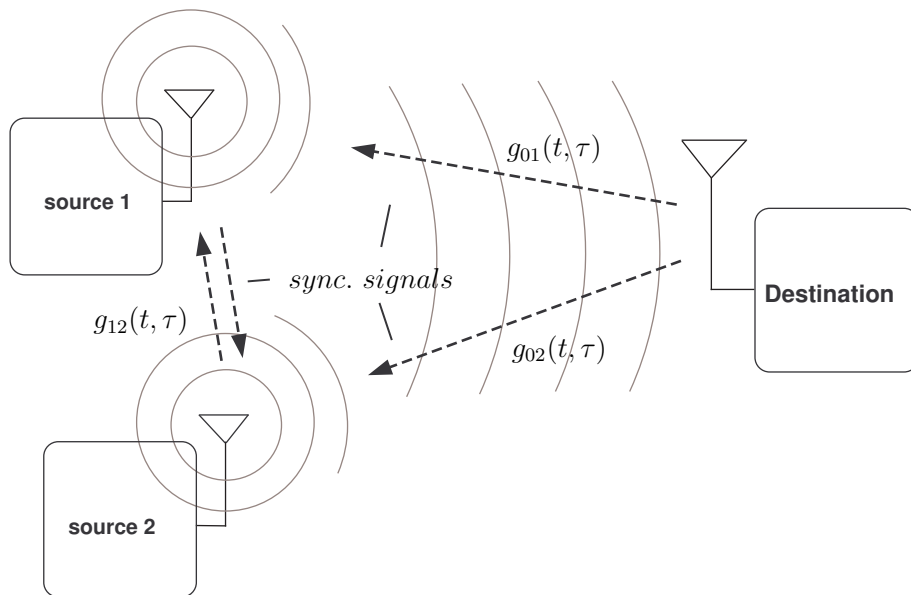


Figure 2.6: Two-source, one-destination system model for a round-trip synchronization architecture.

The key concept of the round-trip architecture is that the phase delay for the two opposing round-trip paths formed by the two-source one-destination triangle are identical. In other words, the phase delay in the  $D \rightarrow S1 \rightarrow S2 \rightarrow D$  circuit is identical to the phase delay in the  $D \rightarrow S2 \rightarrow S1 \rightarrow D$  circuit<sup>1</sup>.

To expose the intuition of a round-trip architecture more simply, it is temporarily assumed that the channels are single path and time-invariant (i.e.,  $g_{ij}(t) = \delta(t - \tau_{ij})$  for  $ij \in \{01, 02, 12\}$ )<sup>2</sup>. If the destination in Figure 2.6 were to transmit a signal  $x(t)$

<sup>1</sup>Here it is assumed that the channel delays are identical in the forward and reverse directions.

<sup>2</sup>Multi-path and time-varying channels are discussed in Chapters 4 and 5.

to source 1, and source 1 relayed this signal to source 2, and source 2 subsequently relayed this signal back to the destination, the propagation time can be calculated from  $\tau_{tot} = \tau_{g01} + \tau_{g12} + \tau_{g10}$ , corresponding to the round-trip path  $D \rightarrow S1 \rightarrow S2 \rightarrow D$ . The signal that the destination receives from this round-trip path can be expressed as

$$r(t) = x(t - \tau_{tot} - \Delta_1 - \Delta_2) \quad (2.2)$$

where  $\Delta_i$  is the relaying latency of the  $i^{\text{th}}$  source. Since the transmission from the destination  $x(t)$  is also received by source 2, the signal is relayed through the round-trip path  $D \rightarrow S2 \rightarrow S1 \rightarrow D$  as well and the propagation delay through this circuit is identical to  $\tau_{tot}$ . Therefore the destination receives two identical signals of the form (2.2) and synchronization is achieved if the relaying latencies  $\Delta_i$  are strictly controlled. How the relaying latencies are controlled is an attribute of the synchronization technique. An implementation utilizing the round-trip architecture will perform well only if the relaying latencies  $\Delta_i$  are strictly controlled ensuring that the round-trip propagation times only depend on channel variations. Also, the implementation must satisfy the common assumption of half-duplex operation.

A practical realization of a round-trip distributed beamforming technique was described in [15], where the challenges of round-trip synchronization were satisfied by constructing the source using two frequency-synthesis phase locked loops (FS-PLL) [16]. A detailed view of this practical source implementation is shown in Figure 2.7.

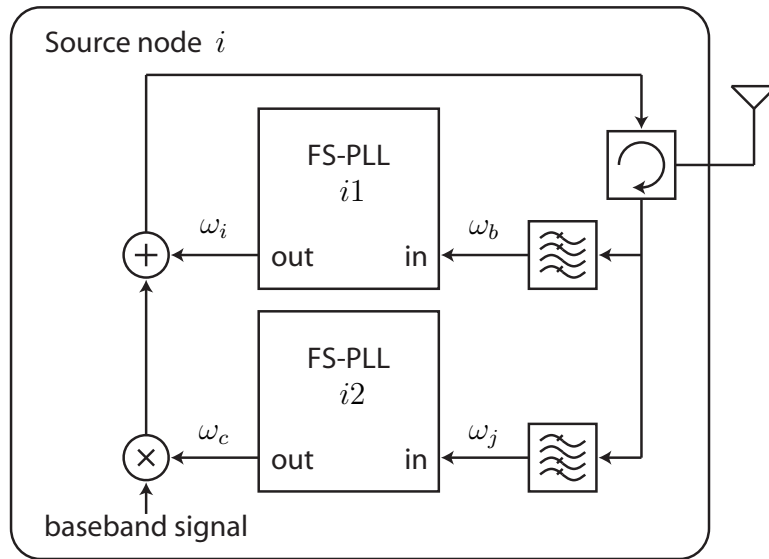


Figure 2.7: Block diagram of  $i^{\text{th}}$  source in the round-trip frequency-synthesis (RTFS) distributed beamforming technique.

In operation, the destination transmits a continuous sinusoidal master beacon at frequency  $\omega_b$  rad/s to the two sources. The sources employ a primary FS-PLL<sup>3</sup> tuned to  $\omega_b$  in order to track the phase of the master beacon. The primary FS-PLL of the  $i^{\text{th}}$  source produces a secondary beacon at frequency  $\omega_i = \frac{N_1}{M_1}\omega_b$  that is used as the relay signal. Simultaneously, the  $i^{\text{th}}$  source uses a secondary FS-PLL tuned to  $\omega_j$  to track the relay signal phase from source  $j$ . The secondary FS-PLL of the  $i^{\text{th}}$  source produces a carrier signal at frequency  $\omega_c = \frac{N_2}{M_2}\omega_j$  to be used to form the distributed beamformer back to the destination. This is expressed by

$$r(t) = a_1 \cos(\omega_{c1}t + \phi_1) + a_2 \cos(\omega_{c2}t + \phi_2) \quad (2.3)$$

where  $\phi_i$ ,  $a_i$ , and  $\omega_{ci}$  are the received phase, amplitude, and frequency, respectively, of the carrier signal from the  $i^{\text{th}}$  source. The power in the received signal as a function of time is given by [17]

$$P_r(t_o) = \frac{1}{2} \left[ a_1^2 + \frac{a_1 a_2 \omega_c}{\pi} \int_{t_o}^{t_o + \frac{2\pi}{\omega_c}} y(t) dt + a_2^2 \right], \quad (2.4)$$

where

$$y(t) = \cos((\omega_{c1} + \omega_{c2})t + (\phi_1 + \phi_2)) + \cos((\omega_{c1} - \omega_{c2})t + (\phi_1 - \phi_2)). \quad (2.5)$$

---

<sup>3</sup>The nomenclature “frequency-synthesis” PLL is used because a frequency multiplier is used to produce an output frequency that differs from the input frequency, but the two frequencies are phase locked.

The power is computed over a period of  $\omega_c$ . It is assumed that  $\omega_{c1} \approx \omega_{c2} \approx \omega_c$  in the locked state, such that the integral of the high frequency term in (2.4)-(2.5) is small. In this case, (2.4) can be simplified to

$$P_r(t_o) = \frac{1}{2} \left[ a_1^2 + \frac{a_1 a_2 \omega_c}{\pi} \int_{t_o}^{t_o + \frac{2\pi}{\omega_c}} \cos(\phi_\Delta(t)) dt + a_2^2 \right] \quad (2.6)$$

where  $\phi_\Delta(t)$  is the effective phase offset in the received carrier signals due to  $\phi_1 - \phi_2$  and  $(\omega_{c1} - \omega_{c2})t$  for  $t \in [t_o, t_o + \frac{2\pi}{\omega_c}]$ .

To review, each source in the RTFS system has a primary and secondary FS-PLL responsible for (i) tracking the phase of the incoming signal so that the relaying latencies are consistent and (ii) producing an output signal at a different frequency to satisfy the half-duplex constraint. Note that all of the signals are transmitted continuously, so with PLLs designed for fast convergence, this technique can track changing channel delays caused by source and/or destination mobility. This technique was shown to be effective in single-path time-invariant and time-varying channels in [15], but the multiple frequencies present in this implementation cause the channel reciprocity assumption to not be valid for general multipath channels. The effective delay imposed by a multipath channel may not be identical at two different frequencies, hence the performance for this approach can degrade in general multipath channels [15].

This thesis considers an extension to the technique in [15] that also uses PLLs to ensure accurate relaying latencies. To better understand this implementation and the distributed beamforming technique proposed in this thesis, it is necessary to be familiar with PLL functionality. Therefore, the next section reviews the basic building blocks of the phase locked loop, and then describes the behavior of the PLL in the unlocked and locked states.

## 2.4 Phase Locked Loop Basics

A phase locked loop (PLL) is a control loop that locks its output signal's phase and frequency to that of its input signal. The PLL is composed of three major components: a phase detector, a loop filter, and a voltage controlled oscillator (VCO). These components are connected as shown in Figure 2.8.

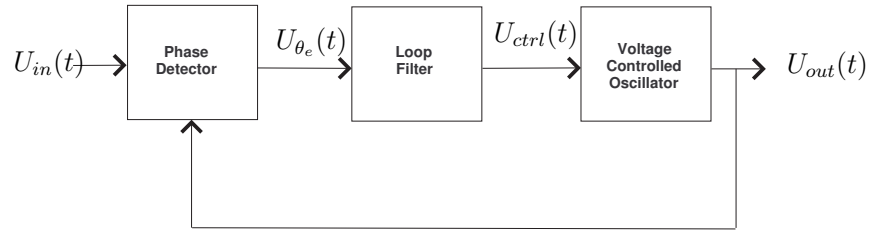


Figure 2.8: Phase locked loop block diagram.

The input to the PLL  $U_{in}(t)$  is commonly a sinusoid with frequency  $\omega_{in}$  and phase  $\theta_{in}$ . The PLL is a closed-loop control system that locks the VCO output signal's phase  $\theta_{out}$  and frequency  $\omega_{out}$  with that of its input signal. The PLL accomplishes this task by finding the phase difference between the output  $U_{out}(t)$  and input  $U_{in}(t)$  using the phase detector. The phase detector outputs a signal  $U_{\theta_e}(t)$  that is approximately proportional to the phase error. The phase detector output is then filtered by the loop filter in order to produce the conditioned VCO control signal  $U_{ctrl}(t)$ . The frequency of the VCO output  $U_{out}(t)$  is adjusted proportionally to the VCO control signal as expressed by

$$\omega_{out}(t) = \omega_q + K_0 U_{ctrl}(t), \quad (2.7)$$

where  $K_o$  is the VCO gain in rad/s·V and  $\omega_q$  is the free-running frequency of the VCO in rad/s. The loop is closed by feeding the VCO output back to the phase detector so that the current phase error can be estimated.

There are several types of phase detectors; [16] describes four different types in detail. The first type, the multiplier phase detector, generates the phase error signal  $U_{\theta_e}(t)$  by multiplying the VCO output  $U_{out}(t)$  and the input signal  $U_{in}(t)$ . The phase error signal produced by a multiplier phase detector consists of a low frequency term and a high frequency term as given by

$$U_{\theta_e}(t) = K_d[\cos((\omega_{out} - \omega_{in})t + (\theta_{out} - \theta_{in})) + \cos((\omega_{out} + \omega_{in})t + (\theta_{out} + \theta_{in}))] \quad (2.8)$$

where  $K_d$  is the phase detector gain in V/rad and is typically set to

$$K_d = \frac{a_{in}a_{out}}{2}, \quad (2.9)$$

where  $a_{in}$  and  $a_{out}$  are the amplitude's of  $U_{in}(t)$  and  $U_{out}(t)$ , respectively. The low-frequency term is the desired portion of the phase error signal  $U_{\theta_e}(t)$ , since, when  $\omega_{out} = \omega_{in}$  and  $\theta_{out} - \theta_{in}$  is small, it is proportional to the phase error.

Other common phase detectors, including the EXOR phase detector, the JK-flipflop phase detector, and phase-frequency detector, all produce a similar phase error signal. These phase detectors are implemented using digital logic, so consequently the phase error signals produced are a variation of a square wave. While the DC average of the square wave, much like the low-frequency term of (2.8), is proportional to the phase error, a square wave also contains high-frequency harmonics that have an adverse effect on the VCO control signal. These harmonics, and the high-frequency term of (2.8), will cause the output frequency to have undesired jitter. However, a properly designed loop filter attenuates the high-frequency components produced by any one of these phase detectors, while passing the low-frequency component. Therefore the loop filter may take on several different versions of a low-pass filter, i.e., a passive lead-lag filter, an active lead-lag filter, or an active PI filter [16].

The design of the loop filter, and the other components of the PLL, is facilitated using the linear model for the PLL illustrated in Figure 2.9. The linear model is used to investigate the performance of the PLL in the locked state, i.e., when  $\omega_{out} = \omega_{in}$  and  $\theta_{out} - \theta_{in}$  is small.

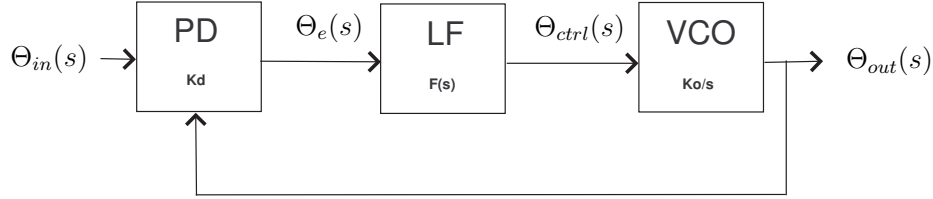


Figure 2.9: Block diagram of the linear PLL model.

In the locked state, the PLL is modeled by a linear transfer function, which relates the input and output phase signals. The phase-transfer function of the PLL can be approximated in terms of the PLL natural frequency  $\omega_n$  and damping factor  $\zeta$  as given by [16]

$$H(s) \approx \frac{2s\zeta\omega_n + \omega_n^2}{s^2 + 2s\zeta\omega_n + \omega_n^2}. \quad (2.10)$$

The phase-transfer function exposes that the 2nd-order PLL is essentially a low-pass filter with unit DC gain. The bandwidth is specified by the frequency where the closed loop gain has dropped by 3dB, which is denoted by  $\omega_{3dB}$ . The designer of the PLL generally knows what the PLL loop bandwidth  $\omega_{3dB}$  should be from investigation of the locked state using the linear model.

A 2nd-order PLL uses a 1st-order loop filter, and  $\omega_n$  and  $\zeta$  are specific to the particular design of the loop filter. Therefore, once the designer chooses a loop bandwidth  $\omega_{3dB}$  and a loop filter implementation, the natural frequency  $\omega_n$  and damping factor  $\zeta$  can be found. Guidelines are given in [16] as to how to choose the poles of the loop filter, as well as  $K_o$  and  $K_d$  for given values of  $\omega_n$ ,  $\zeta$ , and  $\omega_{3dB}$ .

### 2.4.1 PLL Operation

To investigate the basic operation of the PLL a specific implementation of a 2nd-order PLL is designed and then simulated. A multiplier phase detector and 1st-order active lead-lag loop filter are used in this example. The frequency of the input is  $\omega_{in} = 2\pi \times 100$  rads/sec, and the input phase  $\theta_{in}$  is randomly generated. The loop bandwidth is set to  $\omega_{3dB} = 2\pi \times 10^6$  rads/sec. The VCO gain is  $K_o = 2\pi \times 10^4$  rad/s·V and the phase detector gain is  $K_d = 1$  V/rad. The loop filter poles were chosen to achieve the specified loop bandwidth [16]. The VCO center frequency is equal to the input  $\omega_q = \omega_{in}$ , but the phase is randomly generated.

Figure 2.10 shows the input and output signals before and after lock with the corresponding behavior of the control signal  $U_{ctrl}(t)$ . In the locked state, the output leads the input by  $\frac{\pi}{2}$  due to the choice of phase detector. The input frequency is equal to the VCO center frequency  $\omega_q$ , so  $U_{ctrl}(t)$  converges to zero in the locked state. If this were not the case, the control signal  $U_{ctrl}(t)$  would need to converge to a non-zero level in order to drive the output frequency  $\omega_{out}$  to a value other than  $\omega_q$ .

For this PLL design,  $U_{ctrl}(t)$  has a considerable amount of jitter in the locked state due to high-frequency feedthrough from the phase detector. This jitter is undesirable in many applications including distributed beamforming because it causes the output frequency to vary. The magnitude of the high-frequency feedthrough can be reduced by lowering the loop bandwidth  $\omega_{3dB}$ , but this lengthens the time-to-lock, denoted as  $T_L$ .

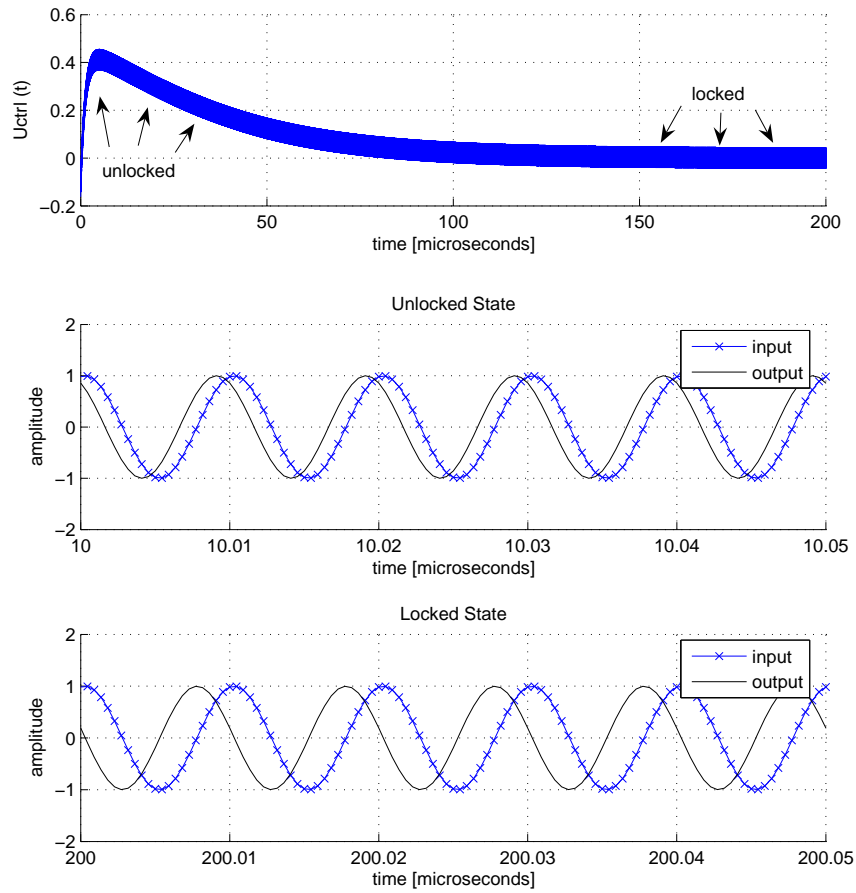


Figure 2.10: Control signal  $U_{ctrl}(t)$  and corresponding PLL input and output signals before and after lock. The PLL closed loop bandwidth  $\omega_{3dB} = 2\pi \times 10^6$  rads/sec facilitates fast convergence, but allows a significant amount of high-frequency feedthrough.

The time-to-lock is independent of the components used in the 2nd-order PLL design, and is approximated by [16]

$$T_L \approx \frac{2\pi}{\omega_n}, \quad (2.11)$$

where  $\omega_n$  is the natural frequency of the PLL. The natural frequency  $\omega_n$  is, in general, proportional to the PLL closed loop bandwidth<sup>4</sup>  $\omega_{3dB}$ . Thus, decreasing  $\omega_{3dB}$  lengthens the time-to-lock  $T_L$ , but decreases the magnitude of the high-frequency feedthrough. This is shown in Figure 2.11 where the loop bandwidth is  $\omega_{3dB} = 2\pi \times 10^5$ rad/sec. The PLL closed loop bandwidth is chosen such that the high-frequency feedthrough is sufficiently attenuated, with the tradeoff that a lower  $\omega_{3dB}$  means that the PLL will take longer to settle. This tradeoff is important to understand because it has considerable impact on the design of the distributed beamforming system proposed in this thesis.

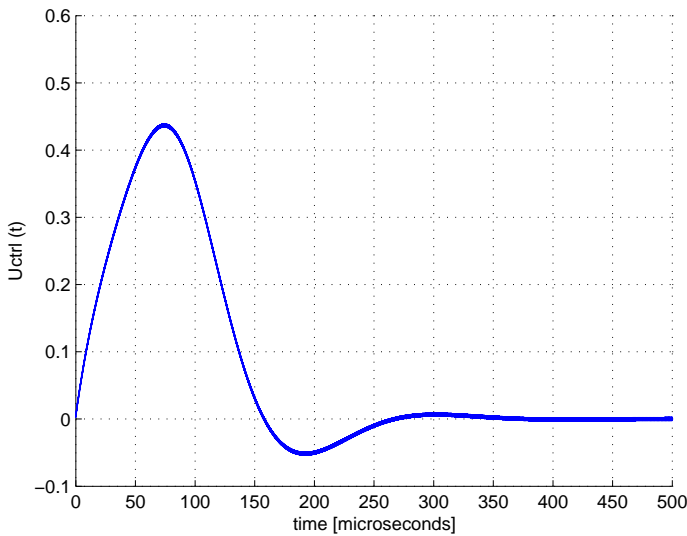


Figure 2.11: Increasing the PLL closed loop bandwidth to  $\omega_{3dB} = 2\pi \times 10^5$ rad/sec facilitates slower convergence, but attenuates the high-frequency feedthrough.

<sup>4</sup>This is investigated in greater detail in Chapter 3.

The background knowledge of the research area and the basic operation of the PLL presented in this chapter is necessary to understand the distributed beamforming system proposed in this thesis. The next chapter introduces the system, and the remaining chapters investigate its performance in time-invariant and time-varying channel models.

# Chapter 3

## Round-Trip Time-Division Distributed Beamforming

The round-trip time-division (RTTD) distributed beamforming system is described in this chapter. The RTTD distributed beamforming method is based on the round-trip frequency-synthesis (RTFS) system first discussed in [15], but the RTTD system uses time-division rather than frequency-division to satisfy the half-duplex constraint. The advantages of a time-division approach are that it does not require any additional bandwidth and, as shown in Chapter 4, channel reciprocity is not compromised in multi-path scenarios. In this chapter, the system model and general synchronization protocol are outlined, and the design and realization of the RTTD sources is considered.

### 3.1 RTTD Protocol Description

The RTTD method is the counterpart of the RTFS method; it separates the transmissions in the time domain rather than the frequency domain to satisfy the half-

duplex constraint. Unlike the RTFS system where the beacons are continuously transmitted, the destination and two sources never transmit simultaneously except when the two sources transmit as a beamformer to the destination. An overview of the RTTD synchronization protocol is shown in Figure 3.1.

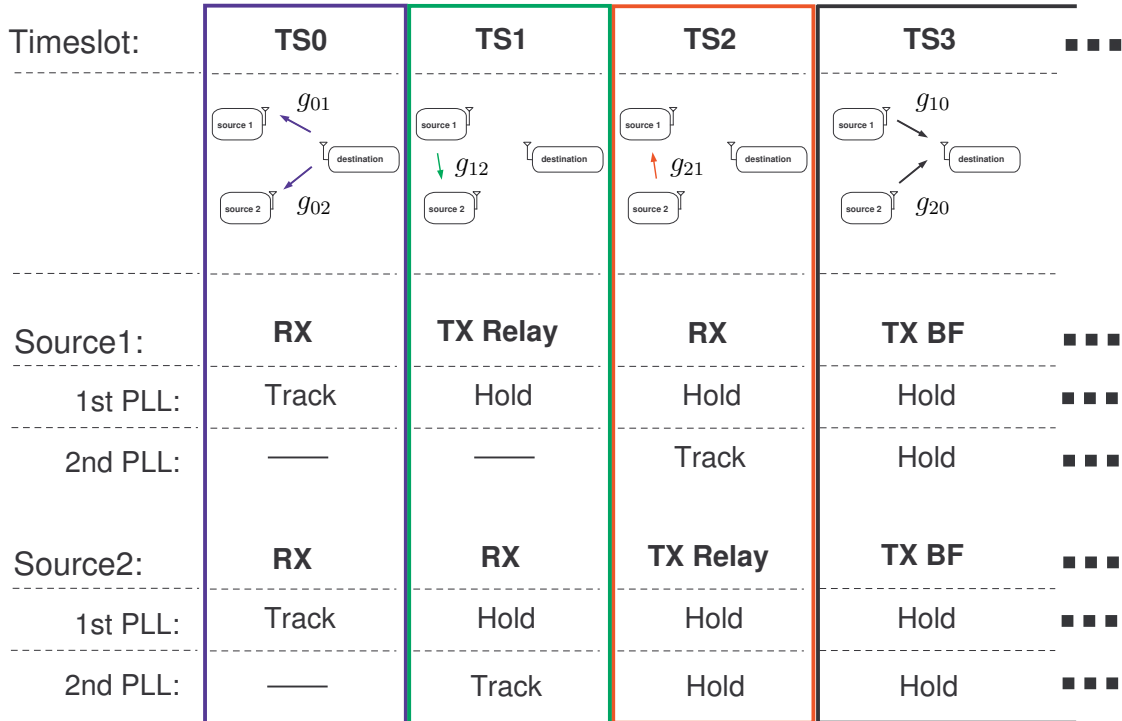


Figure 3.1: Round-trip time-division system model and synchronization protocol.

In the first timeslot, denoted as TS0, the destination transmits a primary beacon to the two sources and the sources use a primary PLL to lock to the transmission. The two sources then exchange secondary beacons in the next two timeslots, denoted as TS1 and TS2, and use secondary PLLs to lock to the relayed signals. During the last timeslot, both sources simultaneously transmit to realize a beamformer in the direction of the destination. Like the RTFS method, the beamformer transmissions of the RTTD system arrive coherently at the destination because the propagation

delay in each round-trip circuit is the same, and the sources use PLLs to precisely control their relaying latencies. A block diagram of the source node realization for the RTTD synchronization method is shown in Figure 3.2. The sources are realized with the primary and secondary PLLs, control logic, and source-specific knowledge about the synchronization protocol shown in Figure 3.1.

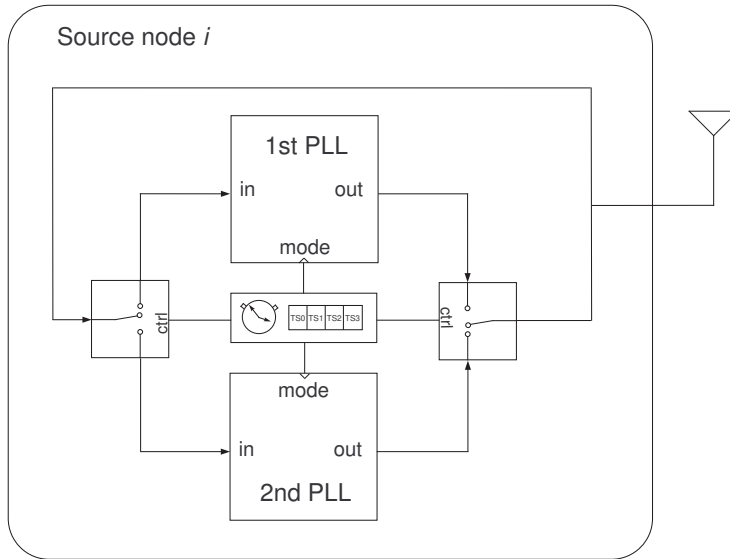


Figure 3.2: Round-trip time-division source block diagram.

To facilitate a discussion of the basic operating principles of the RTTD system in further detail, any type of propagation delay in the channels is temporarily ignored. Chapters 4 and 5 investigate the performance of the RTTD system when propagation delays are considered. In addition, it is temporarily assumed that the source PLLs obtain perfect lock and their outputs equal their inputs in frequency and phase.

The synchronization process begins with the destination transmitting a primary beacon signal  $x(t) = \sin(\omega_c t + \theta_c)$  to the two sources for the duration of timeslot TS0. It is assumed that the timeslot duration, denoted as  $T_{sync}$ , is fixed for all synchronization timeslots. The two sources simultaneously track the primary beacon during timeslot TS0 using their primary PLLs. At the end of TS0, the output of

each primary PLL is equal to the primary beacon in frequency and phase. In order for the primary PLLs to remain locked to the primary beacon even after the beacon vanishes at the end of TS0, the primary PLLs enter a hold-over mode before TS0 ends. While in hold-over mode, the outputs of each primary PLL are available for transmission during later timeslots (TS1-TS2) even though the primary beacon vanishes at the end of TS0. The implementation of hold-over mode is discussed in detail in Section 3.2.

During timeslot TS1 the primary PLL output of source 1 is relayed to source 2. Source 2 tracks the relayed signal from source 1 using its secondary PLL. At the end of TS1, source 2 transitions its secondary PLL to hold-over mode before the secondary beacon from source 1 vanishes.

During timeslot TS2, source 2 relays a secondary beacon from its primary PLL output to source 1. Source 1 uses its secondary PLL to track the relayed signal. Once the secondary PLL of source 1 has achieved lock and before TS2 ends, it makes the transition to hold-over mode. At the end of TS2, the two sources have both of their PLLs in hold-over mode, the PLL outputs are locked to the appropriate phase and frequency, and the sources are ready to realize a beamformer during the final timeslot TS3.

During timeslot TS3, the sources simultaneously transmit carrier waveforms from the outputs of their secondary PLLs. These transmissions are received by the destination and are given by

$$r_{s2}(t) = x(t - \Delta_1 - \Delta_2) \quad (3.1)$$

$$r_{s1}(t) = x(t - \Delta_2 - \Delta_1) \quad (3.2)$$

where  $\Delta_i$  is the relaying latency of the  $i^{\text{th}}$  source. The transmissions will coherently

combine at the destination so long as the relaying latencies of the sources are small. In the implementation of the RTTD system considered in this thesis, they are strictly controlled by using PLLs. The received signal is expressed by

$$r(t) = a_1 \cos(\omega_{c1}t + \phi_1) + a_2 \cos(\omega_{c2}t + \phi_2) \quad (3.3)$$

where  $\phi_i$ ,  $a_i$ , and  $\omega_{ci}$  are the received phase, amplitude, and frequency, respectively, of the carrier signal from the  $i^{\text{th}}$  source. Assuming that the source PLLs obtain perfect lock with their inputs during the synchronization protocol and that the relaying latencies are strictly controlled, the power in the received signal, given by (2.5), is maximized. Error due to inaccurate lock and channel effects, however, cause the beamformer quality to decrease.

The source PLLs may not exactly lock to the frequency and phase of their input signal. The VCO control signals may have error due to noise, residual convergence offsets of the PLL (also referred to as "gross-transient effects" in this thesis), and high-frequency feedthrough produced by the phase detector and not fully suppressed by the loop filter. As a result, there may be phase and frequency error in the PLL outputs in hold-over mode, and consequently between the two beamforming transmissions at the destination during timeslot TS3. A phase error between the carrier waveforms causes the received power (given by (2.5)) to be less than the maximum achievable amount, and a frequency error causes the waveforms to drift out of phase. The amount of phase and frequency error is reduced by attenuating the high-frequency feedthrough and noise as much as possible while allowing the VCO control signal to converge to its proper locked-state value within the timeslot duration  $T_{sync}$ . Designing the PLLs to achieve this is considered in Section 3.2.

The beamformer quality over the TS3 timeslot depends on channel conditions and the ability of the RTTD system to provide a small phase and frequency error at the start of TS3. When the beamformer eventually drifts out of phase, the synchronization sequence performed over the TS0-TS2 timeslots can be executed again to resynchronize the sources. The next section considers specific requirements of the RTTD sources and purposes a PLL design methodology unique to the RTTD distributed beamforming method.

## 3.2 RTTD Source Node Design Considerations

The source node realization of Figure 3.2 is described in detail in this section. Assumptions regarding the sources' ability are outlined and the implementation of hold-over mode is presented. A methodology for designing the RTTD system PLLs is purposed and a specific PLL implementation is chosen. For the chosen PLL implementation, a design example is provided in order to show how one can establish a guideline for choosing the closed loop bandwidth of the source PLLs based on knowledge of the timeslot duration  $T_{sync}$ . The guideline will serve as a design tool for realizing the RTTD sources such that they are able to guarantee a minimum duration of beamforming, and provide longer durations of beamforming on average.

### 3.2.1 Source Requirements and PLL Design Methodology

To avoid transmission collision and to ensure that the sources control signal routing appropriately, the following assumptions regarding the sources' knowledge and inherent ability are made:

- *Assumption 1*: It is assumed that the sources have knowledge of which source they are (1 or 2) and what schedule they are to follow.
- *Assumption 2*: It is assumed that the sources can detect the start of transmissions perfectly.

These assumptions are necessary in order for the sources to execute the schedules of Figure 3.1. *Assumption 2* is of particular importance because accurate timing of the timeslot duration is needed in order for the sources to transition to hold-over mode before the timeslot ends. The transition to hold-over mode must be executed before the input signal vanishes in order to avoid an inaccurate lock. With knowledge of the schedules and timeslot duration, and the ability to detect the start of transmissions accurately, the sources are able to ensure that the PLLs lock to the appropriate signal and then enter hold-over at the correct time.

The RTTD sources are required to implement a PLL hold-over mode that ensures that the PLLs remain locked to a certain phase and frequency. The implementation of the PLL hold-over mode is straightforward. The VCO control signal,  $U_{ctrl}(t)$ , is captured upon entering hold-over mode and it is held constant for the remainder of the synchronization process and until the sources are resynchronized. Hence, the VCO output frequency of the PLLs remains constant as expressed by

$$\omega_{out} = \omega_q + K_0 U_{ctrl}(T_{hold}), \quad (3.4)$$

for  $t \geq T_{hold}$ , where  $T_{hold}$  is the time at which hold-over begins. As Figure 3.3 shows, the transition to hold-over mode always occurs at the end of the timeslot, i.e.  $T_{hold} \approx T_{sync}$ . This is a reasonable assumption because it ensures that transmission energy is not wasted. Figure 3.3 illustrates only an arbitrary example of a PLL control signal behavior, however, because the control signal behavior of a PLL has a statistical nature. The behavior depends on the initial phase and frequency of the input signal, the VCO output initial phase and frequency, and the design of the PLL. Hence, the error introduced into (3.4), caused by the gross-transient convergence and high-frequency feedthrough behavior of the PLL, also has a statistical nature.

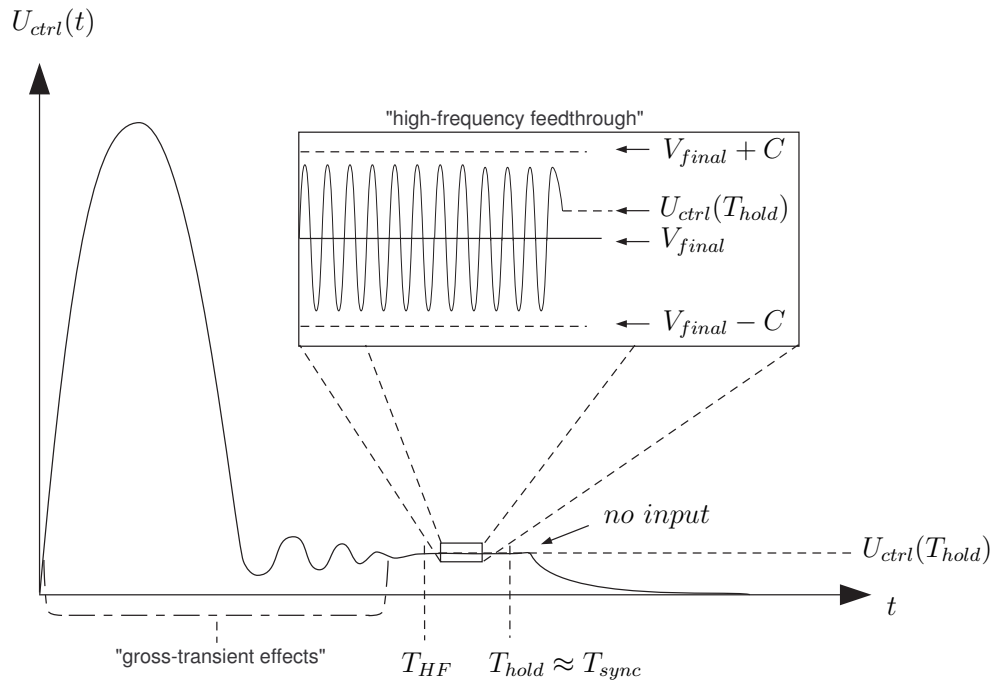


Figure 3.3: Example of the transition to the PLL hold-over mode. The control signal  $U_{ctrl}(t)$  is captured before the input signal vanishes and where the high-frequency feedthrough, with magnitude  $K_d|F(2\omega_c)|$ , is the dominant source of error ( $t \geq T_{HF}$ ). The PLL holds  $U_{ctrl}(T_{hold})$  for the remainder of the synchronization process, or until the sources are resynchronized.

The approach used in this thesis is that the RTTD system PLLs should be designed in such a way that the worst-case frequency error in (3.4) is explicitly known with high confidence. This methodology for designing the PLLs was chosen because in cases when the worst-case frequency error in the PLL outputs is known, a minimum beamformer duration is guaranteed. With knowledge of a guaranteed minimum beamformer duration, the RTTD sources can resynchronize without notification from the destination that the beamformer quality has decreased below an acceptable threshold. The beamformer duration is predictable and reliable when designing the RTTD sources using this methodology.

As illustrated in Figure 3.3, error in (3.4) is caused by the gross-transient and high-frequency feedthrough behavior of the PLL control signal. There is a greater potential error when gross-transient effects are present in the control signal, but when the control signal has converged such that the high-frequency feedthrough is the dominant source of error, the potential error is reduced significantly and remains constant while the input signal is present. Hence, in an attempt to reduce the potential error in the transition to hold-over mode, while maintaining the ability to precisely calculate the worst-case possible frequency error, the RTTD system PLLs are designed in such a way that the dominant source of error at the end of the timeslot is due to high-frequency feedthrough. No explicit description of PLL control signal behavior at any given time (including the time-to-lock approximation  $T_L$ ) is provided in [16], so the time at which high-frequency feedthrough begins to dominate the behavior of a PLL control signal is defined in this thesis by

$$T_{HF} = \min \gamma > 0 \text{ s.t. } |U_{ctrl}(t) - V_{final}| < C \quad \forall t \geq \gamma, \quad (3.5)$$

where  $V_{final} = \frac{\omega_c - \omega_q}{K_o}$  and is the DC offset of the control signal  $U_{ctrl}(t)$  in the locked state, and the threshold  $C$  is a voltage that is chosen to be double the magnitude of the high-frequency feedthrough, i.e.,  $C = 2K_d|F(2\omega_c)|$ . When the threshold is twice the magnitude of the high-frequency feedthrough, the error caused by the gross-transient behavior must be no larger than the magnitude of the high-frequency feedthrough in order for the control signal voltage level  $U_{ctrl}(t)$  to be less than the threshold  $C$ . Hence, the high-frequency feedthrough is considered to be the “dominant” source of error for  $t \geq T_{HF}$ .

The design of the RTTD system PLLs should accommodate the statistical nature of  $T_{HF}$  so that the dominant source of error in the transition to holdover mode is most likely due to high-frequency feedthrough, i.e., with 99% confidence,  $P(T_{HF} \leq T_{sync}) = 0.99$ . Designing the PLLs in this way ensures that the worst-case frequency error is known in (3.4) because it is nearly certain that the error in the control signal magnitude is less than the threshold  $C$ . A higher confidence level could be used, but this would cause additional error in the PLL outputs due to an increased high-frequency feedthrough magnitude. Using a higher confidence level would lead to a more pessimistic view of the RTTD system’s performance. For any confidence level, the same design tradeoffs pertaining to the RTTD system are exposed. Hence, designing the PLLs in this manner is reasonable in that it provides enough confidence that the worst-case error is explicitly known, but it is not so strict that it yields results that are too pessimistic of the RTTD system’s performance. This is investigated further in Section 3.2.3. Section 3.2.3 also demonstrates a PLL design example and shows how a guideline can be established for choosing the closed loop bandwidth  $\omega_{3dB}$  of the RTTD PLLs based on knowledge of the timeslot duration  $T_{sync}$ . In order to do this, however, a specific PLL implementation is selected in the next section.

### 3.2.2 RTTD Source PLL Implementation

The PLLs implemented in this thesis use a multiplier phase detector and a 2nd-order active PI loop filter. The RTTD system does not require any specific implementation, but these choices are satisfactory for the reasons discussed in the remainder of this section.

The multiplier phase detector is chosen because it only produces a single high frequency feedthrough term compared to the multiple harmonics produced by the other phase detectors. This simplifies the analysis, but in general, the multiplier phase detector will expose the same trade-offs as other phase detectors would in designing the PLLs for the RTTD system. With this choice of phase detector, the phase detector gain<sup>1</sup> is  $K_d = \frac{a_{in}a_{out}}{2}$ . The VCO gain of the RTTD PLLs is set to  $K_o = 2\pi \times 10^5$  rad/s·V in this thesis.

The 2nd-order active PI loop filter of the form given by

$$F(s) = \frac{1 + s(\alpha_2)}{s\alpha_1(1 + s\alpha_3)}, \quad (3.6)$$

is chosen because it offers infinite DC gain and the 2nd-order implementation helps to attenuate high frequency feedthrough. It is important that the loop filter has infinite DC gain because the VCO free-running frequencies may not be precisely tuned to the input frequency<sup>2</sup>. In this case, the PLL must generate a non-zero mean control signal at the output of the loop filter in order to drive the VCO to the desired frequency. The infinite DC gain of the loop filter allows the mean phase detector output to be zero in the locked state, but a non-zero mean control signal is still generated to compensate for the frequency offset. A higher order loop filter would provide even more high-frequency feedthrough attenuation, but loop

---

<sup>1</sup> $a_{in}$  and  $a_{out}$  are the amplitudes of the PLL input and output.

<sup>2</sup>This concept is analyzed in greater detail in [15]

stability becomes more of an issue [16]. Hence, the 2nd-order implementation is chosen because it offers some attenuation of high-frequency feedthrough, but loop instability is not of concern. With this choice of loop filter, the magnitude of the high frequency feedthrough in the PLLs, which is derived in Appendix A, can be expressed by

$$K_d|F(2\omega_c)| = \frac{a_{in}a_{out}|F(2\omega_c)|}{2} = \frac{\omega_{3dB}}{K_o} \frac{(\frac{\omega_{3dB}}{\omega_c})^2 + 2c_1c_2(\frac{\omega_{3dB}}{\omega_c})}{4c_2^3 + 2c_2^2c_1(\frac{\omega_{3dB}}{\omega_c})}, \quad (3.7)$$

where  $c_1$  and  $c_2$  are scaling factors used in the PLL design process outlined in [16] and are equal to  $\sqrt{10}$  and 1.33, respectively. The PLL design guidelines outlined in [16] also give direction as to how to choose the filter coefficients  $\alpha_1$ ,  $\alpha_2$ , and  $\alpha_3$  of (3.6), which are derived from the corner frequencies of the loop filter shown in Figure 3.4. The guidelines in [16] use the scaling factors  $c_1$  and  $c_2$  to derive the corner frequencies of the loop filter from the closed loop bandwidth  $\omega_{3dB}$ .

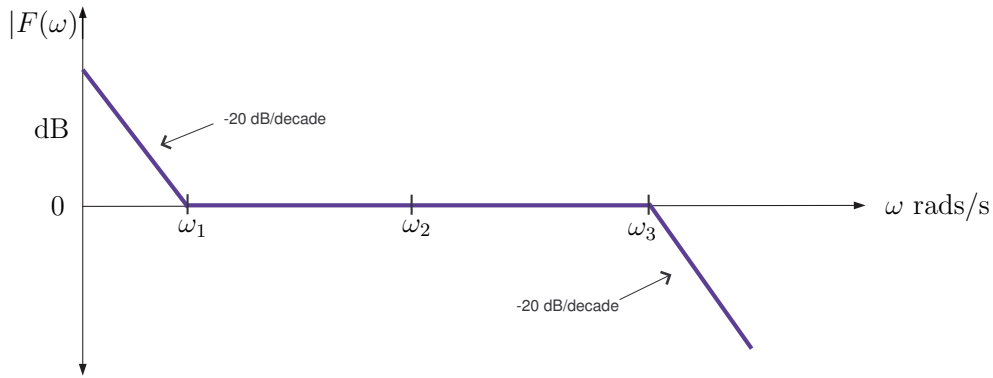


Figure 3.4: Bode diagram of 2nd-order active PI loop filter.

While guidelines for choosing the filter parameters are given in [16], they assume that the designer has a sense of what PLL closed loop bandwidth  $\omega_{3dB}$  is needed for their specific application. It is known from Section 3.2.1 that the RTTD system PLLs should be designed such that  $P(T_{HF} \leq T_{sync}) = 0.99$ , but it is unknown for a

given  $T_{sync}$  how  $\omega_{3dB}$  should be chosen to ensure that this happens. The following section demonstrates how one would find a suitable PLL design for the RTTD system when given knowledge of the timeslot duration  $T_{sync}$ .

### 3.2.3 RTTD Source PLL Design Guideline

The main objective of this section is to demonstrate how a guideline can be established for choosing the closed loop bandwidth of the RTTD system PLLs such that the PLL design methodology outlined in Section 3.2.1 is satisfied. The guideline established in this section is only valid for the PLL implementation outlined in Section 3.2.2, but the process to derive the guideline can be reproduced for other implementations. As discussed in Section 3.2.1, the PLLs of the RTTD system are designed in such a way that  $P(T_{HF} \leq T_{sync}) = 0.99$ . Designing the PLLs in this way ensures that the worst-case frequency error in the PLL outputs is known with high confidence. Hence, the following question is addressed in this section: What should the closed loop bandwidth  $\omega_{3dB}$  of the RTTD system PLLs be for a given timeslot duration  $T_{sync}$  to ensure that  $P(T_{HF} \leq T_{sync}) = 0.99$ ?

The closed loop bandwidth that ensures that  $P(T_{HF} \leq T_{sync}) = 0.99$  for a given timeslot duration  $T_{sync}$  is denoted as  $\omega_{3dB_{RTTD}}$ . A poor choice for  $\omega_{3dB}$  increases the amount of potential error in the PLL outputs. Referring to Figure 3.5, if the closed loop bandwidth of the PLLs is too small, i.e.  $\omega_{3dB} < \omega_{3dB_{RTTD}}$  and  $P(T_{HF} \leq T_{sync}) \ll 0.99$ , then it is more likely that gross-transient effects are present at the end of the timeslot. In this case, the potential error is greater and it is difficult to predict. If the closed loop bandwidth of the PLLs is too large, i.e.  $\omega_{3dB} > \omega_{3dB_{RTTD}}$  and  $P(T_{HF} \leq T_{sync}) \gg 0.99$ , then it is almost certain that the high-frequency feedthrough dominates the PLL control signal behavior at the end of the timeslot. In this case, however, the magnitude of the high-frequency feedthrough is

not attenuated as much as it could be, which also causes the potential error in the PLL outputs to be greater. Hence,  $\omega_{3dB}$  should be large enough to nearly eliminate the effects of the gross-transient behavior of the PLLs, but not too large that the magnitude of the high-frequency feedthrough increases, i.e.  $\omega_{3dB} = \omega_{3dB_{RTTD}}$  and  $P(T_{HF} \leq T_{sync}) = 0.99$ .

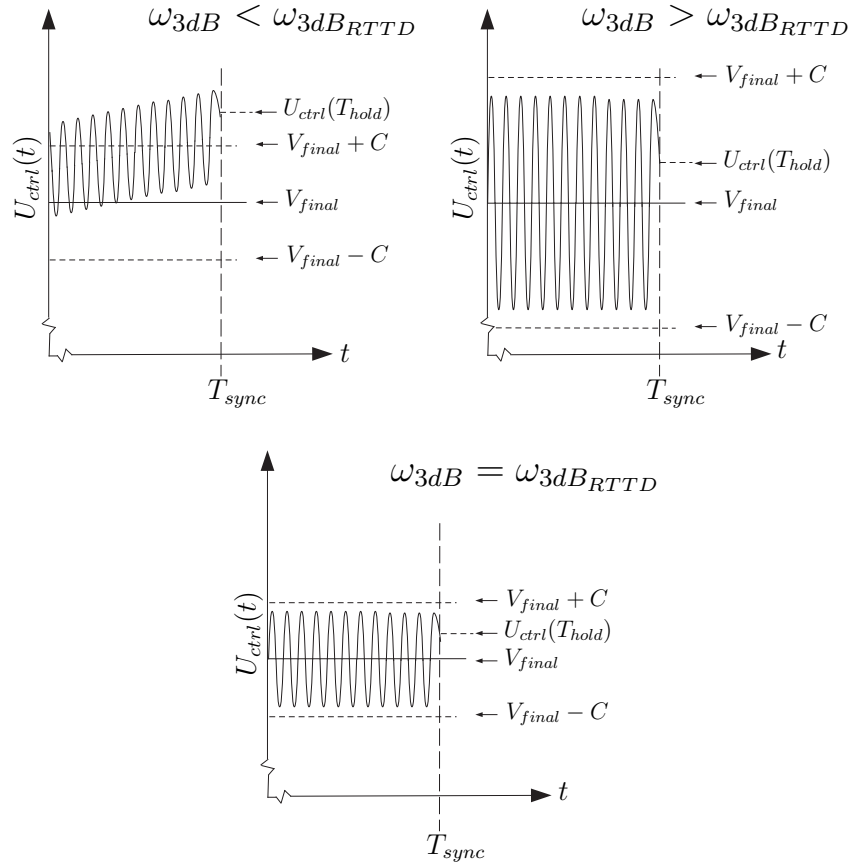


Figure 3.5: Designing the RTTD PLLs with a closed loop bandwidth that is too large or too small leads to increased potential error, and in the case where  $\omega_{3dB} < \omega_{3dB_{RTTD}}$ , the error is unpredictable.

In order to develop a guideline for choosing the PLL closed loop bandwidth  $\omega_{3dB}$  based on knowledge of the timeslot duration  $T_{sync}$  only, a PLL design is selected and simulated over 1000 iterations to find an empirical distribution of  $T_{HF}$  for that

design. The empirical distribution of  $T_{HF}$  is used to find a general relationship between  $\omega_{3dB}$  and  $T_{sync}$ , and thus a guideline for finding  $\omega_{3dB_{RTTD}}$  established.

The PLL simulated to find the results of Figure 3.6 has a closed loop bandwidth of  $\omega_{3dB} = 2\pi 4 \times 10^5$  rads/sec. The frequency of the input carrier signal is  $\omega_c = 2\pi 800 \times 10^6$  rads/sec. The VCO center frequency of the PLL is tuned to the input frequency, but has a randomly generated error of  $\pm 100$  ppm for each iteration. The input phase and initial VCO phase are randomly distributed on  $[-\pi, \pi]$  for each iteration. A histogram of the recorded  $T_{HF}$  values and corresponding cumulative distribution function are plotted in Figure 3.6.

As Figure 3.6 shows, the simulated PLL reaches  $T_{HF}$  before  $t \approx 20$   $\mu$ secs with approximately 99% certainty. With the lack of a design guideline, the designer of the RTTD system PLLs would need to find the PLL closed loop bandwidth of  $\omega_{3dB} = 2\pi 4 \times 10^5$  rads/sec through trial and error when a timeslot duration of  $T_{sync} = 20$   $\mu$ secs is specified. Designing the RTTD system PLLs in such a way would be time consuming and inefficient. Hence, the empirical distribution of  $T_{HF}$  found in Figure 3.6 is used along with the relationship between  $\omega_{3dB}$  and the time-to-lock approximation<sup>3</sup>  $T_L$  to develop a guideline for choosing  $\omega_{3dB}$  based on knowledge of  $T_{sync}$ . The relationship between  $\omega_{3dB}$  and  $T_L$  for the chosen PLL implementation of this thesis is derived in Appendix A and the result is given by

$$T_L \approx \frac{2\pi c_2}{\omega_{3dB} \sqrt{\frac{1}{c_1}}}, \quad (3.8)$$

where  $c_1$  and  $c_2$  are the scaling factors that relate the corner frequencies  $\omega_2$  and  $\omega_3$  of the loop filter to the frequency where the open-loop gain is 1, denoted as  $\omega_T$ . These are set to  $\sqrt{10}$  and 1.33 in [16], respectively. The time-to-lock approximation

---

<sup>3</sup>The time-to-lock approximation was reviewed in Section 2.4.

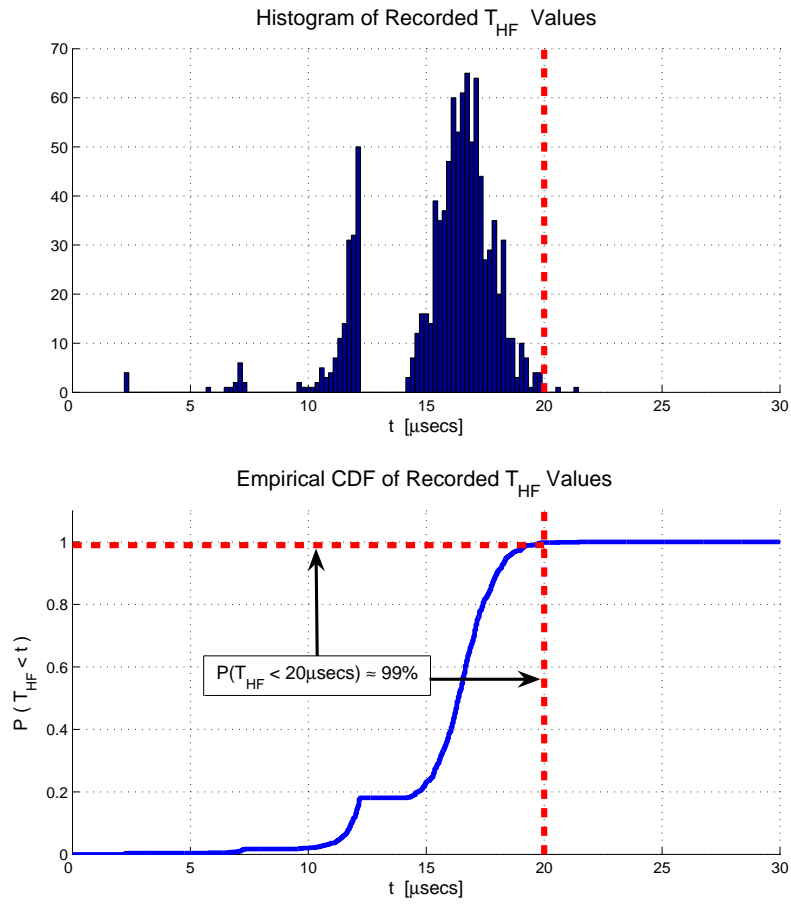


Figure 3.6: Histogram and empirical cumulative distribution function of recorded  $T_{HF}$  values of a simulated PLL which has a closed loop bandwidth of  $\omega_{3dB} = 2\pi 4 \times 10^5$  rads/sec.

for the simulated PLL is found from (3.8) to be  $T_L \approx 6 \mu\text{secs}$ . Comparing the time-to-lock approximation to the timeslot duration  $T_{sync} = 20 \mu\text{secs}$ , it is found that the time-to-lock approximation is  $T_L = 0.3T_{sync}$ . The guideline for choosing  $\omega_{3dB}$  is found by substituting  $T_L$  with  $0.3T_{sync}$  in (3.8), and then solving for  $\omega_{3dB}$ . The resultant guideline can be expressed by

$$\omega_{3dB_{RTTD}} \approx \frac{2\pi c_2}{0.3T_{sync}\sqrt{\frac{1}{c_1}}}, \quad (3.9)$$

where  $\omega_{3dB_{RTTD}}$  is the PLL closed loop bandwidth for the RTTD system PLLs which satisfies the design methodology outlined in Section 3.2.1. This guideline is only valid for the PLL implementation outlined in Section 3.2.2. This guideline cannot be used for other PLL implementations that use other types of loop filters, different VCO gains, and it is only valid for PLL implementations that follow the guidelines outlined in ([16]).

To verify that this guideline is suitable for finding  $\omega_{3dB_{RTTD}}$  for the values of  $T_{sync}$  considered in this thesis, a PLL which has a closed loop bandwidth of  $\omega_{3dB} = 2\pi \times 10^5$  rads/sec is simulated over 1000 iterations (increased by a factor of 2 compared to the PLL design simulated in Figure 3.6). The results shown in Figure 3.7 suggest that the guideline expressed in (3.9) is suitable for finding  $\omega_{3dB_{RTTD}}$  for the timeslot durations considered in this thesis, but this is not a conclusive proof. The relationship between  $T_L$  and  $T_{sync}$  remained the same for both timeslot durations considered, i.e.  $T_L = 0.3T_{sync}$ . The PLL closed loop bandwidth is inversely proportional to  $T_L$  and  $T_{sync}$ .

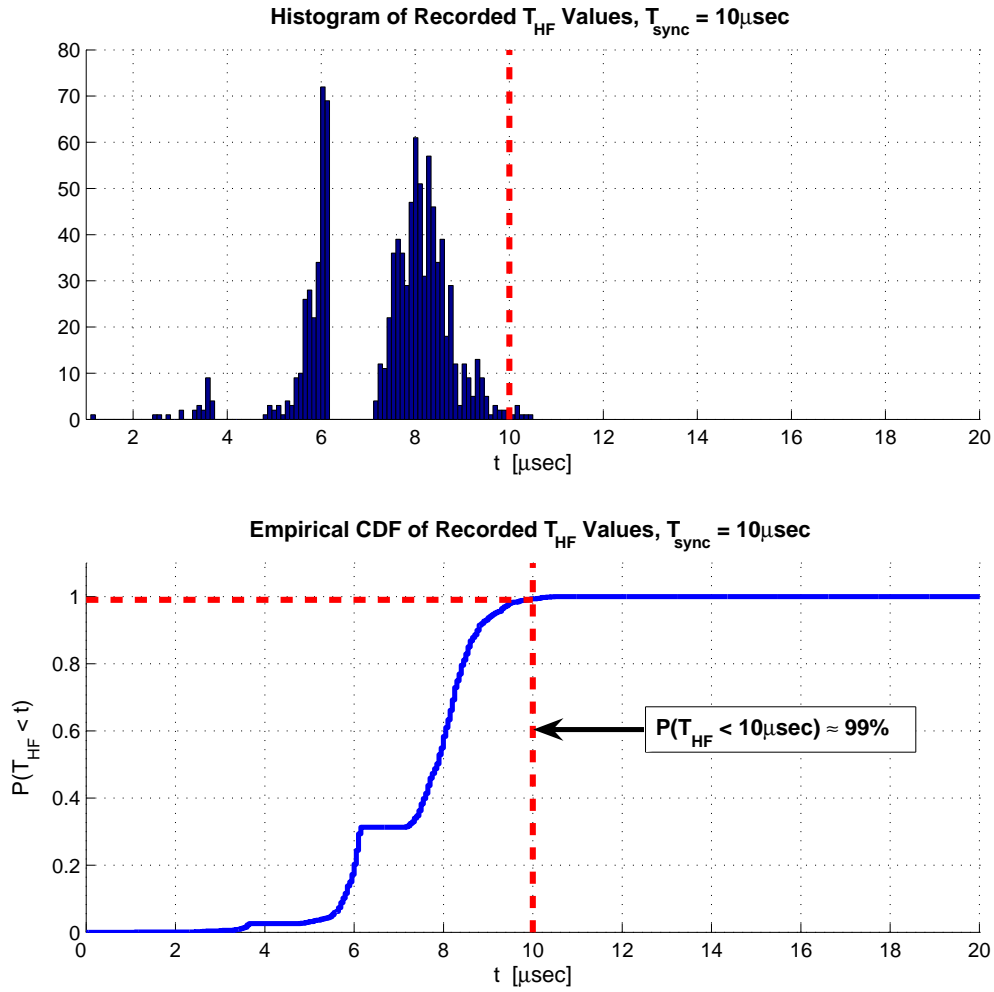


Figure 3.7: Histogram and empirical cumulative distribution function of recorded  $T_{HF}$  values of a simulated PLL which has a closed loop bandwidth of  $\omega_{3dB} = 2\pi 8 \times 10^5$  rads/sec. The PLL reaches  $T_{HF}$  before the timeslot duration  $T_{sync} = 10 \mu\text{sec}$  with 99% confidence, so these results suggest that the guideline expressed in (3.9) is suitable for finding  $\omega_{3dBRTD}$  for the timeslot durations consider in this thesis.

To show that the design methodology outlined in Section 3.2.1, and executed in this section, is a reasonable method for designing the PLLs of the RTTD system, several PLL designs are simulated 1000 iterations and the frequency error at  $t = T_{sync} = 20 \mu\text{secs}$  is found. The mean-squared frequency error,  $E[(\omega_c - \omega_q)^2]$ , is plotted versus  $\omega_{3dB}$  in Figure 3.8.

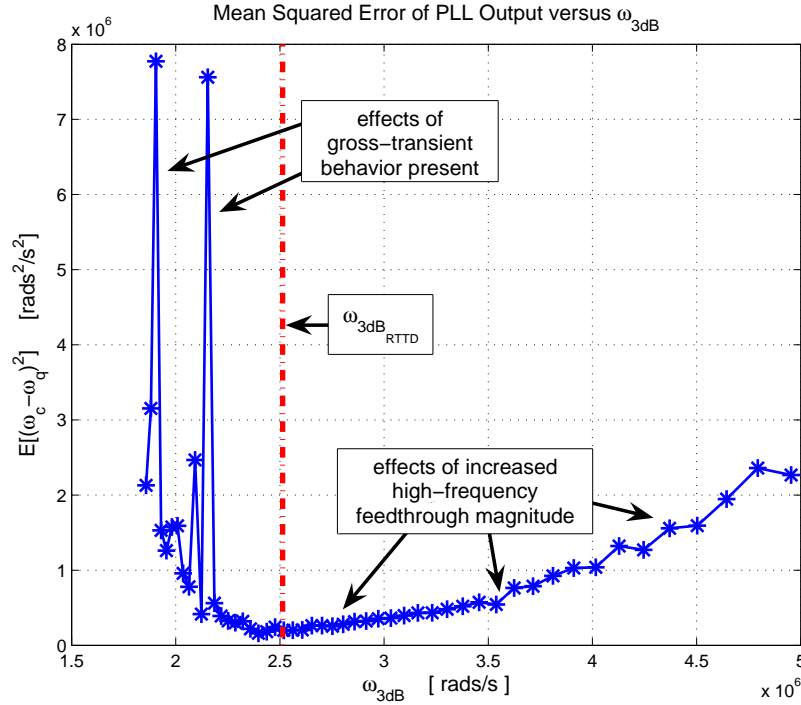


Figure 3.8: Mean-squared frequency error,  $E[(\omega_c - \omega_q)^2]$ , plotted versus PLL closed loop bandwidth  $\omega_{3dB}$ .

The results of Figure 3.8 show that the design methodology used in this thesis for designing the RTTD system PLLs is a reasonable approach in that it reduces the potential error in the PLL outputs such that the good performance of the RTTD system can be highlighted, but it also guarantees a minimum beamformer duration with 99% confidence. The performance of the RTTD system in time-invariant channels is investigated in Chapter 4.

# Chapter 4

## RTTD Distributed Beamforming in Time Invariant Channels

The performance of the RTTD system is investigated when the channels are modeled as single-path and multi-path time-invariant channels. The effects of these channels on the RTTD synchronization protocol are considered, and the synchronization overhead in the system is quantified analytically in each case. Also in this chapter, a performance measure is derived which takes into account the duration of the beamformer and the synchronization overhead needed to accomplish acceptable beamformer quality. The effects of the source PLL design on the RTTD system performance is evaluated using simulation results, but these results are for a specific timeslot duration  $T_{sync}$ . In order to investigate the performance of the RTTD system beyond a specific value of  $T_{sync}$ , a worst-case analysis is conducted. This chapter begins by discussing the performance measure that is used to evaluate the RTTD system.

## 4.1 RTTD System Performance Measure

The performance of the RTTD system is evaluated by determining the efficiency of the system, or in other words, the percentage of time that the sources are able to beamform. The RTTD synchronization protocol requires some amount of time to synchronize the RTTD sources in order to realize a beamformer, and the beamformer duration depends on how well the two RTTD sources are synchronized in frequency and phase at the end of timeslot TS2. The time needed to synchronize, denoted as  $T_{OH}$ , is how the synchronization overhead<sup>1</sup> is quantified in the RTTD system. Temporarily ignoring any effects of the channels, the amount of synchronization overhead in the RTTD system is  $T_{OH} = 3T_{sync}$ . The beamformer duration, denoted as  $T_{BF}$ , is how the quality of the beamformer is quantified. The duration of the beamformer is open for interpretation, however, because it depends on how much phase error between the two beamforming transmissions is acceptable. The acceptable received phase error between the two beamforming transmissions at the destination is denoted as  $\Phi_{BF}$ , and it is set to  $\Phi_{BF} = 10^\circ$  in this thesis. The beamformer duration is calculated by

$$T_{BF} = \begin{cases} \left| \frac{\Phi_{BF} + \phi_{r\Delta} \times \text{sgn}(-\omega_{r\Delta})}{\omega_{r\Delta}} \right| & , \text{ for } |\phi_{r\Delta}| < \Phi_{BF} \\ 0 & , \text{ for } |\phi_{r\Delta}| \geq \Phi_{BF}, \end{cases} \quad (4.1)$$

where  $\phi_{r\Delta}$  and  $\omega_{r\Delta}$  are the received phase and frequency error at the start of beamforming, respectively. The beamformer duration is used in conjunction with the synchronization overhead to determine the efficiency of the RTTD system as expressed by

$$R_{BF} = \frac{T_{BF}}{T_{BF} + T_{OH}}. \quad (4.2)$$

---

<sup>1</sup>Synchronization overhead in the RTTD system is discussed in greater detail for each of the time-invariant channel models in Section 4.2 and Section 4.3.

This performance measure was chosen because it encompasses the negative effect of the synchronization overhead in the RTTD system, as well as, the positive benefit of beamforming for some duration of time. The RTTD system synchronization protocol requires that the RTTD sources invest transmission energy and time before they are able to beamform. The resources consumed during synchronization are not utilized effectively unless the achieved beamformer duration is at least greater than the amount of synchronization overhead. This efficiency performance measure will be used in the remaining sections of this chapter to evaluate the RTTD distributed beamforming system for various PLL designs, and for increasing levels of synchronization overhead. The next section investigates the performance of the RTTD distributed beamforming system in single-path time-invariant (SPTI) channels.

## 4.2 RTTD System Operation in SPTI Channels

In this section, the communication channels in the RTTD system are considered to be single-path and time-invariant. The single-path time-invariant (SPTI) channels are modeled with fixed propagation delays and unity gain, i.e.,  $g_{ij} = g_{ji} = g(t - \tau_{ij})$ , where  $ij \in \{01, 02, 12\}$ . The propagation delays in the channels cause a phase/time delay in the sinusoidal transmissions, and the RTTD sources must compensate for the phase delays in order to achieve a beamformer. The effects of SPTI propagation delays on the RTTD synchronization protocol are considered in the next section.

### 4.2.1 SPTI Channel Effects and Synchronization Overhead

Channel propagation delay was not considered when the RTTD distributed beamforming technique was introduced in Section 3.1, so the schedules were shown to be fixed in time with each source starting and ending the same timeslot simultaneously

with the destination. The propagation delays of SPTI channels, however, cause the perception of the schedule to vary with each transmitter in the system. For example, consider Figure 4.1 which shows the effective schedule from the perspective of the destination in three cases: (i)  $\tau_{01} > \tau_{02}$ , (ii)  $\tau_{01} < \tau_{02}$ , and (iii)  $\tau_{01} = \tau_{02}$ . The perspective of the destination is considered because it shows the time needed for the protocol to be executed and the time at which the destination begins to receive the beamformer.

Figure 4.1 shows that the channel propagation delays cause the timeslots to become disconnected in time, and the sources have “down time” when they are neither transmitting nor receiving. The SPTI propagation delays of the channels introduce latency, and the sources must wait for the right time to transmit or receive. Hence, the synchronization protocol is not executed in three timeslot durations. The beginning of the final timeslot TS3 is ambiguous at the destination because the source 2 beamformer transmission is solely received for a short duration before the source 1 transmission is received. The beamformer is not realized, however, until both transmissions are received simultaneously, so the time required to execute the synchronization protocol in SPTI channels is expressed by

$$T_{OH_{SP}} = 3T_{sync} + 2\tau_{01} + 2\tau_{12}. \quad (4.3)$$

The time needed to synchronize in SPTI channels, denoted as  $T_{OH_{SP}}$ , is how the synchronization overhead is quantified for the RTTD system in SPTI channels. Notice that the synchronization overhead in this case is only dependent on the choice of the timeslot duration  $T_{sync}$  and the propagation delays of the SPTI channels. The synchronization overhead increases linearly with  $T_{sync}$ , but increasing the timeslot duration  $T_{sync}$  may allow the PLLs to obtain a tighter lock because a smaller closed loop bandwidth  $\omega_{3dB}$  could be used. A smaller  $\omega_{3dB}$  would result in more high-

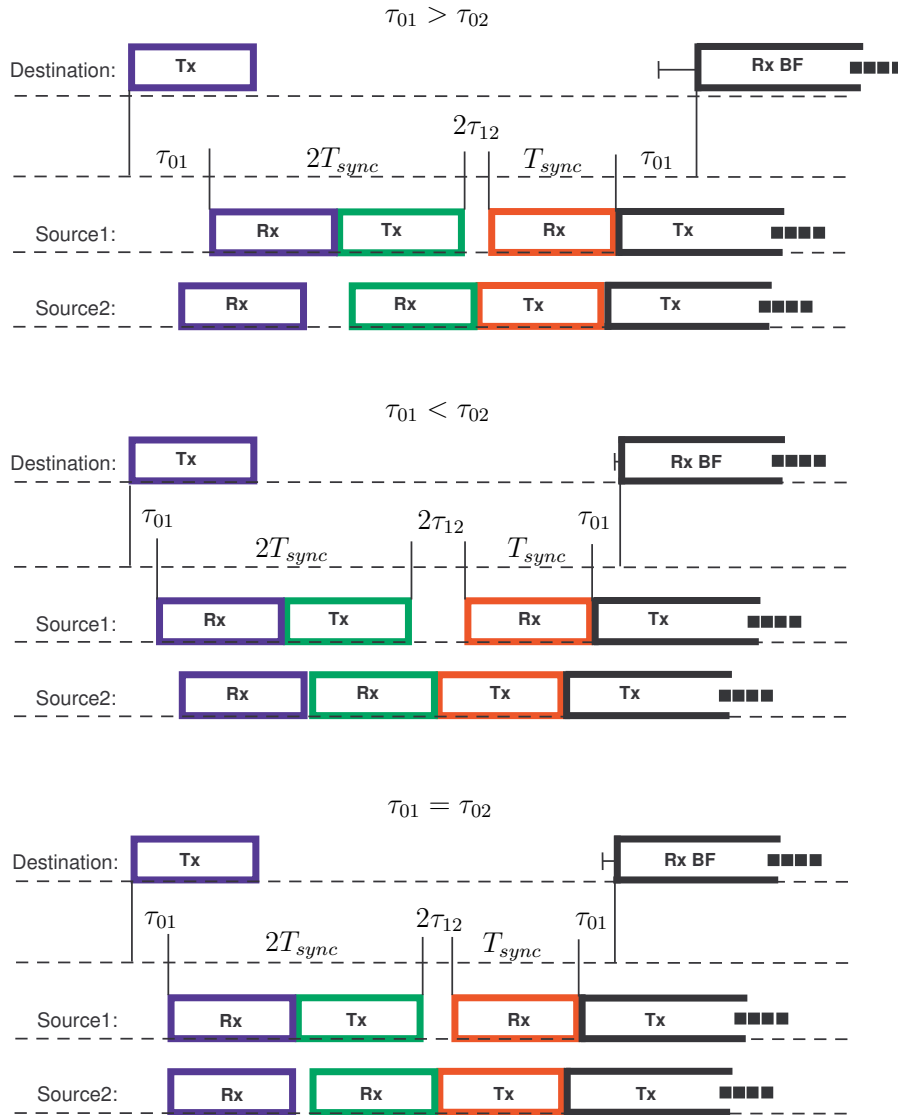


Figure 4.1: Schedule execution in SPTI channels from the perspective of the destination for three cases: (i)  $\tau_{01} > \tau_{02}$ , (ii)  $\tau_{01} < \tau_{02}$ , and (iii)  $\tau_{01} = \tau_{02}$ .

frequency feedthrough attenuation, and thus less frequency and phase error in the PLL outputs. Hence, increasing the timeslot duration  $T_{sync}$  has both a positive and negative effect on the RTTD system performance. The net effect of increasing  $T_{sync}$  will be investigated in Section 4.2.4, but first the effect of the source PLL design on the RTTD system efficiency is investigated for a fixed timeslot duration in the next section.

## 4.2.2 Effects of PLL Design on RTTD System Efficiency

For a fixed level of synchronization overhead, the RTTD system performs better and is more efficient when longer durations of beamforming are achieved. In order to achieve longer beamformer durations, the amount of frequency and phase error at the start of beamforming should be reduced. This is done by designing the RTTD system PLLs with a closed loop bandwidth that reduces the potential error in PLL outputs in their transitions to holdover mode. In addition, as discussed in Section 3.2.1, in order for the RTTD sources to determine when they should resynchronize without feedback from the destination, the worst-case beamformer duration should be explicitly known. Hence, the RTTD system PLLs are designed in such a way that the potential error in the PLL outputs is reduced and the worst-case error is known with high confidence. It was shown in Section 3.2.3 that the potential error due to the gross-transient and high-frequency feedthrough behavior of the PLLs is close to the minimum when the PLLs are designed using the closed loop bandwidth  $\omega_{3dB_{RTTD}}$ . Hence, it is expected that the efficiency of the RTTD system in SPTI channels is close to the maximum when the RTTD system PLLs are designed using  $\omega_{3dB_{RTTD}}$ .

The average efficiency of the RTTD system is found through simulation for several PLL designs with closed loop bandwidths in the range of  $[0.25\omega_{3dB_{RTTD}}, 4\omega_{3dB_{RTTD}}]$ .

The average efficiency for each closed loop bandwidth is taken over 500 simulations of the RTTD system. The channel delays  $\tau_{0j}$  are uniformly distributed on  $[0 \mu\text{sec}, 10 \mu\text{sec}]$  for each iteration, and the inter-source delay is derived using the Law of Cosines and a uniformly distributed angle on  $[0, \pi]$ . The timeslot duration is set to  $T_{sync} = 20 \mu\text{sec}$ .

The PLLs for each closed loop bandwidth are designed by following the guidelines given in [16]. For each design, however, the VCO gain of the PLLs remains constant at  $K_{o_{ij}} = 2\pi \times 10^5$ , and the carrier frequency of the primary beacon remains constant at  $\omega_c = 2\pi 800 \times 10^6$  rads/sec. The PLLs are tuned to the primary beacon, but have a uniformly distributed error of  $\pm 100\text{ppm}$ . The phase of the primary beacon  $\theta_c$  and the phases of the PLL oscillators  $\theta_{q_{ij}}$  are uniformly distributed on  $[-\pi, \pi]$ . The received phase error constraint is set to  $\Phi_{BF} = 10^\circ$ . The average efficiency of the RTTD system is plotted versus  $\omega_{3dB}$  in Figure 4.2.

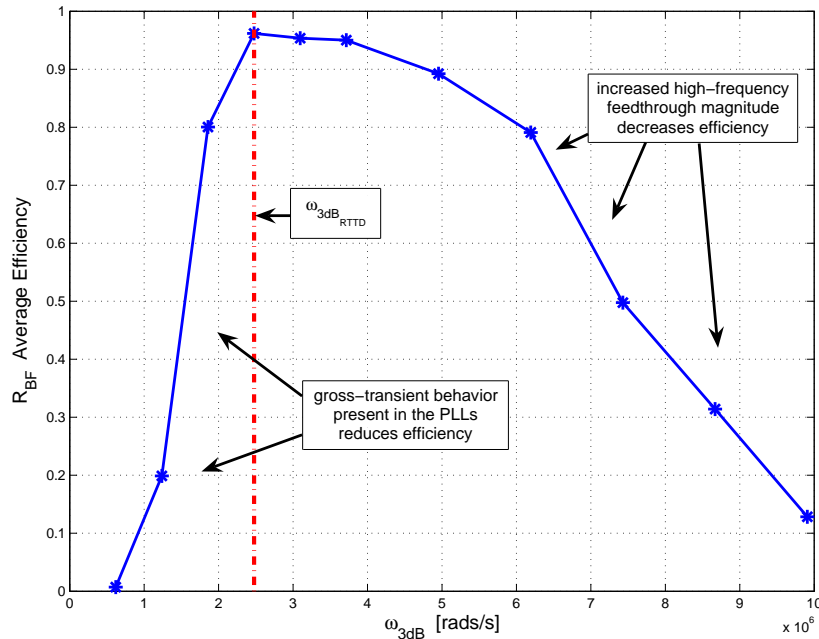


Figure 4.2: Efficiency of the RTTD system versus  $\omega_{3dB}$  for  $T_{sync} = 20 \mu\text{sec}$ .

Figure 4.2 shows that the source PLL design has significant impact on the performance of the RTTD system for a given level of synchronization overhead. It is clear to see in this figure the negative effects of having increased high-frequency feedthrough magnitude or gross-transient behavior in the PLL outputs. For any given timeslot duration  $T_{sync}$ , there is an optimal PLL design that will maximize the average efficiency of the RTTD system. As seen in Figure 4.2, the average efficiency of the RTTD system appears to be maximized when the PLLs are designed using the recommended closed loop bandwidth  $\omega_{3dB_{RTTD}}$ , but it is uncertain whether this is truly the optimal PLL design. In general, however, these results show that the recommended closed loop bandwidth  $\omega_{3dB_{RTTD}}$  is a reasonable choice for the RTTD system PLLs for a given timeslot duration  $T_{sync}$ .

The results shown in Figure 4.2 demonstrate that the RTTD system is able to achieve a beamformer duration in SPTI channels that merits the resource investments made during synchronization. These results, however, are only valid for  $T_{sync} = 20 \mu\text{sec}$ . To investigate the RTTD system efficiency for other values of  $T_{sync}$ , an analytical expression for the worst-case efficiency of the RTTD system, as a function of  $T_{sync}$ , is derived in the next section for cases when the channels are modeled as single-path and time-invariant. A worst-case analysis is possible because the worst-case frequency and phase error in the PLL outputs is explicitly known when the PLLs designed using  $\omega_{3dB_{RTTD}}$ .

### 4.2.3 Worst-Case Performance Analysis for SPTI Channels

In order to investigate the performance of the RTTD system beyond a specific value of  $T_{sync}$ , an expression for the worst-case efficiency of the RTTD system is derived in this section. For any given timeslot duration  $T_{sync}$ , the RTTD system is least efficient when the achieved beamformer duration is minimized. The worst-case

synchronization overhead level for a given timeslot duration  $T_{sync}$  and SPTI channel delay configuration, however, is given by

$$T_{OH_{SPWC}} = 3T_{sync} + 2\tau_{01_{max}} + 2\tau_{12_{max}}, \quad (4.4)$$

where  $\tau_{ij_{max}}$  is the longest possible propagation delay in the  $g_{ij}$  channel. In order to have a general sense of the worst-case synchronization overhead level without needing to explicitly know the channel delays,  $T_{OH_{SPWC}}$  is approximated by ignoring the channel delay terms in (4.4). The approximation is more accurate for cases when  $T_{sync} \gg \tau_{max}$  and it yields slightly more optimistic results than the actual expression, but the results are independent of the channel delays and the placement of the transmitters. The worst-case synchronization level in SPTI channels is be approximated by

$$T_{OH_{SPWC}} \approx 3T_{sync}. \quad (4.5)$$

Assuming that the designer of the RTTD system always chooses the recommended closed loop bandwidth  $\omega_{3dB_{RTTD}}$  for a given timeslot duration  $T_{sync}$ , an analytical expression for the worst-case beamformer duration can be derived. The worst-case beamformer duration is determined by the worst-case possible frequency and phase error between the two beamforming transmissions at the end of TS2. To understand how each PLL contributes to the worst-case error at the start of beamforming, consider the output frequency of a PLL in the RTTD system given by

$$\omega_{out_{ij}} = \omega_{in} + K_o U_{ctrl_{ij}}(t), \quad (4.6)$$

If the PLL is designed using  $\omega_{3dB_{RTTD}}$ , then the worst-case frequency error at the PLL output occurs when the captured VCO control signal is  $U_{ctrl_{ij}}(T_{hold}) = V_{final_{ij}} \pm$

$C$ . Hence, the worst-case frequency error in the PLL output, with 99% confidence can be expressed by

$$|\omega_e| = K_o C, \quad (4.7)$$

where  $C = 2K_d|F(2\omega_c)|$ . One example that yields the worst-case frequency and phase error at the start of beamforming is when the captured VCO control signals of the PLLs in the  $D \rightarrow S1 \rightarrow S2 \rightarrow D$  circuit are equal to  $V_{final_{ij}} + C$ , and the captured VCO controls signals of the PLLs in the  $D \rightarrow S2 \rightarrow S1 \rightarrow D$  circuit are equal to  $V_{final_{ij}} - C$ . The frequency of each PLL in this example can be expressed by

$$\omega_{out_{11}} = \omega_c + \omega_e, \quad (4.8)$$

$$\omega_{out_{21}} = \omega_c - \omega_e, \quad (4.9)$$

$$\omega_{out_{12}} = \omega_{out_{21}} - \omega_e, \text{ and} \quad (4.10)$$

$$\omega_{out_{22}} = \omega_{out_{11}} + \omega_e. \quad (4.11)$$

The worst-case frequency error at the start of beamforming is found by taking the difference between  $\omega_{out_{22}}$  and  $\omega_{out_{12}}$ , as expressed by

$$\begin{aligned} \omega_{BF_{SP}} &= (\omega_{out_{11}} + \omega_e) - (\omega_{out_{21}} - \omega_e) \\ &= (\omega_c + \omega_e + \omega_e) - (\omega_c - \omega_e - \omega_e) \\ &= 4K_o C. \end{aligned} \quad (4.12)$$

In addition to frequency error at the start of beamforming, there is an initial phase error between the beamforming transmissions. The phase error accumulates during the synchronization protocol due to inaccurate frequency lock of the PLLs as seen in Figure 4.3.

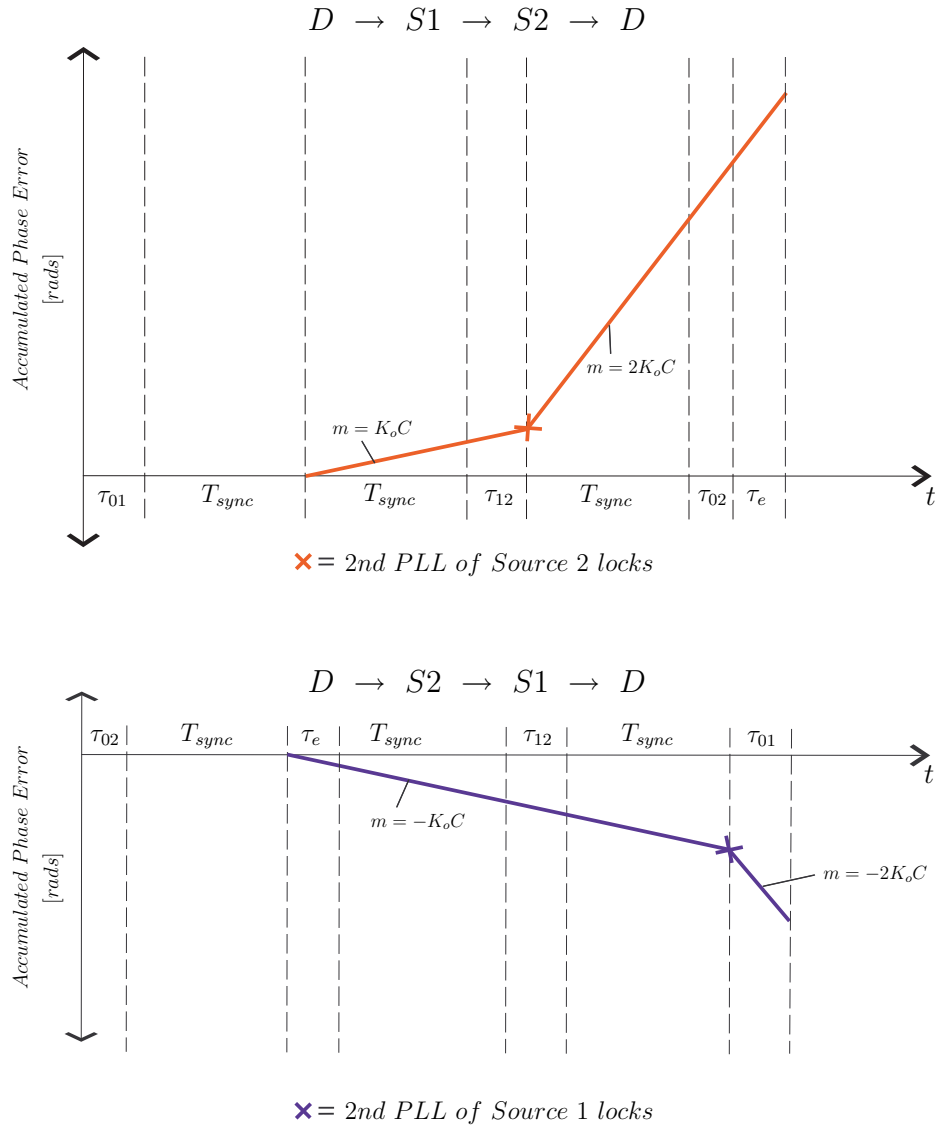


Figure 4.3: Phase error accumulation in each round-trip circuit during the synchronization protocol. The arrival delay between the beamformer transmissions at the destination is denoted as  $\tau_e$  and is calculated by  $\tau_e = \tau_{01} - \tau_{02} + \tau_{12}$ .

As shown in Figure 4.3, the accumulated phase error during the synchronization process in the  $D \rightarrow S2 \rightarrow S1 \rightarrow D$  circuit is

$$\theta_{e_1} = -K_o C(\tau_e + T_{sync} + \tau_{12} + T_{sync}) - 2K_o C\tau_{01}, \quad (4.13)$$

where  $\tau_e = \tau_{01} - \tau_{02} + \tau_{12}$ , and is the arrival delay between the beamformer transmissions at the destination. The accumulated phase error in the  $D \rightarrow S1 \rightarrow S2 \rightarrow D$  circuit is given by

$$\theta_{e_2} = K_o C(T_{sync} + \tau_{12}) + 2K_o C(T_{sync} + \tau_{02} + \tau_e). \quad (4.14)$$

The worst-case initial phase error at the start of beamforming is found by calculating the difference between  $\theta_{e_2}$  and  $\theta_{e_1}$  for  $\tau_{ij} = \tau_{ij_{max}}$  as expressed by

$$\begin{aligned} \phi_{BF_{SP}} &= \theta_{e_2} - \theta_{e_1} \\ &= 5K_o C T_{sync} + 5K_o C \tau_{01_{max}} - K_o C \tau_{02_{max}} + 5K_o C \tau_{12_{max}}. \end{aligned} \quad (4.15)$$

Similar to the worst-case synchronization overhead level approximation, the worst-case phase error at the start of beamforming can be approximated. The approximation will be more optimistic than the true worst-case phase error, and will be more accurate for cases when  $T_{sync} \gg \tau_{max}$ , but the approximation yields results that are independent of the channel delays and transmitter placement. The approximation for the worst-case phase error at the start of beamforming is given by

$$\phi_{BF_{SP}} \approx 5K_o C T_{sync} \approx 10K_o K_d |F(2\omega_c)| T_{sync}. \quad (4.16)$$

The worst-case beamformer duration is found by calculating the earliest possible time at which the beamforming transmissions could exceed the phase constraint  $\Phi_{BF}$ . Substituting the worst-case phase and frequency error expressions into the beamformer duration expression in (4.1) yields the worst-case beamformer duration expression

$$T_{BF_{SP}} = \frac{\Phi_{BF} - \phi_{BF_{SP}}}{\omega_{BF_{SP}}} \approx \frac{\Phi_{BF} - 10K_oK_d|F(2\omega_c)|T_{sync}}{8K_oK_d|F(2\omega_c)|}. \quad (4.17)$$

The worst-case efficiency of the RTTD system in SPTI channels is then calculated by substituting (4.17) and (4.4) into the efficiency expression given in (4.2). The worst-case efficiency of the RTTD system in SPTI channels is given by

$$R_{BF_{SP}} = \frac{T_{BF_{SP}}}{T_{BF_{SP}} + T_{OH_{SPWC}}} \approx \frac{\Phi_{BF} - 10K_oK_d|F(2\omega_c)|T_{sync}}{\Phi_{BF} + 14K_oK_d|F(2\omega_c)|T_{sync}}. \quad (4.18)$$

The worst-case efficiency  $R_{BF_{SP}}$  is a pessimistic measure of the RTTD system performance. For example, the average efficiency of the RTTD system using a timeslot duration of  $T_{sync} = 20 \mu\text{sec}$ , and with PLLs designed using the recommended  $\omega_{3dB_{RTTD}}$ , was found to be 0.96 in Figure 4.2. The worst-case efficiency, however, is calculated to be 0 because it is possible that the phase error constraint is violated at the start of beamforming. Hence, the worst-case efficiency is most useful for investigating the RTTD system performance in cases when the numerator of (4.18) is greater than zero, i.e.  $10K_oK_d|F(2\omega_c)|T_{sync} < \Phi_{BF}$ . Although the worst-case efficiency of the RTTD system  $R_{BF_{SP}}$  is a pessimistic performance measure, it is used to analytically investigate the performance of the system beyond a specific value of  $T_{sync}$  in the next section.

#### 4.2.4 RTTD System Performance in SPTI Channels

It is ambiguous whether the RTTD system performs better or worst for longer synchronization timeslot durations in SPTI channels. When a longer timeslot duration is used, the RTTD system PLLs can be designed using a smaller  $\omega_{3dB}$ , which reduces the amount of error in the PLL outputs and at the start of beamforming. A longer timeslot duration, however, causes increased synchronization overhead, initial phase error, and latency<sup>2</sup>. To better understand the effect of  $T_{sync}$  on the RTTD system performance, the approximate and actual worst-case efficiency are plotted versus  $T_{sync}$  in Figure 4.4. The average efficiency for a limited number of  $T_{sync}$  values is also shown. The average efficiency is taken over 500 simulations of the RTTD system.

As seen in Figure 4.4, the approximations for worst-case synchronization overhead and initial phase error yield more optimistic results than the actual worst-case efficiency. The approximate worst-case efficiency is more representative of the actual worst-case efficiency for  $T_{sync} \gg \tau_{ijmax}$ , but in general, it gives a sense of how the RTTD system performance changes with  $T_{sync}$  without needing to explicitly know the channel delays.

For  $T_{sync} < 100 \mu\text{sec}$ , the worst-case efficiency is low because the level of synchronization overhead is greater than the worst-case duration of the beamformer  $T_{OHSP} \geq T_{BFSP}$ . The average efficiency of the RTTD system, however, does not fall below 0.5 until  $T_{sync} < 2 \mu\text{sec}$ . While the RTTD system may not be very efficient for shorter timeslot durations, a designer may choose a  $T_{sync}$  in this region to achieve less latency. For longer timeslot durations, Figure 4.4 shows that the worst-case efficiency of the RTTD system in SPTI channels approaches 1. For  $T_{sync} > 1 \text{ msec}$ ,

---

<sup>2</sup>The amount of time between starting the synchronization process and receiving the beamformer transmission.

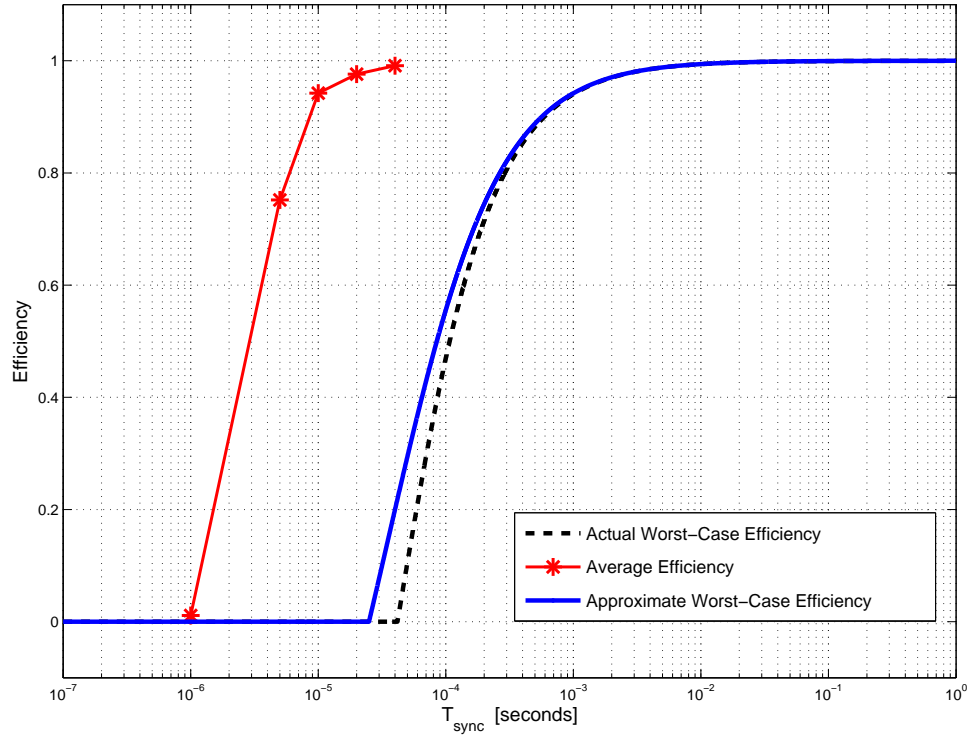


Figure 4.4: Effects of the timeslot duration  $T_{sync}$  on the efficiency of the RTTD system in SPTI channels. The actual worst-case efficiency takes channel delays into account, and the worst-case approximation ignores channel delays and estimates the synchronization overhead by  $T_{OH} \approx 3T_{sync}$ .

however, the increase in worst-case efficiency becomes less significant for larger values of  $T_{sync}$ . Although the overall efficiency of the RTTD system may not increase by a significant amount in this region, a designer may choose a longer timeslot duration to lengthen the beamformer duration. The approximate worst-case beamformer duration is plotted versus  $T_{sync}$  in Figure 4.5 to show that it continues to lengthen with larger values of  $T_{sync}$ .

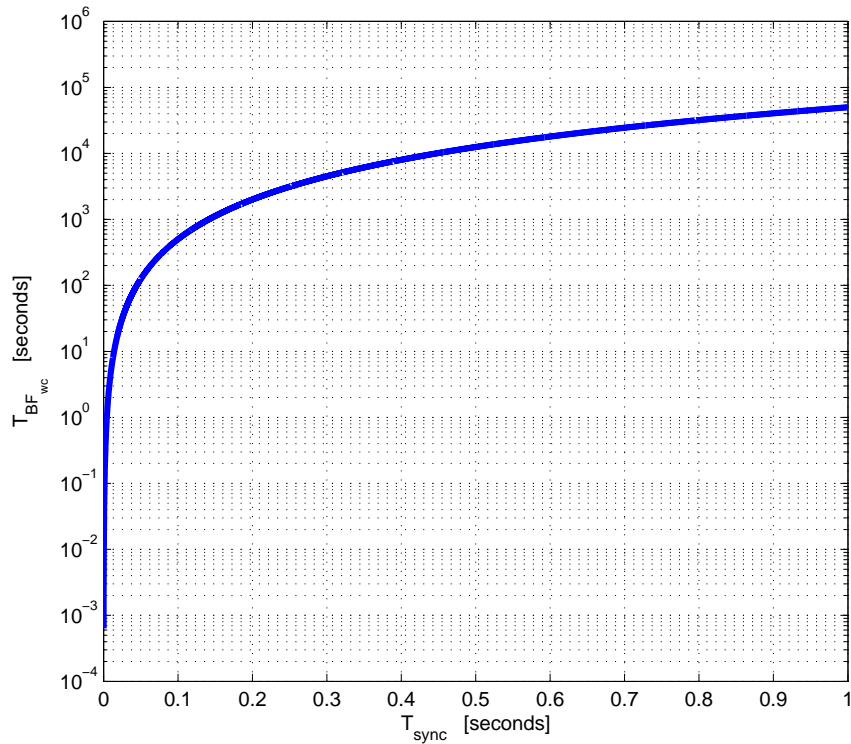


Figure 4.5: Approximate worst-case beamformer duration  $T_{BF_{wc}}$  versus timeslot duration  $T_{sync}$ .

Although the results in this section show that the efficiency of the RTTD system in SPTI channels approaches 1 for larger values of  $T_{sync}$ , these results were found using ideal PLLs. The only cause of frequency and phase error considered was the transient effects of the VCO control signals. As  $T_{sync}$  increases, the closed loop bandwidth of the PLLs reduces and the error in the VCO control signals diminishes.

Hence, the effects of inaccurate frequency lock become negligible such that the beamforming transmissions effectively have the same phase and frequency at the start of beamforming. If practical considerations like noise and oscillator drift are taken into account, however, then an optimum timeslot duration would exist based on the operating environment.

The results presented in this section show that the RTTD system in SPTI channels is able to achieve high efficiency with longer beamformer durations, or less latency with shorter beamformer durations. The next section investigates whether the RTTD system exhibits these same properties in multi-path time-invariant (MPTI) channels.

### 4.3 RTTD System Operation in MPTI Channels

This section considers the performance of the RTTD distributed beamforming system in cases where the communication channels have multiple propagation paths. In multi-path channels, a portion of the transmission energy travels through several paths with greater propagation delays than a line-of-sight (LOS) path<sup>3</sup>. Hence, a receiving RTTD source detects the LOS component at the beginning of a timeslot, and then reflections of the transmission a short time after. With each new arrival of a reflection, the effective phase of the transmission changes. The sources lock to the effective phase of a transmission once all of the reflections have arrived because it remains constant until the end of the timeslot. At the end of a timeslot the LOS component is no longer present, but the scattered reflections may still be observed in the channel. Hence, an RTTD source may detect reflections of a carrier signal from a previous timeslot in addition to the reflections of the transmission being received.

---

<sup>3</sup>The minimum propagation delay path in a MPTI channel

The reflections of a transmission caused by MPTI channels combine with the LOS component either constructively or destructively at the receiving source. This thesis is only concerned with the amount of time that phase disturbances are present at the source inputs, and channel fading is not considered. To isolate the effect of the phase disturbances, the magnitude of the received transmissions are normalized to 1 at the PLL inputs. The source PLLs are implemented with multiplier phase detectors, and the gain of these types of phase detectors is sensitive to the input amplitude. To negate this effect, the magnitude of the transmissions is normalized to 1 so that the VCO control signals of the PLLs have consistent behavior for any given  $\omega_{3dB}$ .

The MPTI channels are modeled with a fixed number of constant propagation delays that are uniformly distributed on the interval  $[\tau_{ijLOS}, \tau_{ijLOS} + \tau_{ijDS}]$ , where  $ij \in \{01, 02, 12\}$ . The minimum propagation delay through the channel  $\tau_{ijLOS}$  corresponds to the LOS component, while  $\tau_{ijLOS} + \tau_{ijDS}$  is the maximum possible delay through the channel. The “delay spread” of a channel, denoted as  $\tau_{ijDS}$ , and the distribution of the delays are dependent on the environment in which the transmitters are located. Typical values for delay spread in several different environments have been measured and tend to be no greater than 5  $\mu\text{sec}$  [18] [19]. The distribution of the propagation delays can simulate a specific environment, but this thesis is only concerned with the maximum amount of time scattered reflections are present in the channels. Hence, a uniform distribution is used.

Unlike the RTFS system where multiple frequencies are used during synchronization, the RTTD system uses a single frequency and therefore channel reciprocity is not compromised. This section considers the effects of MPTI channels on the RTTD sources’ ability to effectively track the phase of the synchronization transmissions, and investigates the performance of the RTTD system in multi-path channels.

### 4.3.1 MPTI Channel Effects and Synchronization Overhead

Phase disturbances caused by multi-path reflections may reduce the amount of time that the RTTD sources have to track the effective phase of a received transmission. Phase disturbances may result from reflections from a previous timeslot, or from the transmission being received. As an example, Figure 4.6 illustrates the effects of MPTI channels on the RTTD synchronization schedule for the case where  $\tau_{01_{LOS}} > \tau_{02_{LOS}}$ . The schedule is shown from the perspective of the destination.

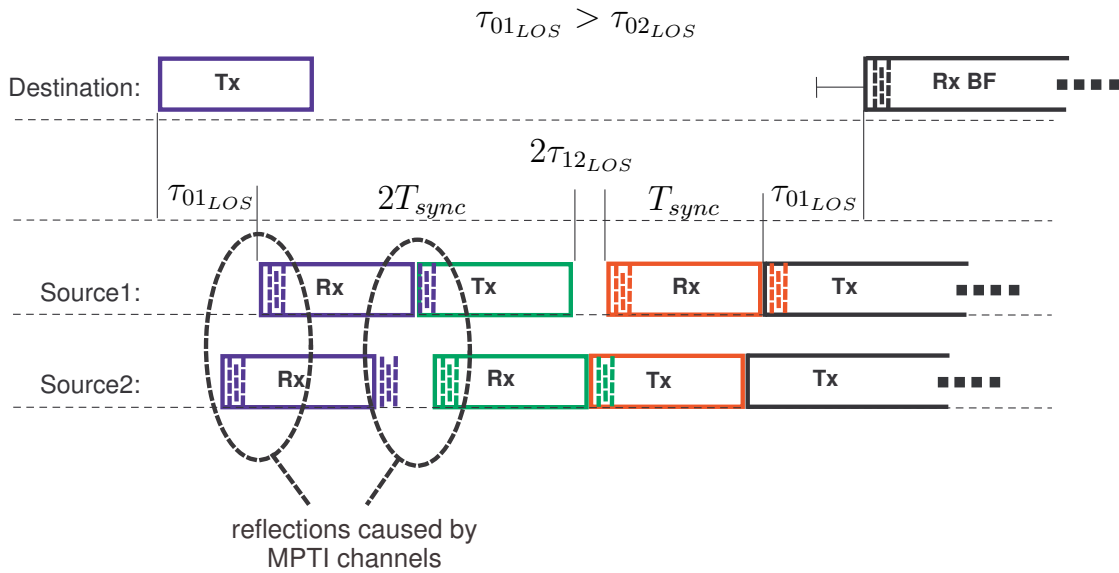


Figure 4.6: Schedule execution in MPTI channels from the perspective of the destination for  $\tau_{01_{LOS}} > \tau_{02_{LOS}}$ .

As Figure 4.6 shows, the RTTD sources may have less time to lock to their received transmissions. Unlike scenarios where the channels are single-path and time-invariant, the effective phase of a received transmission may not be constant for the duration of a timeslot due to multi-path phase disturbances. For example, the time in which the sources have to lock to the constant effective phase of the primary beacon is shorter because the phase of the primary beacon varies at the

source inputs with each new arrival of a multi-path reflection<sup>4</sup>. As another example, the inter-source channel may have a LOS propagation delay that is comparable to the amount of delay spread in the channel. In this case, source 1 begins to receive the relayed beacon during TS2 while reflections from TS1 are still present in the channel. Hence, the amount of time that source 1 has to track the effective phase of the relayed transmission is reduced.

The RTTD sources in MPTI channels may require more time to ensure that the  $T_{HF} \leq T_{sync}$ . To investigate how much additional time is needed, the PLL design of Section 3.2.3 is simulated 1000 iterations for an input that has passed through a multi-path channel that has uniformly distributed delay spread with  $\tau_{DS_{max}} \in [0, 5] \mu\text{sec}$  and  $\tau_{LOS} = 0 \mu\text{sec}$ . The number of multi-path reflections is limited to 20 in these simulations. The empirical histogram and CDF of recorded  $T_{HF}$  values are presented in Figure 4.7.

Figure 4.7 shows that the PLL reaches  $T_{HF}$  before  $t \approx 25 \mu\text{sec}$  with approximately 99% certainty. In order to ensure that  $P(T_{HF} \leq T_{sync}) = 0.99$ , the timeslot duration should be lengthened by the maximum amount of expected delay spread  $\tau_{DS_{max}}$ . Lengthening each timeslot duration by  $\tau_{DS_{max}}$  serves as a straightforward solution in dealing with multipath channels. This adjustment is done after the PLLs have been designed using the guidelines presented in Section 3.2.3 for the chosen timeslot duration. By using this approach, there is no added complexity in designing the source PLLs for MPTI channel scenarios. For both SPTI and MPTI channels, the source PLL design is consistent for a chosen  $T_{sync}$ .

Despite consistent PLL designs, however, the performance of the RTTD system in MPTI channels differs from that in SPTI channel scenarios. Because the timeslot duration is lengthened in MPTI channels, the amount of synchronization overhead

---

<sup>4</sup>The source PLLs begin to track the input when the LOS component is detected, and then enter holdover mode one timeslot duration later.

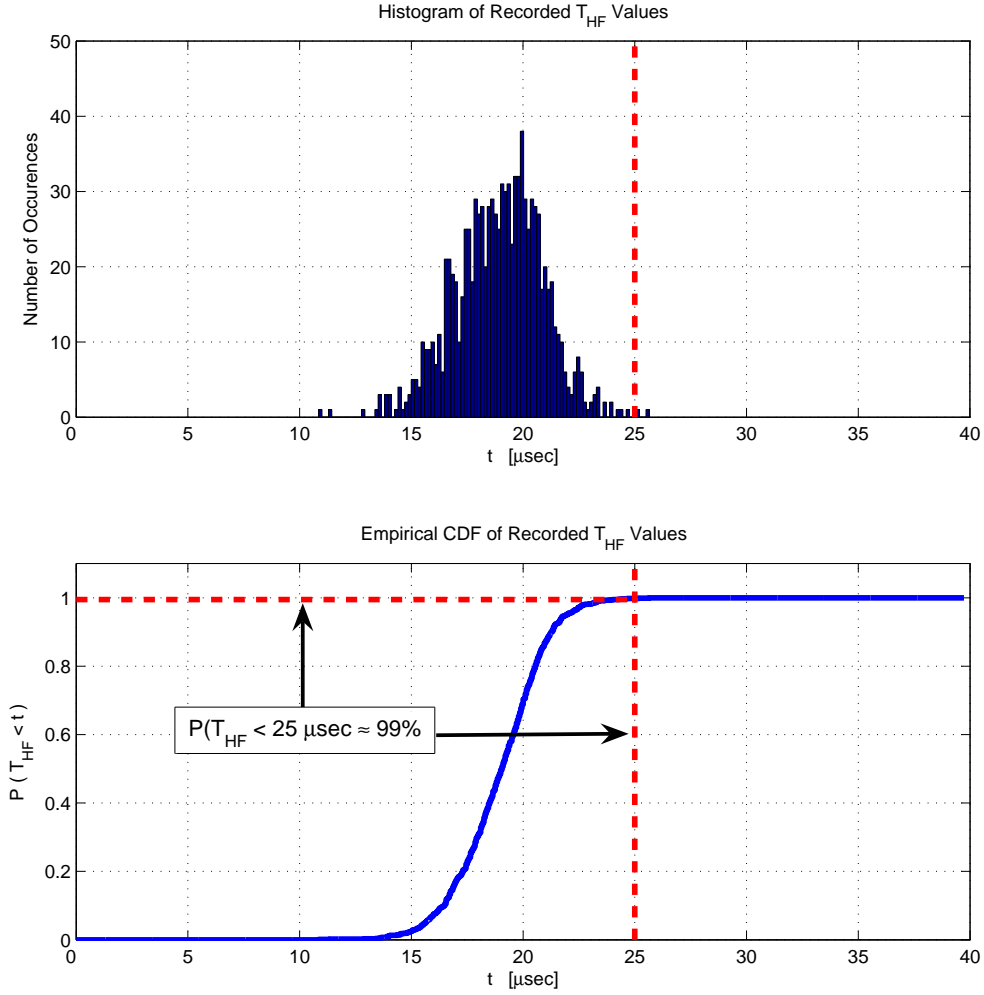


Figure 4.7: Histogram and empirical CDF of recorded  $T_{HF}$  values of a simulated PLL with  $\omega_{3dB} = 2\pi 4 \times 10^5$  rads/sec for an input that has uniformly distributed delay spread where  $\tau_{DS_{max}} \in [0, 5] \mu\text{sec}$  and  $\tau_{LOS} = 0 \mu\text{sec}$ .

is increased. The synchronization overhead of the RTTD system in MPTI channels can be expressed by

$$T_{OH_{MP}} = 3T_{sync} + 2\tau_{01_{LOS}} + 2\tau_{12_{LOS}} + 3\tau_{DS_{max}} + \tau_{01_{DS}}. \quad (4.19)$$

The synchronization overhead in MPTI channel scenarios  $T_{OH_{MP}}$  is similar to  $T_{OH_{SP}}$ , but is slightly larger due to the additional time needed for delay spread compensation. In addition, the destination does not begin to receive the beamformer until the delay spread from the source 1 transmission during TS3 diminishes. The major contributions to synchronization overhead in SPTI channel scenarios, however, are still present in MPTI channel scenarios. The timeslot duration  $T_{sync}$  and LOS propagation delays in the  $g_{01}$  and  $g_{12}$  channels still contribute substantially to the synchronization overhead level.

With the added synchronization overhead needed to combat the effects of MPTI channels, it is expected that the RTTD system efficiency is decreased when compared to the performance in SPTI channels. Not only does the added synchronization overhead decrease the performance, but the additional time during synchronization allows for more phase error accumulation. The worst-case phase and frequency error at the start of beamforming is considered for MPTI channel scenarios in the next section, and the worst-case efficiency of the RTTD system in MPTI channels is derived.

### 4.3.2 Worst-Case Performance Analysis for MPTI Channels

In order to investigate the performance of the RTTD system in MPTI channels beyond a specific value of  $T_{sync}$ , a worst-case analysis similar to that in Section 4.2.3 is conducted in this section. To determine the worst-case efficiency of the RTTD

system in MPTI channels, expressions for the worst-case synchronization overhead level and worst-case initial phase error are rederived. Additional synchronization overhead is used in MPTI channel scenarios to limit the frequency error in the source PLL outputs to  $|\omega_e| \leq K_o C$  rads/sec. Hence, the frequency error at the start of beamforming in MPTI channels is the same as it is in SPTI channel scenarios as expressed by

$$\omega_{BF_{MP}} = \omega_{BF_{SP}} = 4K_o C. \quad (4.20)$$

The worst-case synchronization overhead level is increased in MPTI channels compared to  $T_{OH_{SPWC}}$  as expressed by

$$T_{OH_{MPWC}} = 3T_{sync} + 2\tau_{01_{max}} + 2\tau_{12_{max}}, \quad (4.21)$$

where  $\tau_{ij_{max}} = \tau_{LOS_{max}} + \tau_{DS_{max}}$ . The delay  $\tau_{ij_{max}}$  in this case represents the maximum LOS propagation delay and the compensation for maximum expected delay spread in the  $g_{ij}$  channel. By ignoring the LOS propagation delays, the worst-case synchronization level in MPTI channels is approximated by

$$T_{OH_{MPWC}} \approx 3T_{sync} + 4\tau_{DS_{max}}. \quad (4.22)$$

The worst-case initial phase error is greater for MPTI channel scenarios than for SPTI channels because the amount of synchronization overhead is greater. The additional time required for delay spread compensation allows for more phase error accumulation during the synchronization process. The worst-case initial phase error in MPTI channels is given by

$$\phi_{BF_{MP}} = 5K_o C T_{sync} + 5K_o C \tau_{01_{max}} - K_o C \tau_{02_{max}} + 5K_o C \tau_{12_{max}} + 9K_o C \tau_{DS_{max}}. \quad (4.23)$$

As one can see in (4.23), the worst-case accumulated phase error in MPTI channels increases by  $9K_oC\tau_{DSmax}$ . This term represents the extended timeslot durations and the delay spread detected by destination. Ignoring channel delays, the worst-case phase error at the start of beamforming in MPTI channels can be approximated by

$$\begin{aligned}\phi_{BFMP} &\approx 5K_oCT_{sync} + 9K_oC\tau_{DSmax} \\ &\approx 10K_oK_d|F(2\omega_c)|T_{sync} + 18K_oK_d|F(2\omega_c)|\tau_{DSmax}.\end{aligned}\quad (4.24)$$

With explicit knowledge of the worst-case synchronization overhead level, and worst-case frequency and phase error at the start of beamforming, analytical expressions for the worst-case beamformer duration and efficiency of the RTTD system in MPTI channels can be found. The approximate worst-case beamformer duration and worst-case RTTD system efficiency in multi-path channel scenarios are given by (4.25) and (4.26), respectively.

$$T_{BFMP} = \frac{\Phi_{BF} - \theta_{BFMP}}{\omega_{BFMP}} \approx \frac{\Phi_{BF} - K_oK_d|F(2\omega_c)|(10T_{sync} - 18\tau_{DSmax})}{8K_oK_d|F(2\omega_c)|} \quad (4.25)$$

$$R_{BFMP} = \frac{T_{BFMP}}{T_{BFMP} + T_{OHMPWC}} \approx \frac{\Phi_{BF} - K_oK_d|F(2\omega_c)|(10T_{sync} - 18\tau_{DSmax})}{\Phi_{BF} + K_oK_d|F(2\omega_c)|(14T_{sync} + 32\tau_{DSmax})} \quad (4.26)$$

The next section utilizes the analytical expressions derived in this section to investigate the RTTD system performance in MPTI channels.

### 4.3.3 RTTD System Performance in MPTI Channels

The RTTD system performance in MPTI channels is investigated for a range of timeslot durations  $T_{sync}$  in this section. The performance achieved in multi-path channels is compared to the results obtained in single-path channels. The worst-case efficiency, approximate worst-case efficiency, and average efficiency of the RTTD

system in both time-invariant channel models are plotted versus  $T_{sync}$  in Figure 4.8.

The average efficiency is found from 500 simulations of the RTTD system.

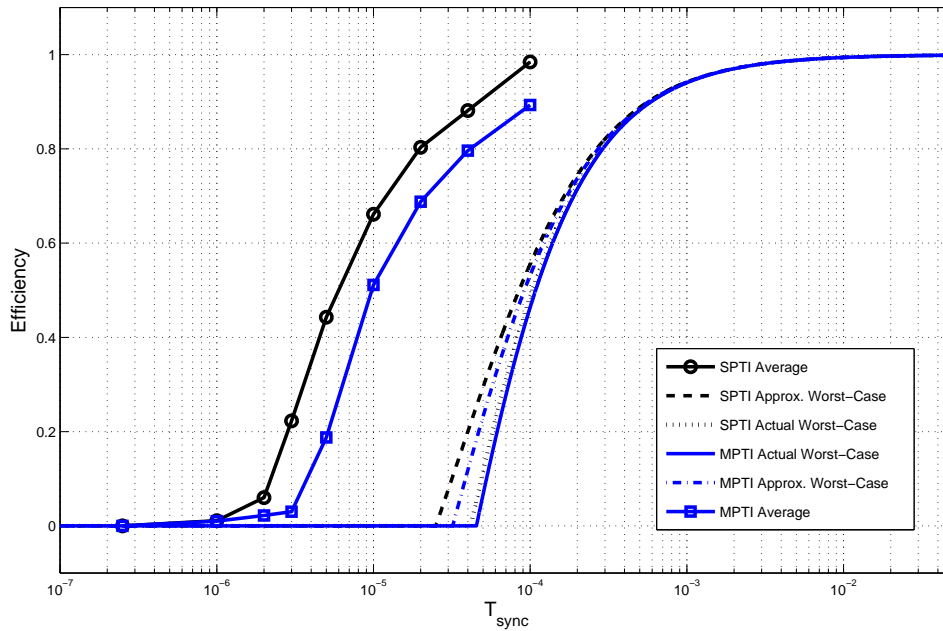


Figure 4.8: The RTTD system efficiency in MPTI channels is compared to that in SPTI channels. The actual worst-case results take into account channel delays, while approximations do not.

In general, Figure 4.8 shows that the added synchronization overhead and phase error accumulation in MPTI channel scenarios decreases the efficiency of the RTTD system compared to the results for SPTI channels. The general relationship between the efficiency of the RTTD system and the timeslot duration  $T_{sync}$ , however, remains consistent. The RTTD system is more efficient in MPTI channel scenarios when longer timeslot durations are used.

The difference between  $R_{BFSP}$  and  $R_{BFMP}$  is more drastic for shorter timeslot durations, i.e.  $T_{sync} < 10^{-5}$ , but the added synchronization overhead and phase error in multi-path channels becomes less significant for longer timeslot durations  $T_{sync}$ . From the results presented in Figure 4.8, it is found that increasing the times-

lot duration by the expected amount of delay spread is a straightforward solution in dealing with multi-path effects, and that the RTTD system is able to achieve a beamformer duration that merits the resources used during synchronization. When compared to the RTTD system performance in SPTI channels, the efficiency of the RTTD system in MPTI channels is reduced for shorter timeslot durations, i.e.  $T_{sync} < 10^{-5}$ . The difference in achieved efficiency is less, however, for longer timeslot durations.

The simulation and analytical results obtained in this chapter show that the RTTD system is capable of implementing a distributed beamformer in time-invariant channels. The achievable beamformer duration for longer timeslot durations leads to high system efficiency. Shorter timeslot durations cause the RTTD system to be less efficiency, but there is less latency. In addition, other potential benefits such as reduced transmit energy and increased battery life are not considered. The next chapter investigates the RTTD system's ability to implement a distributed beamformer in time-varying channels.

# Chapter 5

## RTTD Distributed Beamforming in Time-Varying Channels

The performance of the RTTD distributed beamforming system is investigated in this chapter for cases when the channels are time-varying and single-path, i.e.  $g_{ij} = g_{ji} = g(t - \tau_{ij}(t))$ . The propagation delays of the channels  $\tau_{ij}(t)$  vary due to source and/or destination movement, and as a result, the input phase to the source PLLs varies as well. The RTTD source PLLs can be designed to accurately track a time-varying input phase, but phase error due to mobility accumulates when the PLLs enter hold-over mode. To fully understand the capabilities of the RTTD system in mobile scenarios, two essential questions are answered in this chapter, and they are: (i) what is the distribution of the received phase error at the destination at the start of beamforming, and (ii) what is the distribution of the received phase error during beamforming? These questions give insight into the RTTD system's ability to achieve phase synchronization, and how long the RTTD system can perform as a distributed beamformer before resynchronization is necessary. This chapter begins with a description of the time-varying channels in the next section.

## 5.1 Time-Varying Channel Model

The relative velocity in each of the time-varying channels shown in Figure 5.1,  $v_{ij}(t)$ , is modeled by a wide-sense stationary, bandlimited Gaussian random process with zero-mean. All three channels are assumed to be identically distributed and independent of one another. The initial distance between transmitters,  $x_{ij}(t = 0)$ , is randomly chosen such that the initial propagation delay is uniform on the interval  $[\tau_{ijmin}, \tau_{ijmax}]$ .

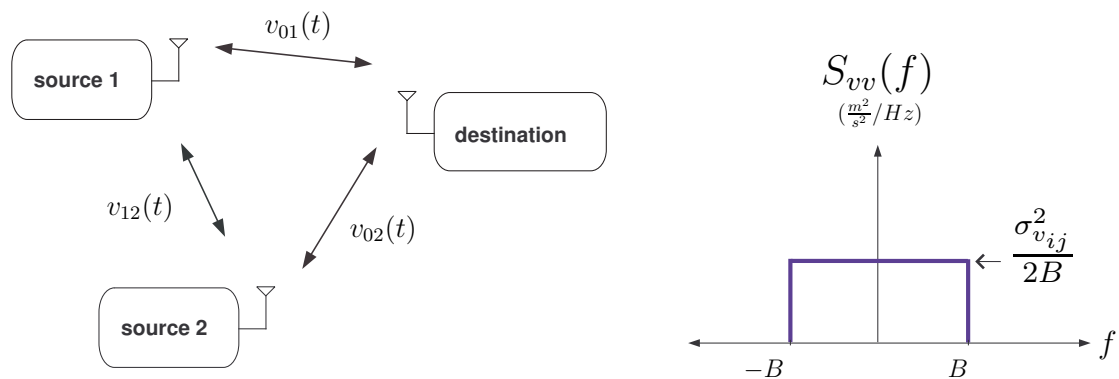


Figure 5.1: RTTD system model in time-varying channels and PSD of channel velocities  $S_{vv}(f)$ .

A negative velocity in the channels corresponds to two transmitters moving towards each other, and a positive velocity corresponds to two transmitters moving away from one another. The PSD of the channel velocities, as seen in Figure 5.1, has a height of  $\frac{\sigma_{v_{ij}}^2}{2B}$  and a bandwidth of  $B$ .

While the time-varying channel model chosen in this thesis may not be representative of the real-life movement exhibited by wireless transmitters, it provides the opportunity to analytically evaluate the RTTD system in a mobile scenario. Because a Gaussian random process is used to model the channel velocities, the dis-

tance between transmitters  $x_{ij}(t)$ , and the corresponding phase delay  $\rho_{ij}(t)$ , are also Gaussian random processes. As a result, the statistical properties of the phase error at the start of beamforming and during beamforming can be found analytically. To investigate the phase error contributed by each mobile channel, the statistical properties of  $x_{ij}(t)$  and  $\rho_{ij}(t)$  are investigated in this section.

### 5.1.1 Statistical Properties of Channel Delays

To understand how each time-varying channel contributes to the phase error in the beamformer, the statistical properties of the channel distance  $x_{ij}(t)$ , and of the corresponding phase delay  $\rho_{ij}(t)$ , are derived in this section. The distance between transmitters  $i$  and  $j$  at time  $t$  can be expressed by

$$x_{ij}(t) = x_{ij}(0) + \int_0^t v_{ij}(u) du. \quad (5.1)$$

The distance  $x_{ij}(t)$  is a Gaussian random process. Hence, the distance at time  $t = T$  is a Gaussian random variable with mean  $x_{ij}(0)$ . The variance of  $x_{ij}(T)$  is given by

$$\begin{aligned} \sigma_{x_{ij}}^2(T) &= \int_{-B}^B S_{vv}(f) |H(f)|^2 df, \\ &= \int_{-B}^B \frac{\sigma_{vv_{ij}}^2}{2B} \left| \frac{1 - e^{-j2\pi fT}}{j2\pi f} \right|^2 df, \\ &= \frac{\sigma_v^2}{2\pi^2 B^2} \left[ -1 + \cos(2\pi BT) + 2\pi BT \int_0^{2\pi BT} \frac{\sin(u)}{u} du \right], \end{aligned} \quad (5.2)$$

where  $H(f)$  is the transfer function for a continuous finite-time integrator [20]. As seen from (5.2), a closed-form solution for  $\sigma_{x_{ij}}^2(T)$  does not exist. The vari-

ance  $\sigma_{x_{ij}}^2(T)$  can be approximated, however, by estimating the velocity autocorrelation function  $R_{vv}(\tau)$  by the variance  $\sigma_v^2$ , and then performing double-integration of  $R_{vv}(\tau) \approx \sigma_{v_{ij}}^2$  on the interval  $[0, T]$  as expressed by

$$\sigma_{x_{ij}}^2(T) \approx \int_0^T \int_0^T \sigma_{v_{ij}}^2 = \sigma_{v_{ij}}^2 T^2. \quad (5.3)$$

The approximation of  $\sigma_{x_{ij}}^2(T)$  is most accurate for cases when  $T \ll \frac{1}{B}$  because the autocorrelation function  $R_{vv}(\tau)$  is approximately equal to the variance  $\sigma_{v_{ij}}^2$  for  $T \ll \frac{1}{B}$ . This estimation is illustrated in Figure 5.2.

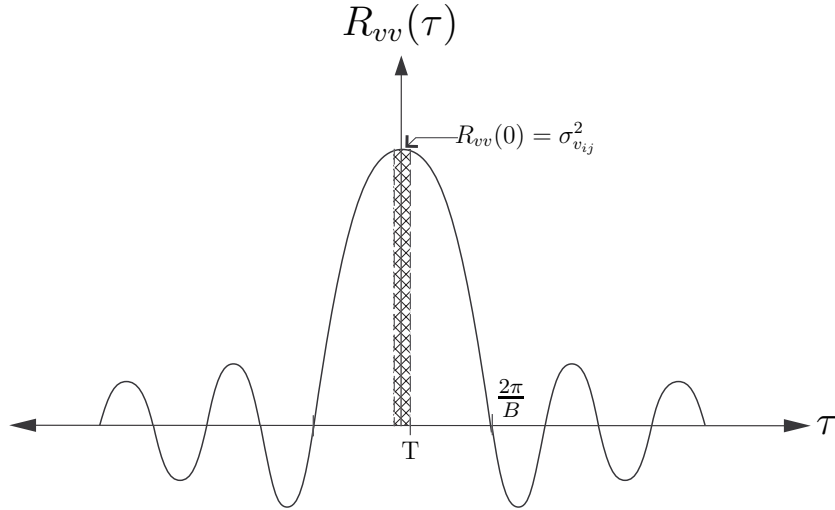


Figure 5.2: The velocity autocorrelation function  $R_{vv}(\tau)$  is approximately equal to the variance  $R_{vv}(0) = \sigma_{v_{ij}}^2$  for cases when  $T \ll \frac{1}{B}$ .

The approximation of  $\sigma_{x_{ij}}^2(T)$  is verified in Figure 5.3 where  $\frac{2B\sigma_x(T)}{\sigma_v}$  is plotted versus  $BT$ . The  $y$ -axis of Figure 5.3 is the standard deviation of distance  $\sigma_x$  normalized by  $\frac{\sigma_v}{2B}$ , and is therefore dimensionless. The  $x$ -axis of Figure 5.3 is for any combination of  $B$  and  $T$ , and is also dimensionless.

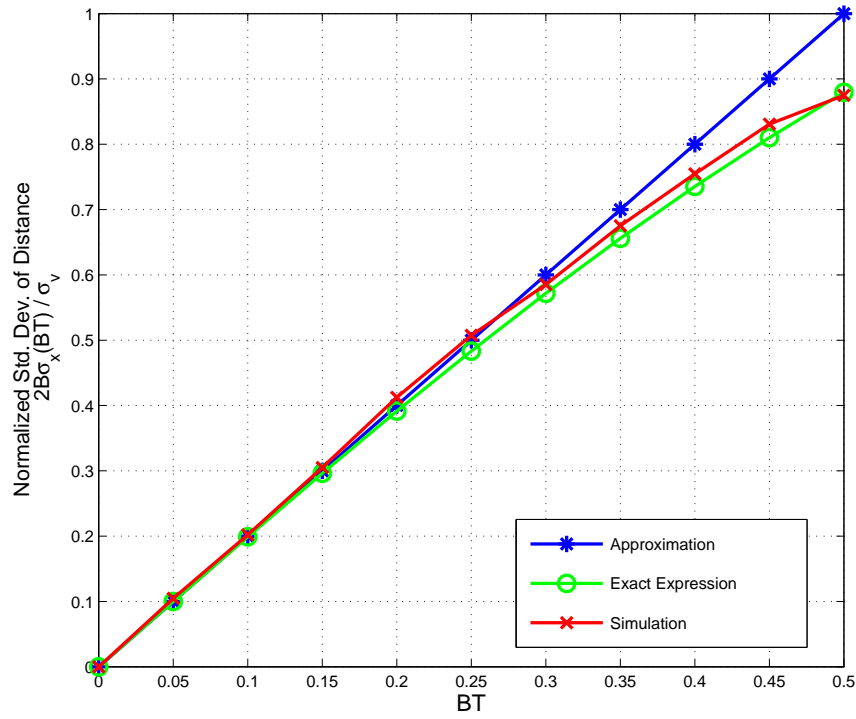


Figure 5.3: The approximate and exact expression of  $\sigma_{x_{ij}}^2(T)$ , as well as simulation results, are compared by plotting  $\frac{2B\sigma_x(T)}{\sigma_v}$  versus  $BT$ .

As seen in Figure 5.3, the approximation of  $\sigma_{x_{ij}}^2(T)$  is most accurate for cases when  $BT \leq 0.3$ . Intuitively, the product of  $B$  and  $T$  can be thought of as a measure of how quickly movement in the channels happens relative to the elapsed time  $T$ . For a small combination of  $BT$ , source/destination movement is sluggish and slow relative to  $T$ . For a larger combination of  $BT$ , the movement relative to  $T$  is more chaotic and fast. More specifically, a higher bandwidth  $B$  causes variation in  $x_{ij}(t)$  to happen more rapidly, and a greater  $T$  allows for more variation in  $x_{ij}(t = T)$  because more time elapses. A greater velocity variance  $\sigma_{v_{ij}}^2$  increases the magnitude of the movements. Increasing  $\sigma_{v_{ij}}^2$  or  $T$  causes the channel distance variance at time  $t = T$  to increase.

The channel phase delays, denoted as  $\rho_{ij}(t)$ , are also Gaussian random processes. Hence, the phase delay of a channel at time  $t = T$  is a Gaussian random variable with mean  $\rho_{ij}(0) = \frac{\omega_c x_{ij}(0)}{c}$ , and variance given by

$$\begin{aligned} \sigma_{\rho_{ij}}^2(T) &= \frac{\omega_c^2 \sigma_{x_{ij}}^2(T)}{c^2}, \\ &= \frac{\omega_c^2 \sigma_{v_{ij}}^2}{2\pi^2 B^2 c^2} \left[ -1 + \cos(2\pi BT) + 2\pi BT \int_0^{2\pi BT} \frac{\sin(u)}{u} du \right], \end{aligned} \quad (5.4)$$

$$\approx \frac{\omega_c^2 \sigma_{v_{ij}}^2 T^2}{c^2}, \quad (5.5)$$

where  $\omega_c$  is the frequency of the synchronization beacons and  $c$  is the speed of light. The statistical properties of the channel phase shifts are used to derive the distribution of the phase error at the start of beamforming in the next section.

## 5.2 Initial Phase Error Distribution

At the destination, the beamforming transmissions may differ in phase because the RTTD source PLLs do not track changes in the channel phase delays when they are in hold-over mode. During synchronization, the channel phase delays may change so much that the initial phase error at the start of beamforming exceeds the phase error constraint  $\Phi_{BF}$ . The time-varying nature of the channel phase delays cause the phase error at the destination to be statistical. Finding the distribution of the initial phase error will give insight into the ability of the RTTD system to achieve phase synchronization despite mobile transmitters.

It is assumed that the timeslot duration  $T_{sync}$  is long enough such that the high-frequency feedthrough in the source PLLs is negligible, and that the frequency and phase error at the source PLL outputs is essentially zero, i.e.  $\omega_{out_{ij}} = \omega_c$  and  $\theta_{out_{ij}} = \theta_{in_{ij}}$ . It is also assumed that channel phase delay changes happen much slower than the timeslot duration, i.e.  $T_{sync} \ll \frac{1}{B}$ . This assumption is necessary to avoid relativistic analysis.

To facilitate the derivation of the initial phase error distribution, the time at which the  $j^{th}$  PLL of the  $i^{th}$  source begins to track its input is denoted as  $t_{RX_{ij}}$ . The time at which the destination begins to receive the beamforming transmission from the  $i^{th}$  source is denoted as  $t_{RX_{Di}}$ . These times are illustrated in Figure 5.4.

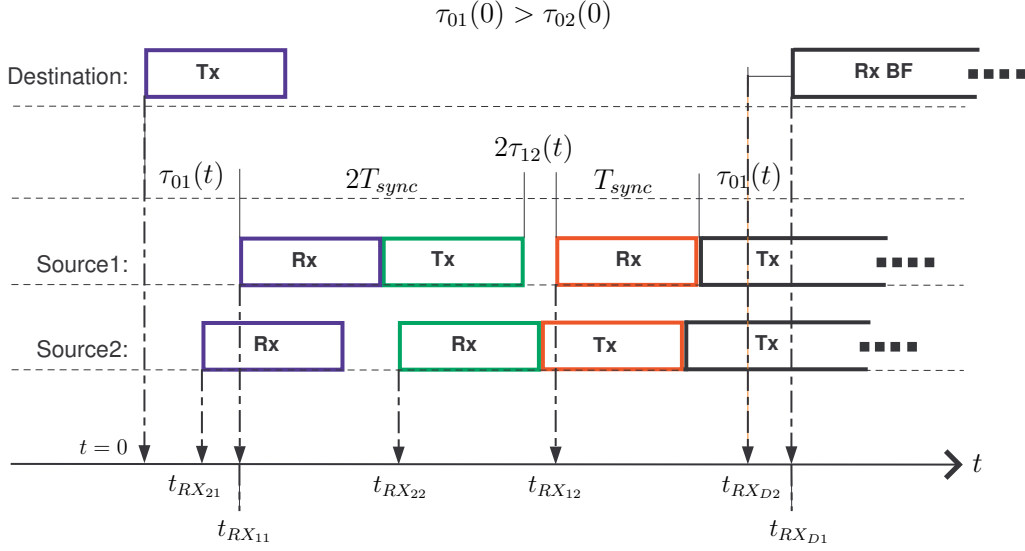


Figure 5.4: Schedule execution in single-path time-varying channels from the perspective of the destination for  $\tau_{01}(0) > \tau_{02}(0)$ .

Using this notation, the received phase at the destination from source 1 can be expressed by

$$\phi_{r_1}(t_{RX_{D1}}) = \theta_c + \rho_{02}(t_{RX_{21}} + T_{sync}) + \rho_{21}(t_{RX_{12}} + T_{sync}) + \rho_{10}(t_{RX_{D1}}), \quad (5.6)$$

and the received phase from source 2 can be expressed by

$$\phi_{r_2}(t_{RX_{D1}}) = \theta_c + \rho_{01}(t_{RX_{11}} + T_{sync}) + \rho_{12}(t_{RX_{22}} + T_{sync}) + \rho_{20}(t_{RX_{D1}}), \quad (5.7)$$

where  $\rho_{ij}(T)$  is the phase delay from the  $i^{th}$  transmitter to the  $j^{th}$  transmitter at time  $t = T$ . Although the destination begins to receive the source 2 beamformer transmission at  $t = t_{RX_{D2}}$ , the phase shift contributed by the  $g_{20}$  channel is not evaluated until the destination begins to receive both transmissions, i.e.  $t = t_{RX_{D1}}$ , which is the start of beamforming.

As seen in (5.6) and (5.7), the phase delay of a channel is evaluated once per round-trip circuit. The time at which each channel phase delay is evaluated, however, differs between the two round-trip circuits. As a result, there is phase error at the destination at the start of beamforming. The initial received phase error,  $\phi_{r\Delta}(t_{RX_{D1}}) = \phi_{r1}(t_{RX_{D1}}) - \phi_{r2}(t_{RX_{D1}})$ , is given by

$$\begin{aligned}\phi_{r\Delta}(t_{RX_{D1}}) &= [\rho_{02}(t_{RX_{21}} + T_{sync}) - \rho_{20}(t_{RX_{D1}})] \\ &+ [\rho_{21}(t_{RX_{12}} + T_{sync}) - \rho_{12}(t_{RX_{22}} + T_{sync})] \\ &+ [\rho_{10}(t_{RX_{D1}}) - \rho_{01}(t_{RX_{11}} + T_{sync})].\end{aligned}\quad (5.8)$$

It is known from Section 5.1 that a channel phase delay, at the specific time  $T$ , is Gaussian distributed with mean  $\rho_{ij}(0)$  and variance  $\sigma_{\rho_{ij}}^2(T)$ , as expressed by

$$f_{\rho_{ij}(T)}(x) = \frac{1}{\sqrt{2\pi\sigma_{\rho_{ij}}^2(T)}} e^{-\frac{(x-\rho_{ij}(0))^2}{2\sigma_{\rho_{ij}}^2(T)}}. \quad (5.9)$$

Hence, the phase error contributed by each channel, i.e.  $\rho_{ij}(T_{2_{ij}}) - \rho_{ij}(T_{1_{ij}})$ , is a Gaussian random variable with zero-mean and variance  $\sigma_{\rho_{ij}}^2(T_{2_{ij}} - T_{1_{ij}})$ , where  $T_{2_{ij}}$  and  $T_{1_{ij}}$  refer to the two different times during the synchronization process that the phase delay in the  $g_{ij}$  channel is evaluated. The elapsed time between instances when a channel is evaluated is dependent on the timeslot duration, as well as the latencies caused by the channel propagation delays. The contributing phase errors of each channel are not identically distributed because these elapsed times differ, as expressed by

$$T_{2_{01}} - T_{1_{01}} = t_{RX_{D1}} - t_{RX_{11}} - T_{sync}, \quad (5.10)$$

$$T_{2_{02}} - T_{1_{02}} = t_{RX_{D1}} - t_{RX_{21}} - T_{sync}, \text{ and} \quad (5.11)$$

$$T_{2_{12}} - T_{1_{12}} = t_{RX_{12}} - t_{RX_{22}}. \quad (5.12)$$

Explicit solutions for  $t_{RX_{ij}}$  do not exist because the channel propagation delays are time-varying. It is assumed, however, that the propagation delay changes happen much slower than the timeslot duration, i.e.  $T_{sync} \ll \frac{1}{B}$ . Hence, the latencies caused by channel propagation delay are assumed to be nearly constant during the synchronization process, i.e.  $\tau_{ij}(T_{2_{ij}}) \approx \tau_{ij}(T_{1_{ij}}) \approx \tau_{ij}(0)$  for  $t < t_{RX_{D1}}$ . As a result, the elapsed times over which the variance of the phase errors are evaluated are given by

$$T_{2_{01}} - T_{1_{01}} \approx 2T_{sync} + \tau_{01}(0) + 2\tau_{12}(0), \quad (5.13)$$

$$T_{2_{02}} - T_{1_{02}} \approx 2T_{sync} + 2\tau_{01}(0) + 2\tau_{12}(0) - \tau_{02}(0), \text{ and} \quad (5.14)$$

$$T_{2_{12}} - T_{1_{12}} \approx T_{sync} + \tau_{12}(0) - \tau_{02}(0). \quad (5.15)$$

It is also assumed that the timeslot duration  $T_{sync}$  is long enough such that the frequency and phase error in the source PLL outputs is negligible. Hence, it is reasonable to assume that  $T_{sync} \gg \tau_{ij}(0)$ , and that the elapsed times can be accurately approximated by

$$T_{2_{01}} - T_{1_{01}} \approx 2T_{sync}, \quad (5.16)$$

$$T_{2_{02}} - T_{1_{02}} \approx 2T_{sync}, \text{ and} \quad (5.17)$$

$$T_{2_{12}} - T_{1_{12}} \approx T_{sync}. \quad (5.18)$$

With the elapsed times approximated by an integer number of timeslot durations, the phase error distribution at the start of beamforming can be rewritten as

$$f_{\phi_{r\Delta}}(x) \approx \frac{1}{\sqrt{2\pi\sigma_{\phi_{r\Delta}}^2(T_{sync})}} \exp\left(\frac{-x^2}{2\sigma_{\phi_{r\Delta}}^2(T_{sync})}\right), \quad (5.19)$$

where,

$$\sigma_{\phi_{r\Delta}}^2(T_{sync}) \approx \sigma_{\rho_{02}}^2(2T_{sync}) + \sigma_{\rho_{12}}^2(T_{sync}) + \sigma_{\rho_{01}}^2(2T_{sync}). \quad (5.20)$$

Using the approximation in (5.5), the variance of the phase error at the start of beamforming is estimated by

$$\sigma_{\phi_{r\Delta}}^2(T_{sync}) \approx 9\frac{\omega_c^2}{c^2}\sigma_v^2T_{sync}^2, \quad (5.21)$$

for identically distributed channels and when  $\tau_{ij}(0) \ll T_{sync} \ll \frac{1}{B}$ . The exact analytical expression, which uses (5.4) to calculate  $\sigma_{\phi_{r\Delta}}^2(T_{sync})$ , can also be used to determine the phase error variance at the start of beamforming<sup>1</sup>. In the next section, simulation results for the initial phase error distribution are compared to the analytical expressions derived in this section.

### 5.3 Simulation Results: Initial Phase Error

The distribution of the initial phase error at the start of beamforming is investigated in this section. The RTTD system is simulated to find an empirical distribution of the initial phase error, and these results are compared to the analytical results derived in Section 5.2. The results are compared when determining how the initial

---

<sup>1</sup>Although the “exact analytical” expression still estimates the elapsed times by an integer number of timeslot durations, it is referred to as such when (5.4) is used to calculate the phase variance of each channel

phase error distribution is affected by the speed of movement, the timeslot duration, and the magnitude of velocity variations.

The RTTD source PLLs are simulated using the linear PLL model, which was reviewed in Section 2.4. In order to use the linear PLL model, it is assumed that the VCO frequencies are all identical and are equal to the master beacon frequency  $\omega_c$ . The linear PLL model still simulates the gross-transient behavior of the PLLs, but the high-frequency feedthrough is not simulated. Each simulation was completed using the parameters listed here:

- the master beacon phase is uniformly distributed on  $\theta_c = [-\pi, \pi)$
- the initial VCOs phases are uniformly distributed on  $\theta_{q_{ij}} = [-\pi, \pi)$
- the phase detector gains are  $K_d = 1$
- the VCO gains are  $K_o = 2\pi \times 10^5$
- the loop filter bandwidth of the PLLs is set to 1 MHz to facilitate fast convergence and eliminate potential error due to gross-transient behavior

### 5.3.1 Effects of Movement Speed

The speed of the movements is measured by the product of the timeslot duration and the velocity bandwidth, i.e.  $BT_{sync}$ . To determine the effects of  $T_{sync}$  and  $B$ , the standard deviation of the initial phase error  $\sigma_{\phi_{r\Delta}}$ , normalized by  $\frac{\sigma_v}{2B}$ , is plotted in Figure 5.5 for any general combination of  $BT_{sync}$  where the product is less than 0.5. The standard deviation of the phase error is normalized by  $\frac{\sigma_v}{2B}$  so that the results of Figure 5.5 can be used to determine the distribution of the initial phase error for any general velocity variance  $\sigma_v^2$ , and for any general velocity bandwidth  $B$  or timeslot duration  $T_{sync}$ .

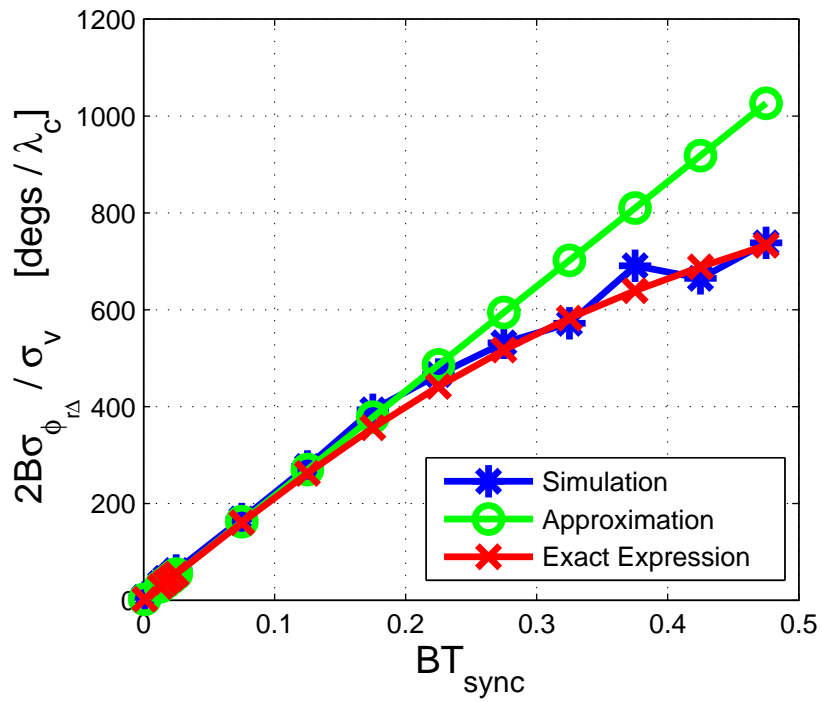


Figure 5.5: The standard deviation of the phase error at the start of beamforming  $\sigma_{\phi_{r\Delta}}$  is investigated for different movement speeds.

The standard deviation of velocity is specified in  $\frac{\lambda_c}{8}$  so that the results of Figure 5.5 are independent of the synchronization beacon frequency  $\omega_c$ . As a result, the  $y$ -axis is measured in  $\frac{\text{deg}}{\lambda_c}$ . Figure 5.5 shows that the standard deviation of the phase error at the start of beamforming is an increasing function of  $BT_{sync}$ . For a given timeslot duration  $T_{sync}$ , the standard deviation of the initial phase error increases if the movement in the channels is quicker and more chaotic. For a given velocity bandwidth  $B$ , a longer timeslot duration increases the standard deviation of the initial phase error. Hence, the timeslot duration should be chosen in consideration of the mobile scenario in order to reduce the initial phase error at the start of beamforming. It should allow for the PLLs to converge, but not be any longer to allow for phase error to accumulate due to mobility.

Figure 5.5 shows that the approximation for  $\sigma_{\phi_{r\Delta}}^2$  is only slightly pessimistic when compared to the simulation data and to the exact analytical expression. The approximation is within 5% of the simulation data and the exact analytical expression when  $BT_{sync} \leq 0.1$ . The simulation data follows the exact analytical expression within 5% for all  $BT_{sync}$ . The next section investigates the initial phase error distribution for increasing magnitudes of velocity variation.

### 5.3.2 Effects of Velocity Variation

The effects of increasing velocity variation on the initial phase error distribution is investigated in this section. The product of  $B$  and  $T_{sync}$  is fixed at  $BT_{sync} = 0.2$ , and the standard deviation of the initial phase error is found for increasing magnitudes of velocity variation. The quantity  $2B\sigma_{\phi_{r\Delta}}$  is plotted versus the standard deviation of velocity  $\sigma_v$  in Figure 5.6. The results of Figure 5.6 are for any general velocity bandwidth  $B$ , or any general timeslot duration  $T_{sync}$ , so long as the product of the two is  $BT_{sync} = 0.2$ .

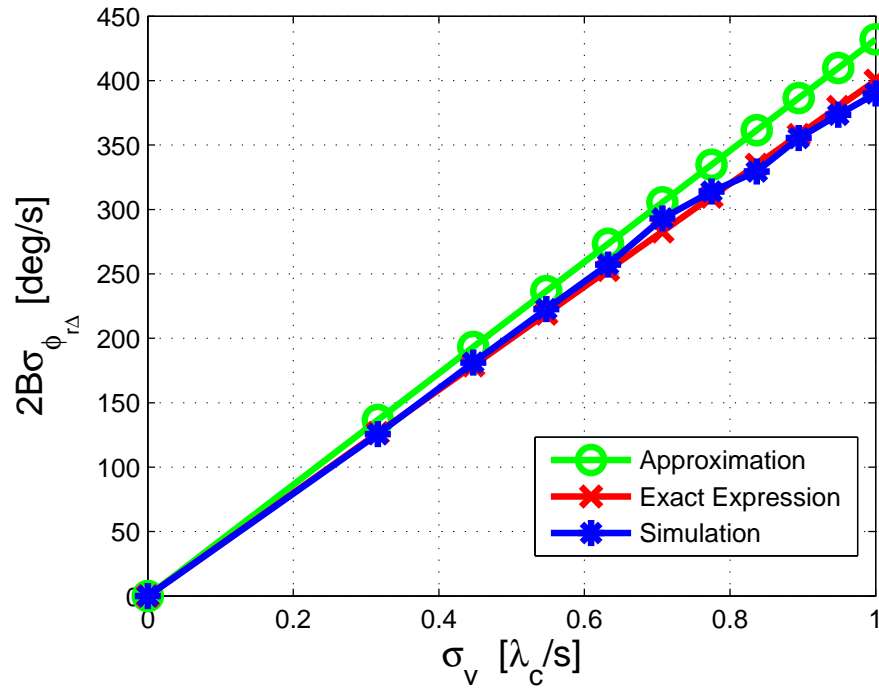


Figure 5.6: The quantity  $2B\sigma_{\phi_{r\Delta}}$  is plotted versus  $\sigma_v$  to show the effects of increasing velocity variation. The product of  $B$  and  $T_{sync}$  is fixed at  $BT_{sync} = 0.2$ .

As seen in Figure 5.6, the standard deviation of the initial phase error increases linearly with the velocity standard deviation. With greater potential channel velocities, the distance between transmitters can change more drastically and cause greater potential phase delays. In the example given in Figure 5.6, the channel velocity changes happen relatively quickly compared to the timeslot duration. Hence, a velocity standard deviation of only  $\sigma_v = 1 \frac{\lambda_c}{\text{s}}$  can potentially cause a significant initial phase error. Assuming a practical velocity bandwidth of  $B = 10$  Hz and a carrier frequency of  $\omega_c = 2\pi 800$  rads/s, the standard deviation of the initial phase error is  $\sigma_{\phi_{r\Delta}} = 20^\circ$  when  $\sigma_v = 1 \frac{\lambda_c}{\text{s}}$ . The timeslot duration in this example, however, would be  $T_{sync} = 20$  msec. Considering that the high-frequency feedthrough of the PLLs is essentially zero when a timeslot duration of this length is used, a timeslot duration this long may be more detrimental to the performance of the RTTD system than beneficial.

The results shown in Figure 5.6, as well as Figure 5.5, demonstrate that the statistical properties of the initial phase error  $\phi_{r\Delta}$  can change significantly depending on the speed and magnitude of the channel velocities. The RTTD system can be designed to achieve a favorable initial phase error distribution in a wide range of mobile scenarios, but it is unclear what limitations exist. The next section investigates under what mobile scenarios the RTTD system is able to satisfy the phase error constraint at the start of beamforming.

### 5.3.3 Initial Phase Error in Mobile Scenarios

To understand the performance of the RTTD system in many different mobile scenarios, the statistical properties of the initial phase error are investigated for several combinations of  $B$ ,  $T_{sync}$ ,  $\sigma_v$ . The quantity  $2B\sigma_{\phi_{r\Delta}}$  is plotted versus  $BT_{sync}$  and  $\sigma_v$  simultaneously in Figure 5.7. The results of Figure 5.7 are for any general  $B$  or  $T_{sync}$ , and are independent of the beacon carrier frequency.

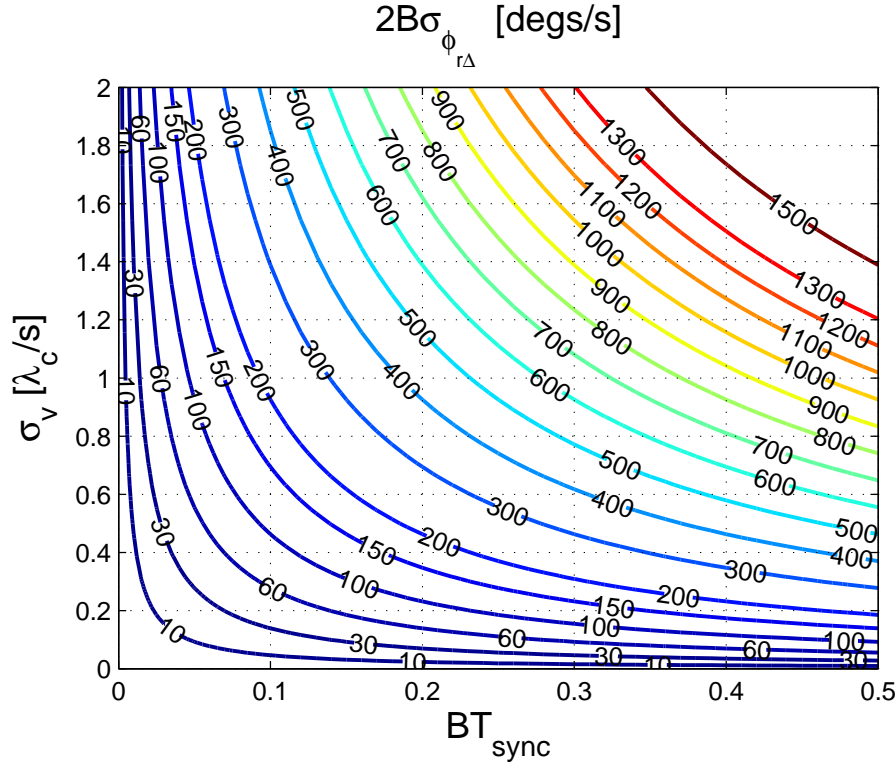


Figure 5.7: The quantity  $2B\sigma_{\phi_{r\Delta}}$  is plotted versus  $BT_{sync}$  and  $\sigma_v$  simultaneously to investigate the statistical properties of the initial phase error in several different mobile scenarios.

The RTTD system performs best when both the speed, and the magnitude, of the movements is smaller. Figure 5.7 highlights a tradeoff between  $BT_{sync}$  and  $\sigma_v$ . The RTTD system can perform well for faster movements, but the magnitude of the velocity changes must remain small. The RTTD system can perform well for greater velocity variations, but the movements must be more sluggish.

Figure 5.7 shows that RTTD system can be designed to achieve a favorable initial phase error distribution in many mobile scenarios. To ensure a small initial phase error, the timeslot duration should be chosen in consideration of the mobile scenario described by  $\sigma_v$  and  $B$ . A shorter timeslot duration is needed for higher levels of mobility (greater  $\sigma_v$  and  $B$ ), but for cases when the transmitters are less mobile, a longer timeslot duration can be used. To demonstrate the ability of the RTTD system to satisfy the phase error constraint  $\Phi_{BF}$  at the start of beamforming, and to investigate how  $T_{sync}$  should be chosen to accommodate a mobile scenario, the probability of satisfying the phase error constraint at the end of synchronization is plotted versus  $T_{sync}$  and  $\sigma_v$  in Figure 5.8. In this example, a carrier frequency of  $\omega_c = 2\pi 800$  MHz is assumed, and the velocity bandwidth is fixed at  $B = 10$  Hz. The approximation for  $\sigma_{\phi_{r\Delta}}$  is used to produce the results of Figure 5.8. The phase error constraint is set to  $\Phi_{BF} = 10^\circ$ .

Figure 5.8 highlights that a shorter timeslot duration is needed for higher levels of mobility (greater  $\sigma_v$ ), while a longer timeslot duration can be used when the transmitters are less mobile. In cases where the transmitters are quite mobile, i.e.  $\sigma_v = 10 \frac{\lambda_c}{S}$ , the timeslot duration can be chosen such that the RTTD system satisfies  $\Phi_{BF}$  with high probability. Standard deviations in velocity any greater than  $\sigma_v = 10 \frac{\lambda_c}{S}$ , however, would require a timeslot duration so short that error due to high-frequency feedthrough would be of concern. On the other hand, for timeslot durations longer than  $T_{sync} = 10$  msec the RTTD transmitters would need to be almost stationary in order to satisfy  $\Phi_{BF}$  with high probability.

The next section investigates the statistical properties of the beamformer phase error to gain a better understanding of the RTTD system efficiency for these same mobile scenarios.

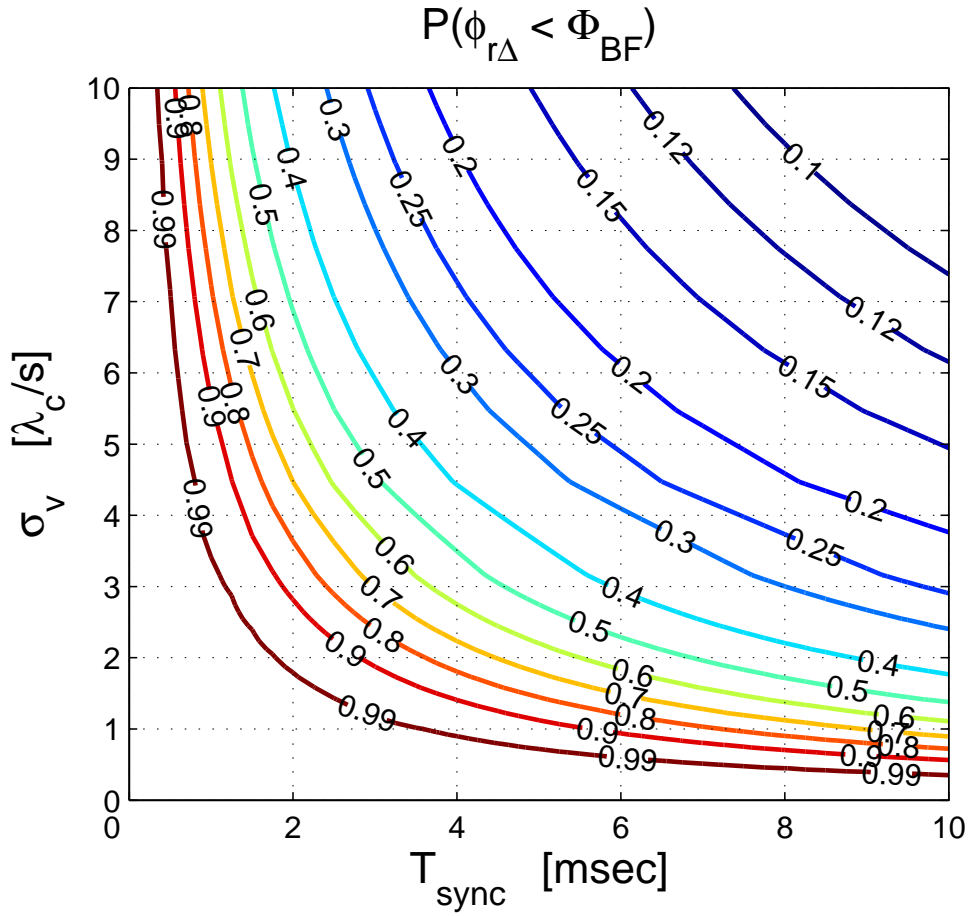


Figure 5.8: The probability  $P(\phi_{r\Delta} \leq \Phi_{BF})$  is plotted versus  $T_{sync}$  and  $\sigma_v$  to show how the timeslot duration should be chosen for increasing levels of velocity variation so that the phase error constraint is satisfied at the start of beamforming.

## 5.4 Phase Error During Beamforming

The distribution of the phase error during beamforming gives insight into how long the RTTD system can perform as a distributed beamformer. When considering the beamformer duration in time-invariant channels, a minimum beamformer duration could be guaranteed because the worst-case frequency and phase error at the start of beamforming was explicitly known, and phase error due to mobility was not of concern. When considering the beamformer duration in time-varying channels, a minimum beamformer duration can no longer be guaranteed. The initial phase and frequency error in time-varying channels is not explicitly known, and the time-varying channel delays cause the phase error in the beamformer to vary.

From the previous section, it is known that the initial phase error at the start of beamforming is Gaussian distributed with zero mean and variance approximated by (5.21). If the initial phase error is temporarily ignored, however, and it is assumed that the RTTD system is designed in such a way that the beamformer transmissions are perfectly synchronized, then the only cause for phase error in the beamformer is limited to mobility. Any potential phase error in the beamformer would be due to the time-varying phase delays in the  $g_{10}$  and  $g_{20}$  channels. The inter-source channel  $g_{12}$  has no effect on the beamformer after synchronization. Phase error in the beamformer occurs when the source-destination phase delays deviate from their values at the start of beamforming, i.e.  $\rho_{i0}(t_{RX_{D1}})$ . Hence, the phase error in the beamformer is expressed by

$$\phi_{r\Delta BF}(t) = \zeta_{10}(t) - \zeta_{20}(t), \quad \text{for } t \geq t_{RX_{D1}}, \quad (5.22)$$

where  $\zeta_{i0}(t)$  represents the phase delay change in the  $g_{i0}$  channel after synchronization, i.e.  $\zeta_{i0}(t) = \rho_{i0}(t) - \rho_{i0}(t_{RX_{D1}})$ . Each contributing phase term  $\zeta_{i0}(t)$  is

a Gaussian random process with zero mean. Hence, the phase delay change at some elapsed time from the start of beamforming, denoted as  $\zeta_{i0}^2(T_\Delta)$ , is a Gaussian random variable with zero mean and variance given by

$$\sigma_{\zeta_{i0}}^2(T_\Delta) = \frac{\omega_c^2 \sigma_{v_{ij}}^2}{2\pi^2 B^2 c^2} \left[ -1 + \cos(2\pi B T_\Delta) + 2\pi B T_\Delta \int_0^{2\pi B T_\Delta} \frac{\sin(u)}{u} du \right], \quad (5.23)$$

where  $T_\Delta$  is the elapsed time from the start of beamforming. The phase error between the two beamforming transmissions at  $t = t_{RX_{D1}} + T_\Delta$  is therefore a Gaussian random variable with zero mean and variance given by

$$\begin{aligned} \sigma_{\phi_{r\Delta BF}}^2(T_\Delta) &= \sigma_{\zeta_{10}}^2(T_\Delta) + \sigma_{\zeta_{20}}^2(T_\Delta) \\ &= 2\sigma_{\zeta_{i0}}^2(T_\Delta). \end{aligned} \quad (5.24)$$

A closed-form solution for  $\sigma_{\phi_{r\Delta BF}}^2(T_\Delta)$  does not exist, however, so an approximation is made by taking its limit as  $T_\Delta \rightarrow \infty$ . The sine integral function approaches  $\frac{\pi}{2}$  for large values of  $T_\Delta$ , and the term  $-1 + \cos(2\pi B T_\Delta)$  becomes insignificant. Hence, the variance of the beamformer phase error is approximated by

$$\sigma_{\phi_{r\Delta BF}}^2(T_\Delta) \approx \frac{\omega_c^2 \sigma_v^2 T_\Delta}{B c^2}. \quad (5.25)$$

This approximation clearly shows that the variance of the beamformer phase error is an increasing function of  $T_\Delta$  and  $\sigma_v^2$ . Greater velocity changes cause more phase error variation, and the phase error variation increases the longer the RTTD sources perform as a beamformer. This approximation is most accurate for larger values of  $T_\Delta$ , but it also serves as an upper-bound for smaller values of  $T_\Delta$ . The approximation is compared to the exact expression and simulation data in the next section.

## 5.5 Simulation Results: Beamformer Phase Error

Simulation results are used in this section to verify the analytical expressions which describe the distribution of the beamformer phase error. This is done by simulating the two beamforming transmissions through their respective source-destination channels and finding the standard deviation of the phase error for increasing values of  $T_\Delta$ . The analytical expressions are then used to investigate the RTTD system's ability to achieve high efficiency. This section begins by validating the analytical results found in Section 5.4.

### 5.5.1 Beamformer Duration and Phase Error

The simulation data is compared to the analytical results by plotting the standard deviation of the phase error  $\sigma_{\phi_{r\Delta BF}}$ , normalized by  $\frac{\sigma_v}{2B}$ , versus  $BT_\Delta$  in Figure 5.9. These results are for any general velocity variance  $\sigma_v^2$ , and for any general velocity bandwidth  $B$  or  $T_\Delta$ . In order to highlight the effects of mobility during beamforming, no initial phase error is considered.

For smaller values of  $T_\Delta$ , Figure 5.9 shows that the standard deviation approximation of  $\phi_{\phi_{r\Delta BF}}$  is more pessimistic when compared to the simulation data and to the exact analytical expression. For example, if a velocity bandwidth of  $B = 10$  Hz and a velocity standard deviation of  $\sigma_v = 1 \frac{\lambda_c}{5}$  is assumed, the approximate standard deviation is  $\sigma_{\phi_{r\Delta BF}} = 19^\circ$  at  $T_\Delta = 20$  msec. The exact standard deviation is only  $\sigma_{\phi_{r\Delta BF}} = 10^\circ$ . The approximation becomes more representative of the actual performance as  $T_\Delta$  increases, so it is most accurate for RTTD systems that employ larger timeslot durations. The exact analytical expression is within 5% of the simulation data for all values of  $T_\Delta$ .

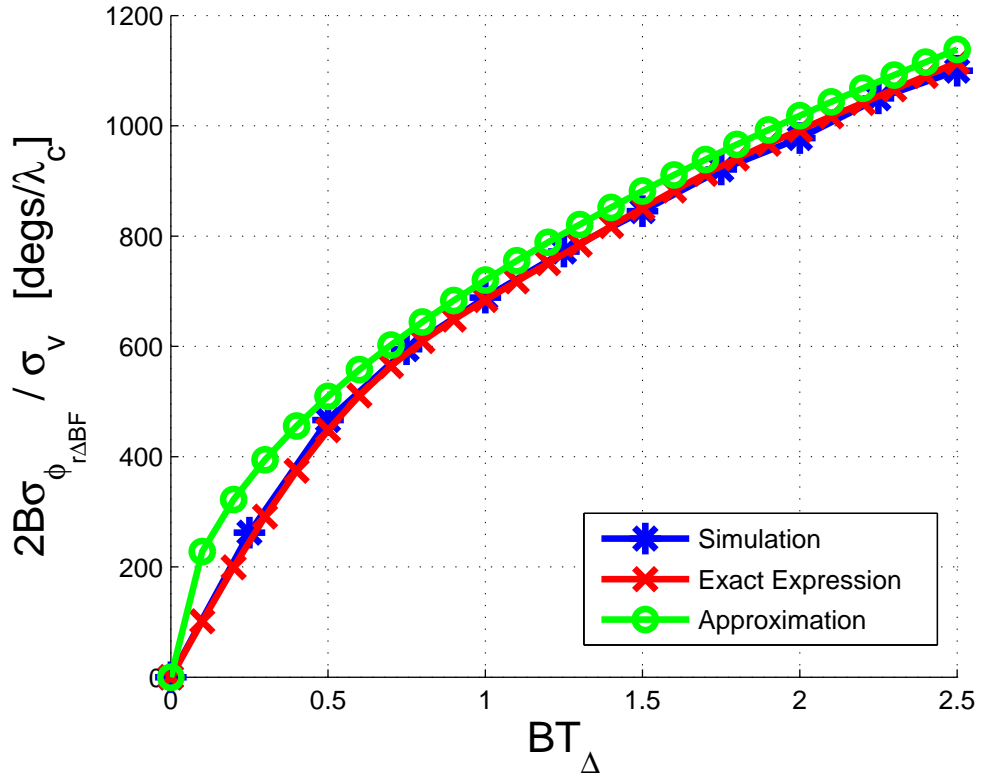


Figure 5.9: The standard deviation of the phase error during beamforming  $\sigma_{\phi_{r\Delta BF}}$  is plotted versus  $BT_{\Delta}$ .

As seen in Figure 5.9, it becomes less likely that the beamformer phase error satisfies the phase error constraint  $\Phi_{BF}$  the longer the RTTD sources perform as a beamformer. Depending on the mobile scenario and how the timeslot duration is chosen, the RTTD sources may not be able to beamform for a duration of time that merits the time spent synchronizing. In order to investigate this further, the next section considers the efficiency of the RTTD system for several mobile scenarios.

### 5.5.2 Efficiency in Mobile Scenarios

The distribution of the beamformer phase error is used to investigate whether the RTTD system can achieve high efficiency in mobile scenarios. The probability of achieving an efficiency of 0.85 is plotted versus  $T_{sync}$  and  $\sigma_v$  simultaneously in Figure 5.10. The velocity bandwidth is assumed to be  $B = 10$  Hz and the synchronization beacon frequency is  $\omega_c = 2\pi 800$  MHz. The exact analytical expression for calculating  $\sigma_{\phi_{r\Delta BF}}$  is used in Figure 5.10 because the timeslot durations considered are relatively short. In addition, because the product of  $B$  and  $T_{sync}$  in Figure 5.10 is kept below 0.01, so no initial phase error is considered. A phase error constraint of  $\Phi_{BF} = 10^\circ$  is assumed.

Figure 5.10 demonstrates that the RTTD system can achieve high efficiency in mobile scenarios where the velocity standard deviation is as much as  $\sigma_v = 10 \frac{\lambda_c}{S}$ . Mobile scenarios such as these, however, require a timeslot duration that is  $T_{sync} \leq 100 \mu\text{sec}$ , and error due to PLL gross-transient behavior and high-frequency feedthrough becomes more of a concern. When a longer timeslot duration is used to negate the effects of PLL transient behavior, however, the RTTD transmitters must be less mobile, i.e.  $\sigma_v \leq 2 \frac{\lambda_c}{S}$ , in order to achieve high efficiency. In general, the RTTD system is able to perform well as a distributed beamformer in mobile scenarios, but the amount of acceptable mobility is limited.

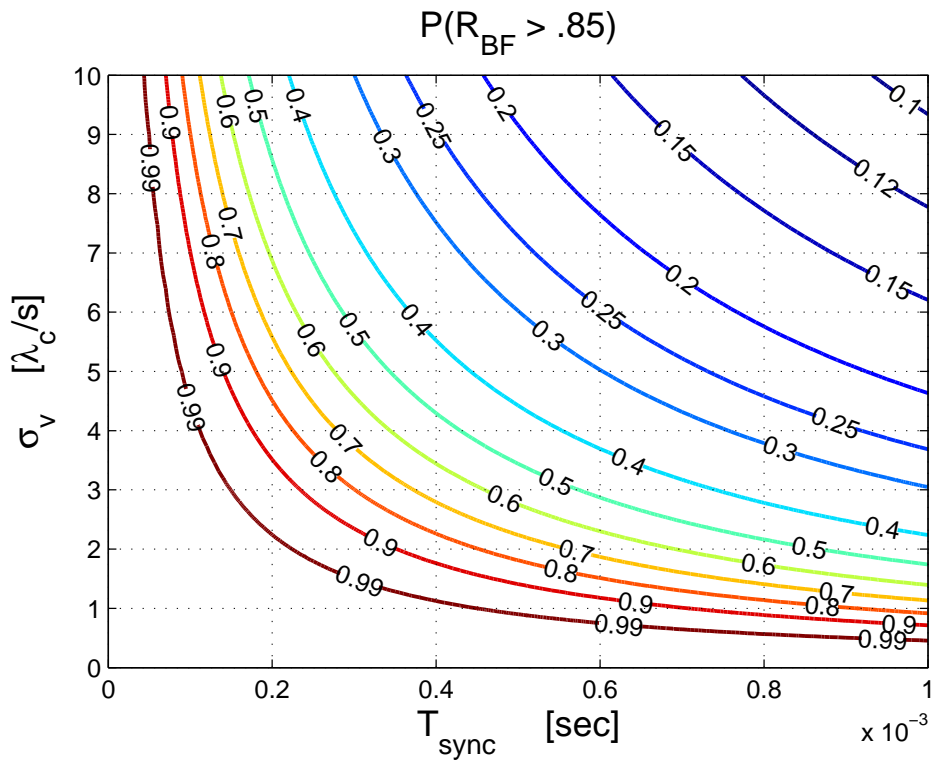


Figure 5.10: The probability of achieving an efficiency of at least 0.85 is plotted versus  $\sigma_v$  and  $T_{sync}$ .

# Chapter 6

## Conclusions

The primary goal of this thesis was to introduce the Round-Trip Time-Division distributed beamforming system, and to demonstrate its basic capabilities in three different channel models. A secondary goal was to develop a foundation of guidelines for designing the system. After investigation of the RTTD system performance in time-invariant and time-varying channels, several conclusions regarding the work in this thesis, as well as potential future work, can be made.

This thesis introduced the RTTD system in Chapter 3. A specific PLL implementation was chosen and a design guideline for choosing the PLL closed loop bandwidth  $\omega_{3dB}$  based on knowledge of the timeslot duration  $T_{sync}$  was provided. The guideline enabled a worst-case analysis and was shown to reduce the average error in the PLL outputs at the end of the timeslot duration. Future work may consider other PLL implementations or other design methodologies which truly minimize the average error in the PLL outputs. An alternate implementation and design of the RTTD PLLs may significantly affect the performance results obtained in Chapters 4 and 5.

The efficiency performance metric described in Chapter 4 of this thesis takes in to account the duration of the beamformer and the time spent synchronizing the

RTTD sources. These two durations of time were used to calculate the percentage of time the RTTD sources would be able to perform as a beamformer. This performance metric is a straightforward way to evaluate the capabilities of the RTTD system in the three channel models. It identified the major design tradeoffs with channel conditions, and highlighted the drawbacks of the time-divisioned approach. Future work may consider, however, other metrics to measure the performance of the RTTD system. Perhaps the savings in transmit energy, or the increases in signal reliability, could be considered and compared to the resources consumed during synchronization.

The performance of the RTTD system was investigated in Chapter 4 for single-path and multi-path time-invariant channels. The only cause for error considered in the PLL outputs was due to the gross-transient and high-frequency feedthrough behavior of the PLLs. As a result, the efficiency of the RTTD system approaches 1 for longer timeslot durations because these effects diminish when the RTTD source PLLs are designed with a low closed loop bandwidth. These results may be impractical because other detrimental effects such as noise and oscillator drift were not considered. In practical scenarios, there is additive AWGN noise at the VCO input. Hence, there will always be phase error accumulation in the PLL outputs and the actual worst-case error is non-deterministic. The worst-case analysis and simulation results in Chapter 4, however, do provide a general sense of the RTTD system performance in time-invariant channels and identify the effects of the timeslot duration. Future work may also consider a different methodology in dealing with the effects of multi-path time-invariant channels.

The performance of the RTTD system was investigated in Chapter 5 for single-path time-varying channels. Although the Gaussian channel model provided the opportunity to analytically investigate the phase error at the start of beamform-

ing, and during beamforming, this channel model may not be representative of the movement exhibited by typical wireless transmitters. As a result, the performance results obtained in this chapter may be pessimistic, but they offer insight into how the RTTD system performs for different mobile scenarios. Future work may consider a more realistic channel model.

Future work may also consider additional RTTD sources, better source construction, different PLL implementations, and more efficient scheduling during synchronization.

# Appendix A

## Appendices

Expressions for the time-to-lock  $T_L$  approximation and the magnitude of the high frequency feedthrough  $K_d|F(2\omega_c)|$  as a function of the PLL closed loop bandwidth  $\omega_{3dB}$  are derived in this appendix. The results of this appendix are used in Chapter 3 where the PLL design guidelines are discussed.

### A.1 Time-to-Lock

An expression for  $T_L$  for 2nd-order PLLs is given in (2.11) of Chapter 2. The PLLs used in the RTTD system in this thesis are 3rd-order, but the expression in (2.11) is still valid for approximating the time-to-lock [16].

A second-order loop filter was chosen in this thesis because an additional high-frequency pole enables the loop filter to attenuate the high-frequency feedthrough from the phase detector<sup>1</sup>. The additional high-frequency pole, however, has little impact on the gross-transient convergence behavior of the PLL loop [16]. Therefore, the additional high frequency pole, at  $\omega_3 = \frac{1}{\alpha_3}$ , can be removed and the loop filter

---

<sup>1</sup>Refer to Figure 3.4.

transfer function simplifies to a first-order active PI filter as given by

$$F(s) = \frac{1 + s(\alpha_2)}{s\alpha_1}. \quad (\text{A.1})$$

The results for a 2nd-order PLL in [16] now apply directly to approximating  $T_L$  for the 3rd-order PLL implementation of chapter 3. The approximation for  $T_L$  is in terms of the PLL natural frequency  $\omega_n$ , so in order to express  $T_L$  in terms of  $\omega_{3dB}$ , the relationship between  $\omega_n$  and  $\omega_{3dB}$  must be found. From [16], it is known that  $\omega_n$  can be expressed by

$$\omega_n = \sqrt{\frac{KoKd}{\alpha_1}}, \quad (\text{A.2})$$

where the time coefficient  $\alpha_1$  is calculated from

$$\alpha_1 = \frac{KoKd}{\omega_2^2 c_1}, \quad (\text{A.3})$$

and  $c_1$  is a scaling factor that relates the corner frequencies  $\omega_2$  and  $\omega_3$  to the frequency where the open-loop gain is 1, denoted as  $\omega_T$ . The scaling factor  $c_1$  is set to  $\sqrt{10}$  in [16], but it has been left as a variable to make the analytical expressions as general as possible. The corner frequencies are given by

$$\omega_2 = \frac{\omega_T}{c_1}, \quad (\text{A.4})$$

and,

$$\omega_3 = \omega_T c_1. \quad (\text{A.5})$$

Substituting (A.4) into (A.3), and the product of that into (A.2), the natural fre-

quency of the PLL can be expressed in terms of  $\omega_T$  as given by

$$\omega_n = \omega_T \sqrt{\frac{1}{c_1}}. \quad (\text{A.6})$$

The frequency  $\omega_T$  is proportional to the PLL closed loop bandwidth  $\omega_{3dB}$  by the scaling factor  $c_2$ , so  $\omega_n$  can now be expressed by

$$\omega_n = \frac{\omega_{3dB} \sqrt{\frac{1}{c_1}}}{c_2}. \quad (\text{A.7})$$

The scaling factor  $c_2$  is set to 1.33 in [16], but it has been left as a variable to make the analytical expressions as general as possible. The approximation for  $T_L$  in terms of  $\omega_{3dB}$  is found by substituting (A.7) into (2.11) from Chapter 2, and the result is given by

$$T_L = \frac{2\pi c_2}{\omega_{3dB} \sqrt{\frac{1}{c_1}}}. \quad (\text{A.8})$$

## A.2 High-Frequency Feedthrough Magnitude

To evaluate the magnitude of the high frequency feedthrough  $K_d|F(2\omega_c)|$  as a function of the PLL closed loop bandwidth  $\omega_{3dB}$ , the substitution  $s = j\omega$  is made into the loop filter transfer function given in (3.6), and magnitude is given by

$$|F(\omega)| = \left| \frac{1 + j\omega\alpha_2}{j\omega\alpha_1(1 + j\omega\alpha_3)} \right|. \quad (\text{A.9})$$

The substitution  $\omega = 2\omega_c$  is made into (A.9) to find the filter magnitude at the double-frequency term  $2\omega_c$  produced by the multiplier phase detector. While the actual double-frequency term may not be exactly  $2\omega_c$  due to VCO center frequency offset, this serves as a reasonable approximation. The transfer function evaluated

at  $2\omega_c$  is given by

$$|F(2\omega_c)| = \left| \frac{1 + 2j\omega_c\alpha_2}{2j\omega_c\alpha_1(1 + 2j\omega_c\alpha_3)} \right|. \quad (\text{A.10})$$

Guidelines for choosing the filter time coefficients  $\alpha_1$ ,  $\alpha_2$ , and  $\alpha_3$  are given in [16], and they can be expressed in terms of the PLL closed loop bandwidth as given by

$$\alpha_1 = \frac{c_2^2 c_1 K_o K_d}{\omega_{3db}^2}, \quad (\text{A.11})$$

$$\alpha_2 = \frac{\omega_{3db}}{c_1 c_2}, \text{ and} \quad (\text{A.12})$$

$$\alpha_3 = \frac{c_2}{\omega_{3db} c_1}. \quad (\text{A.13})$$

The scaling factor  $c_1$  is calculated from (A.4), and the scaling factor  $c_2$  is the ratio of  $\omega_{3dB}$  to  $\omega_T$ . The double-frequency magnitude of the filter in terms of  $\omega_{3dB}$  is found by substituting (A.11)-(A.13) into the transfer function expression in (A.10), and simplifying. The result is given by

$$|F(2\omega_c)| = \frac{\omega_{3dB}}{K_o K_d} \frac{\left(\frac{\omega_{3dB}}{\omega_c}\right)^2 + 2c_1 c_2 \left(\frac{\omega_{3dB}}{\omega_c}\right)}{4c_2^3 + 2c_2^2 c_1 \left(\frac{\omega_{3dB}}{\omega_c}\right)}. \quad (\text{A.14})$$

Finally, the high frequency feedthrough magnitude  $K_d|F(2\omega_c)|$  is found by multiplying (A.14) by the phase detector gain  $K_d$ , as expressed by

$$K_d|F(2\omega_c)| = \frac{\omega_{3dB}}{K_o} \frac{\left(\frac{\omega_{3dB}}{\omega_c}\right)^2 + 2c_1 c_2 \left(\frac{\omega_{3dB}}{\omega_c}\right)}{4c_2^3 + 2c_2^2 c_1 \left(\frac{\omega_{3dB}}{\omega_c}\right)}. \quad (\text{A.15})$$

# Bibliography

- [1] Stutzman, W. L. and Thiele, G. A. *Antenna Theory and Design*. John Wiley and Sons, New York, (1981).
- [2] Visser, H. J. *Array and Phased Array Antenna Basics*. John Wiley and Sons, New York, (2005).
- [3] Hu, A. and Servetto, S. *IEEE Transactions on Information Theory* **52**(6), 2725–2748 (2006).
- [4] Sendonaris, A., Erkip, E., and Aazhang, B. *IEEE Transactions on Communications* **51**(11), 1927–1938 Nov. (2003).
- [5] Sendonaris, A., Erkip, E., and Aazhang, B. *IEEE Transactions on Communications* **51**(11), 1939–1948 Nov. (2003).
- [6] Laneman, J. N. and Wornell, G. W. *IEEE Transactions on Information Theory* **49**(10), 2415–2425 (2003).
- [7] Mudumbai, R. Madhow, U. and Barriac, G. *submitted for review to IEEE Transactions on Wireless Communications* (2006).
- [8] Strogatz, S. *SYNC: The Emerging Science of Spontaneous Order*. Hyperion, New York, (2003).
- [9] Mirollo, R. and Strogatz, S. *SIAM Journal on Applied Mathematics* **50**(6), 1645–1662 (1990).
- [10] Hong, Y. and Scaglione, A. *IEEE Journal on Selected Areas of Communications* **23**(5), 1085–1099 (2005).
- [11] Werner-Allen, G. T. A. P. M. W. and Nagpal, R. In *Proceedings of the 3rd int. conf. on Embedded networked sensor systems*, 142–153, (2005).
- [12] Tu, Y. S. and Pottie, G. J. In *Proceedings of the IEEE Vehicular Technology Conference (VTC)*, volume 1, 130–134, Spring (2002).

- [13] Barriac, G., Mudumbai, R., and Madhow, U. In *Information Processing in Sensor Networks (IPSN), Third International Workshop*, 81–88, Berkeley, CA, April 26-27 (2004).
- [14] Mudumbai R. Hespanha, J. Madhow, U. and Barriac, G. In *Proceedings of the IEEE IEEE International Symposium on Information Theory*, volume 1, 130–134, (2005).
- [15] Brown III, D. R. In *Proceedings of the 5th IEEE Signal Processing Advances in Wireless Communications*, 278–282, June 5-8 (2005).
- [16] Best, R. E. *Phase-Locked Loops: Design, Simulation, and Applications*. McGraw-Hill, New York, (2003).
- [17] Papoulis, A. *The Fourier Integral and Its Applications*. McGraw-Hill, New York, (1962).
- [18] Newhall, WG Saldanha, K. and Rappaport, T. In *IEEE Vehicular Technology Conference*, (19965).
- [19] Cheon, C. Liang, G. and Bertoni, L. *IEEE Selected Areas in Communications* **19**(11), 2191–2200 (2001).
- [20] Kamen, E. *Introduction to Signals and Systems*. Macmillan, New York, (1987).